CLASSIFICATION METHODS *FOR* REMOTELY SENSED DATA

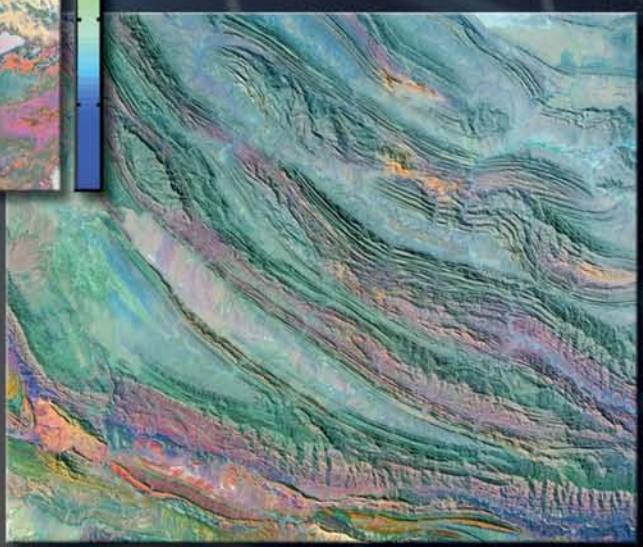

SECOND EDITION

BRANDT TSO • PAUL M. MATHER

CRC Press
Taylor & Francis Group

CLASSIFICATION METHODS *FOR* REMOTELY SENSED DATA

SECOND EDITION

CLASSIFICATION METHODS *FOR* REMOTELY SENSED DATA

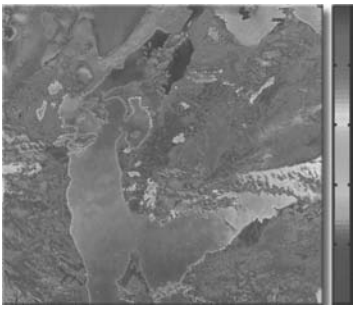

SECOND EDITION

BRANDT TSO • PAUL M. MATHER

CRC Press
Taylor & Francis Group
Boca Raton London New York

CRC Press is an imprint of the
Taylor & Francis Group, an **informa** business

CRC Press
Taylor & Francis Group
6000 Broken Sound Parkway NW, Suite 300
Boca Raton, FL 33487-2742

Printed in the United States of America on acid-free paper
10 9 8 7 6 5 4 3 2 1

International Standard Book Number-13: 978-1-4200-9072-7 (Hardcover)

Library of Congress Cataloging-in-Publication Data

Tso, Brandt.
Classification methods for remotely sensed data / Brandt Tso, Paul Mather.
-- 2nd ed.
p. cm.
Includes bibliographical references and index.
ISBN 978-1-4200-9072-7 (hardcover : alk. paper)
1. Remote sensing. 2. Pattern recognition systems. I. Mather, Paul M. II. Title.

G70.4.T784 2009
621.36'78--dc22 2009004453

Visit the Taylor & Francis Web site at
http://www.taylorandfrancis.com

and the CRC Press Web site at
http://www.crcpress.com

Contents

Preface to the Second Edition

The first edition of this book was written between 1998 and 2000, and was published in 2001. In the ten years that have elapsed since the start of this project, developments in image classification technology have been considerable. In order to keep this book relevant and up to date, two new chapters have been added and the existing chapters have been updated. The new chapters cover the topics of support vector machines (SVMs) and decision trees, both of which are now the subject of research articles in the major journals. SVMs represent a recent development in the computational aspects of image classification, and one of the problems they face is in the allocation of data to one of several (rather than one of two) classes. A number of approaches to this problem are presented in Section 4.4, but further experimentation is required. The number of potential approaches to the use of decision trees is considerable, and these are covered in Chapter 6. Developments such as boosting and random forest generation are described in Section 6.8. Lopping branches that do not contribute to the effectiveness of the decision tree is an important aspect of the design of the tree, which is covered in Section 6.7.

Acknowledgment is due to our institutions, the Management College, National Defense University and to The University of Nottingham, for providing support while this book was being revised. Brandt Tso also recognizes the benefits of his year as a postdoctoral fellow in the Remote Sensing Laboratory, Naval Postgraduate School, Monterey, California.

Preface to the First Edition

We classify objects in order to make sense of our environment, by reducing a multiplicity of phenomena to a relatively small number of general classes. On a country walk, for example, you might point to cows, trees, tractors, or swans. What you are actually doing is identifying an observed object and allocating it to a preexisting class, or giving it a name. Before setting out on the walk, you knew that swans existed, and you could specify their characteristics. When you saw a large white bird, possibly swimming in a canal or river, with an orange and black beak, you compared those characteristics to those of a swan and thus identified the bird, giving it the name or label of *swan*. We must be careful, therefore, to distinguish between the definition of the classes to which objects may belong and the identification or labeling of individual objects, and to avoid confusion between the two meanings of the word *classification*—the definition of categories of objects and the assignment or allocation of individual objects to these classes.

The example of the swan can also help to define other concepts. First, you must already have a model (or idealized representation) of the key features of a swan before you can recognize one. You learned, presumably in your childhood, the names of categories and subcategories of animals, plants, and other objects. Now you use that knowledge to identify and name the things you see and hear. In the literature of classification, this approach is termed *supervised learning*, meaning that you have divided the phenomena of interest into a number of *a priori* groups. You have observed a number of examples from each group, and have characterized them in terms of a number of discriminating features. The sample set is called *training data*, and this approach is known as *supervised classification*. In fact, it is supervised identification because it is assumed that the classification (the definition of the groups and their characteristics) has been defined before any previously unknown objects were identified.

An alternative approach, known as *unsupervised classification* or *clustering*, is also widely used. In this approach it is assumed that (1) you have little knowledge of the characteristics of the data set, (2) that you wish to determine whether any natural groupings exist in those data, and if so, (3) whether they can be identified in terms of phenomena of interest. In a sense, this procedure is akin to exploring the data (and visualization methods can help considerably in the process) whereas the supervised approach is inductive.

This book is about pattern recognition for remotely sensed data. We prefer the term *pattern recognition* to *classification* because the latter term can be misleading, as noted above. However, the two terms are used in this book, partly for reasons of tradition. A *pattern* is a set of measurements made on an object. It can be described as a mathematical vector of measurements. For example, a person's height and weight can be represented by the vector [192, 50] (in cm and kg, respectively). If a supervised approach is used, then the pattern is compared in some way to members of the sets of patterns that define the categories of interest, and the given pattern is

assigned to one of these categories (one of which may be "unknown"). This approach can be described as inductive. Alternatively, a clustering strategy may be used that is based on the similarity between patterns, in order to determine whether any distinct groups of patterns exist in the data.

In Earth observation by remote sensing, the objects to be labeled are normally the individual pixels forming a multispectral or hyperspectral image. Each pixel is represented by a pattern vector consisting of a set of measurements, one per image band plus, possibly, other measurements such as texture. If each spectral band is represented by one axis of a multidimensional space (the *feature space*), then the pixel can be represented as a point in that space. For simplicity, let the number of features be two, and let the x-axis represent the first feature and the y-axis represent the second. A pixel with a feature vector of [1, 5] can therefore be shown on a graph as a point with Cartesian coordinates [1, 5]. Now imagine that all the pixels in the two-band image have been plotted on the graph, and that they fall into clearly defined groups. We can separate these groups by lines or curves. These lines or curves are called *decision boundaries*, for they show the positions of the boundaries of individual categories. If a point lies on one side of the boundary, it is given a label such as "A," whereas if it lies at the other side of the boundary it is given the label "B." In higher-dimensional problems, the lines and curves become *hyperplanes* and *hypersurfaces*. So the labeling problem can be thought of as one that involves the positioning of hyperplanes or hypersurfaces, representing decision boundaries, in a multidimensional feature space. The algorithm that determines the position of the pixel with respect to the decision boundaries, and thus allocates a specific label to that pixel, is called a *decision rule*. The word *classifier* is widely used as a synonym for the term *decision rule*.

The use of pattern recognition methods in remote sensing has a long history. Air photo interpreters were perhaps the first to use intuitive methods to determine the information contained in reconnaissance photographs, and these methods continue to be of great importance, particularly in the gathering of military intelligence, as the human eye–brain combination can make decisions and judgments on complex problems in milliseconds, using experience as a guide. Automatic methods are more suitable to the routine processing of images that show predictable patterns. Such methods have been developed and applied in a number of disciplines, ranging from speech and handwriting recognition, industrial process management, and medical diagnosis, as well as in the collection of military intelligence. The main distinguishing characteristic of Earth observation data is its volume. Hence, methods that can be applied in other applications may not be suited to the analysis of remotely sensed data because of the computational requirements. A further point to note is that there is often a discrepancy between the dimensionality of remotely sensed data sets and the volume of training data that is available. Where training data is sparse relative to the dimensionality of the data, it becomes difficult to estimate the characteristics of each training class, and so error may become significant. This phenomenon of increasing error with increasing data dimensionality is sometimes known as the *Hughes effect*.

Advances in technology have led to rapid developments in methods of pattern recognition, leading to the formulation of new and more sophisticated decision rules.

Some of those new methods have been introduced into the field of remote sensing and have shown encouraging results. A further feature of remote sensing applications in recent years is the use of combinations of data derived from different sensors or from different time periods, plus terrain and other data extracted from geographic information system (GIS) databases. In addition, the spectral information contained in remotely sensed images is often augmented by derived measures such as values of texture and context. In dealing with multidata sources, a significant problem is the considerable increase in the computational cost. Other problems, such as data scale and data reliability, must also be considered. There is an increasing interest in seeking methods for efficiently manipulating multisource data in order to increase classification accuracy. It should always be remembered, though, that sophisticated algorithms cannot compensate for lack of training data or an inadequate definition of the problem (in terms of the number and nature of the classes to be recognized relative to the scale of the study).

Texture is the tonal variation within an area. A simple example that illustrates the concept is the pattern on a carpet. If we treat each pattern as a whole, then the carpet can easily be described. If the carpet is seen as a set of small rectangular units, then the problem of describing its properties is more difficult. In some cases, texture information seems to be more effective than tonal information to describe the objects, and one can develop *texture features* corresponding to different kinds of patterns to improve the performance of a classifier.

Contextual information describes how the object of interest may be affected by its neighbors. For instance, English words starting with the letter "q" are more likely to be immediately followed by the letter "u" than "z" or "c." In the case of classification of an agricultural area, a pixel labeled as "carrot" is more likely to be surrounded by pixels of the same class rather than by other classes such as "water" or "wheat." The ability to model such contextual behavior may reduce confusion in the classification process.

The decision to write this book was triggered by our experience in attempting to use new methods of describing and labeling pixels in a remotely sensed image. While a number of valuable but more general textbooks are available for undergraduate use, we know of no coherent source of advanced information and guidance in the area of pattern recognition for research scientists and postgraduate research students in remote sensing, together with students taking advanced remote sensing courses. We hope that this book will contribute to the increased understanding and adoption of recently developed techniques of pattern recognition, and that it will provide readers with a link between the remote sensing literature and that of statistics, artificial intelligence, and computing. We do suggest, however, that attention be paid to experimental design and definition of the problem, for an advanced pattern recognition procedure is no substitute for thinking about the problem and defining an appropriate set of features.

Chapter 1 introduces the basic concepts of remote sensing in the optical and microwave region of the electromagnetic spectrum. This chapter is intended to introduce the field of remote sensing to readers with little or no background in this area, and it can be omitted by readers with adequate background knowledge of remote sensing.

Chapter 2 introduces the principles of pattern recognition. Traditional decision rules, including the supervised minimal distance classifier, Gaussian maximum likelihood, and unsupervised clustering techniques are described, together with other methods such as fuzzy-based procedures and decision trees. The chapter also contains brief accounts of dimension reduction methods, including orthogonal transforms, the assessment of classification accuracy, and the principles underlying the choice of training data.

Chapter 3 describes widely used neural network models and architectures including the multilayer perceptron (also called the feed-forward neural network), Kohonen's self-organized feature map, counterpropagation, the Hopfield network, and networks based upon adaptive resonance theory (ART).

Chapter 4 deals with pattern recognition techniques based on fuzzy systems. The main topics of this chapter are the construction of fuzzy rules, fuzzy mapping functions, and the corresponding decision processes.

Chapter 5 presents a survey of methods of quantifying image texture, including fractal- and multifractal-based theory, the multiplicative autoregressive random field model, the grey level co-occurrence matrix, and frequency domain filtering.

Chapter 6 addresses the theory and the application of Markov random fields. The main application of Markov random fields is to model contextual relationships. Other related topics, including function formulation, image restoration, robust estimation in the presence of noise (outliers), and the derivation of Markov-based texture measures, are also presented.

Chapter 7 provides several approaches for dealing with multisource data. The methods described include the extension of Bayesian classification theory, evidential reasoning, and Markov random fields.

No one is more aware of a book's deficiencies and inadequacies than its authors. Even Socrates, after a lifetime of learning, is reported to have been impressed by the extent of his own ignorance. Had more time and space been available, the book would have contained a longer account of the use of wavelets in texture analysis, and of the applications of decision tree classifiers. Publishers, who live in the real world, impose constraints of time and space while authors naturally attempt to rewrite their manuscripts every month in order to include the latest developments. We hope that we have reached a happy compromise that should satisfy most readers. We have included references to further work in order to guide the more advanced reader toward the relevant literature.

Most of the research underlying the ideas presented in this book was carried out while Dr. Brandt Tso was a postgraduate student, and later a postdoctoral fellow, in the School of Geography, The University of Nottingham, under the supervision of Professor Paul M. Mather. The second author provided encouragement, support, contributions to the first three chapters, and numerous rewrites of the draft. We realize that any book written by human authors is necessarily flawed, and we accept responsibility for any errors that may be contained in these pages.

The School of Geography, The University of Nottingham, provided computing facilities as well as a stimulating and encouraging environment for research. The second author is grateful to his many postgraduate research students from different parts of the world who have, over the past decade or so, educated and trained him in

many areas of remote sensing. In particular, he would like to thank Valdir Veronese, Taskin Kavzoglu, Carlos Vieira, and Mahesh Pal, who have carried out research projects in areas relevant to the subject matter of this book. The contribution of others, while not directly related to the topic of image classification, has helped by broadening the intellectual debate within my research group as well as helping in many other ways. We also thank Dr. M. Koch of Boston University for help and guidance with the Red Sea Hills data set, which is used in a number of examples in this book. The help, good humor, and patience of Tony Moore of Taylor & Francis is greatly appreciated. Finally, both authors recognize the contributions of their families, and dedicate this book to them.

Brandt Tso
Taipei, 2000

Paul M. Mather
Nottingham, 2000

Author Biographies

Dr. Brandt Tso has served as a scientific officer in the Taiwan military service, studying modeling and pattern recognition techniques since 1988. Dr. Tso completed his Master's degree in information science at the Management College, National Defense University, Taiwan. Between 1994 and 1998, Dr. Tso was awarded a scholarship by the Taiwan government to pursue a Ph.D. degree in the School of Geography, The University of Nottingham, U.K., under the supervision of Professor Paul M. Mather, concentrating on the field of remotely sensed data classification. In 2003, Dr. Tso was an invited postdoctoral fellow in the Remote Sensing Laboratory, Physics Department, Naval Postgraduate School, Monterey, California, U.S.A., to study more complex remotely sensed data classification skills. Currently, Dr. Tso is an associate professor in the information science department, Management College, National Defense University, Taiwan. His main research interests include remotely sensed data recognition, real scene image retrieval, and machine learning algorithms. He has published numerous research papers relating to these fields.

Professor Paul M. Mather graduated with a degree in geography from the University of Cambridge in 1966. He then moved to The University of Nottingham to conduct research for his Ph.D. in geomorphology, which was awarded in 1969. As lecturer, senior lecturer, and full professor (1988), his attention was focused on the use of multivariate analysis in physical geography, a subject on which he published a detailed and well-received monograph in 1976. By the 1980s his interest in multivariate analysis had branched out to include remote sensing. In 1987 the first edition of his book *Computer Processing of Remotely Sensed Data* was published. It is now in its third edition (2004) with a fourth edition in preparation. He has always been fascinated by the applications of computers in physical geography and the environmental sciences, and is a proficient Fortran programmer. He retired in 2006, and was made Emeritus Professor. He received the Back Award from the Royal Geographical Society for his work in remote sensing in 1992, and in 2002 was awarded the Order of the British Empire (OBE) by Her Majesty Queen Elizabeth II for services to remote sensing. He has lectured in a number of countries around the world.

1 Remote Sensing in the Optical and Microwave Regions

Remotely sensed image data is widely used in a range of oceanographic, terrestrial, and atmospheric applications, such as land-cover mapping, environmental modeling and monitoring, and the updating of geographical databases. Hence, the quantized pixel values making up an image may be converted to physical values of radiance and related to some property of the surface being sensed. An example of this approach is the calibration of thermal infrared imagery to produce maps of temperature fields, such as sea surface temperature. In other applications, thematic information is required. A thematic map is one that displays the spatial variation of a specified phenomenon, such as land surface elevation, soil type, geology, or vegetation. It is this second approach that is considered in this book. The term *pattern recognition* is used to describe the procedures involved in relating vectors of measurements that are spatially referenced to individual pixel locations to the types or categories into which the phenomenon of interest is subdivided. If, for example, the phenomenon of interest is agricultural crops, then the categories are the individual crop types. Each crop type is represented in the thematic image by a numerical label. Vectors of measurements that are spatially referenced to individual pixel locations include image pixel values plus derived values such as texture, coherence, or context, as well as other geographical data that can be related to the pixel location, such as terrain elevation and slope, geology, and soil type.

Digital thematic maps can be represented in two ways, using either the raster or the vector models. The *vector model* uses the classical cartographic representation of map objects in terms of points, lines, and areas. Using this model, a continuously varying spatial attribute such as terrain elevation is represented by contour lines and spot heights, while an attribute such as soil type or underlying geology is represented in terms of boundary lines that enclose areas that are homogenous with respect to the property of interest and at the chosen scale of observation. The *raster model* represents spatial attributes in terms of their values over a contiguous set of small individual (and usually square) areas. Thus, variations in land surface elevation over a region of interest are represented by numerical values stored in a rectangular grid or raster, each element of which is the average elevation of the ground area represented by that element or cell of the grid. This representation of terrain height variation is known as a *digital elevation model* or DEM.

In the same way, variations in geology in a study region are stored in raster format as a set of labels. Each cell in the data array is given a numeric label that is linked to a

description. For example, pixels with the Label 1 may be described as Carboniferous Limestone, while pixels given the Label 2 might be described as Silurian Grit. In this book, we are concerned with spatial data (specifically, remotely sensed images) that are represented in terms of rectangular rasters.

In the examples given in the preceding paragraphs, each cell of the raster stores either a physical value (such as elevation in meters above a given datum) or a label (such as 1 or 2, indicating rock types such as granite and basalt). In practice, rasters (and particular raster data sets containing images for display) are generally stored in the form of integer rather than floating-point numbers, in order to conserve storage space. Thus, a DEM may be represented in terms of an array of integers in the range 0 to 255, with each integer value representing a range of land surface elevations. The idea is similar to the use of a key in a printed map in which elevation is generally shown in shades of green and brown, with the map key showing the relationship between these hues and specific elevation ranges. In the same way, the values 0 to 255 contained in the DEM are connected to a range of real elevation values by the use of a table rather than a key. The table, known as a *lookup table* or LUT, allows the user to determine the actual range of elevations denoted by a particular label, such as 215. In some applications, the physical elevation value is required (for instance, if slope angle is to be calculated). Other questions can be answered by using the counts or labels directly. If Label 18 is used to represent land with a surface elevation between 200 and 205 meters, then the locations of such areas can be achieved by searching the raster for all values of 18 rather than converting the raster labels back to physical values and searching for cells holding numbers in the range 200 to 205.

Remotely sensed images are stored and manipulated in raster form. Each element of the raster is known as a pixel, and the value contained in any pixel location is simply a quantized count or a label rather than a physical value. For some applications, such as pattern recognition, these counts can be used directly as we are interested in interpixel similarities and differences. In other applications, such as sea-surface temperature determination, the pixel counts must be converted to physical values of radiance or reflectance, with corrections applied for such factors as sensor calibration changes and atmospheric influences. The range of quantized counts used in a raster representation of an image ranges from 0 to 255 (8-bit representation, for images derived from sensors such as Landsat Enhanced Thematic Mapper + (ETM++ and SPOT High Resolution Visible [HRV]), to 0 to 1023 (10-bit representation, as used for Advanced Very High Resolution Radiometer [AVHRR] data to more complex formats. For example, raw synthetic aperture radar data are commonly represented in terms of two 16-bit integers per pixel, with the first integer representing the real part and the second integer representing the imaginary part of a complex number. Whatever the precision (8-, 10-, or 16-bit) these pixel values are stored as rectangular rasters, and can be held in a computer in the form of a two-dimensional array. The data set used in pattern recognition consists of a number of co-registered raster images representing, for example, the measurements in the individual bands of a multispectral or hyperspectral image, the ground elevation (DEM), or some other spatial property of interest. The number of features used to represent terrain conditions is known as the *dimensionality* of the data. Multispectral and radar data have a low dimensionality; for instance, SPOT HRV produces three bands of data,

and Landsat-7 ETM+ generates seven bands in wavelengths ranging from the optical to the thermal infrared, plus a panchromatic band, while the radar satellite ERS-2 operates in a single band. Hyperspectral sensors such as Airborne Visible/Infrared Imaging Spectrometer (AVIRIS), Compact Airborne Spectrographic Imager (CASI) and the Digital Airborne Imaging Spectrometer (DAIS) have the ability to collect data in tens or hundreds of narrow spectral bands. One problem in the classification of high-dimensional remotely sensed data is the paucity of samples ("training data") relative to the dimensionality of the feature space. This problem leads to difficulties in estimating statistical parameters such as the mean and covariance matrix.

The aim of pattern recognition in the context of remote sensing is to link each object or pixel in the study area to one or more elements of a user-defined label set, so that the radiometric information contained in the image is converted to thematic information, such as vegetation type. The process can be regarded as a mapping function that constructs a linkage between the raw data and the user-defined label set. A simple example is shown in Figure 1.1. Normally, each object or pixel is linked to a single label. However, it is also possible to perform a *one-to-many* mapping, so that a given pixel can be associated with more than one label, with the differing degrees of association between the pixel and each label being expressed as probabilities of membership. Alternatively, a *many-to-one* scheme will link groups of pixels to a single label. This approach can be used, for example, to give the same label to all of the pixels in a single agricultural field.

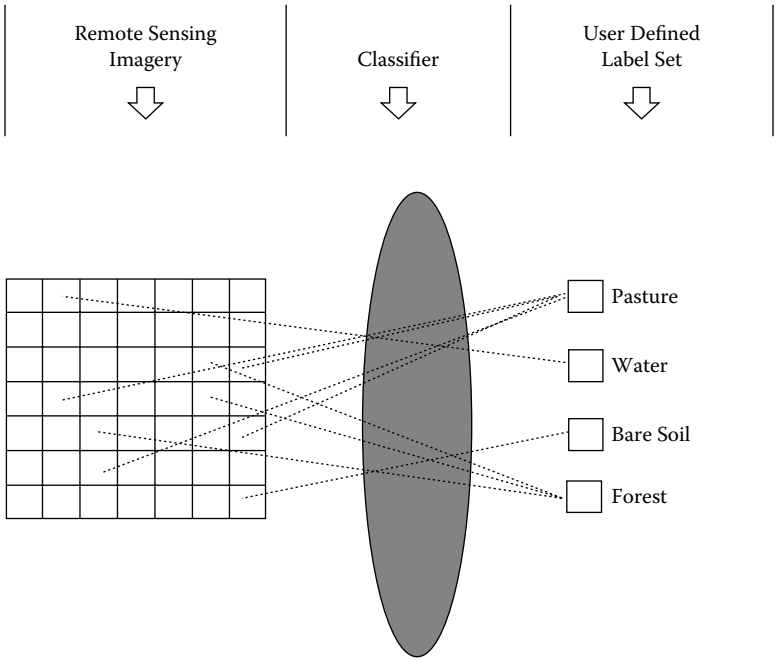

FIGURE 1.1 The concept of the classifier as a link between an image (left) and a set of labels.

Each application generally requires a different methodology, and each methodology is likely to generate different results. If reliable results are to be obtained, the analyst should understand the behavior of the method being used in order to achieve a satisfactory performance. For instance, the performance of a statistical procedure is strongly affected by the accuracy of the estimates of parameters such as the mean vector and the variance–covariance matrix for each class, which are obtained from samples of pixels called *training data sets*. Equally, the design of the architecture of a feed-forward neural net has an equally important impact on performance of the network.

The aim of this book is to provide a survey of pattern recognition methodology for use with remotely sensed imagery. Besides describing traditional approaches, more advanced techniques using artificial neural networks, support vector machines, fuzzy theory, and decision trees are introduced, and considerable space is devoted to the discussion of textural and contextual features. Some particular issues, such as pattern recognition using multiple data sources, change detection, and the analysis of mixed pixels, are also illustrated.

In the main part of this introductory chapter, the principles underlying remote sensing in the optical and microwave regions of the spectrum are described. Some important preprocessing techniques, such as corrections for atmospheric and topographic effects and noise filtering models, are also presented. These techniques are helpful in improving thematic accuracy in some kinds of applications, for example, in change detection.

1.1 INTRODUCTION TO REMOTE SENSING

Remote sensing is the use of sensors installed on aircraft or satellites to detect electromagnetic energy scattered from or emitted by the Earth's surface. This energy is associated with a wide range of wavelengths, forming the electromagnetic spectrum. Wavelength is generally measured in micrometers (1×10^{-6} m, μm). Discrete sets of continuous wavelengths (called *wavebands*) have been given names such as the *microwave band*, the *infrared band*, and the *visible band*. An example is given in Figure 1.2, which shows only a part of the overall electromagnetic spectrum. It is apparent that the visible waveband (0.4 to 0.7 μm), which is sensed by human eyes, occupies only a very small portion of the electromagnetic spectrum.

A specific remote sensing instrument is designed to operate in one or more wavebands, which are chosen with the characteristics of the intended target in mind. Thus, a sensor designed to detect electromagnetic radiation in the visible spectrum that has been reflected by chlorophyll in ocean waters will use different wavebands than would a sensor designed to detect the characteristics of soils. Apart from the reflectance characteristics of the target, an important factor governing the choice of waveband is the effect of interactions between the atmosphere and electromagnetic radiation. Such radiation passes downward through the atmosphere on its way from the sun to the Earth, and reflected radiation passes upward through the atmosphere on its way from Earth to the sensor. Absorption and scattering are the main mechanisms that alter the intensity and direction of electromagnetic radiation within the atmosphere. In some regions of the optical spectrum, these mechanisms (principally absorption) ensure that remote sensing is impossible. Spectral regions of

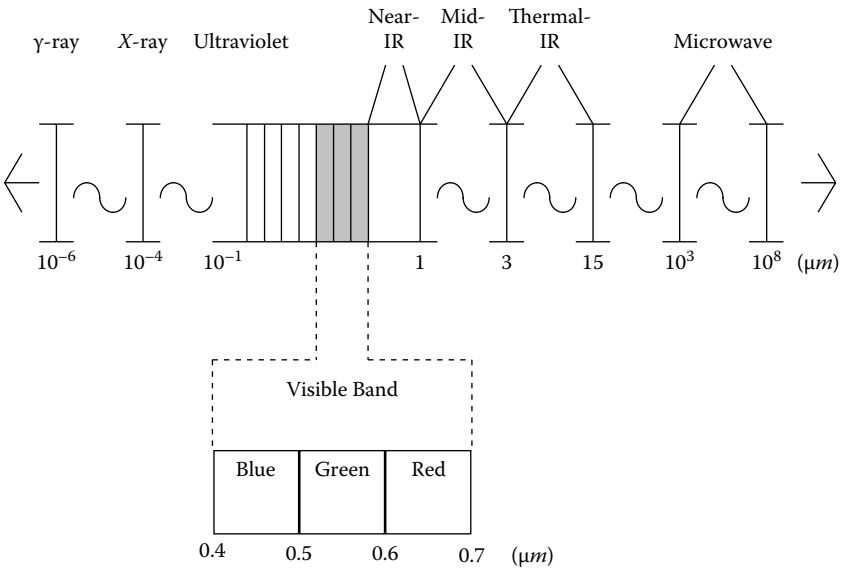

FIGURE 1.2 Regions of the electromagnetic spectrum that are of interest in remote sensing applications.

lower absorption are known as *atmosphere windows* (Figure 1.3), though it should be remembered that scattering and absorption affect all wavebands in the optical spectrum to a greater or lesser degree, and these effects are variable both in space and time.

1.1.1 Atmospheric Interactions

Electromagnetic radiation interacts with the Earth's atmosphere, the degree of interaction depending on the wavelength of the radiation and the local characteristics of the atmosphere. The basic interactions are known as *scattering* and *absorption*. Scattering is more likely to occur at shorter wavelengths. The most common scattering behavior is known as *Rayleigh scattering*, which is the main cause of haze in remotely sensed imagery. The atmosphere has different levels of absorption at different wavelengths. Regions of the spectrum that have a relatively high transmission are called atmospheric windows (Figure 1.3). The energy in some wavebands (e.g., from 15 to 10^3 μm) is almost completely absorbed by the atmosphere. These wavelengths cannot, therefore, be used for remote sensing. Wavebands with a high transmission could be potential candidates for remote sensing missions.

1.1.2 Surface Material Reflectance

The choice of wavebands for remote sensing in the optical region is also affected by the characteristics of the surface material. Energy that is incident upon a target can be separated into three components, namely, energy that is transmitted,

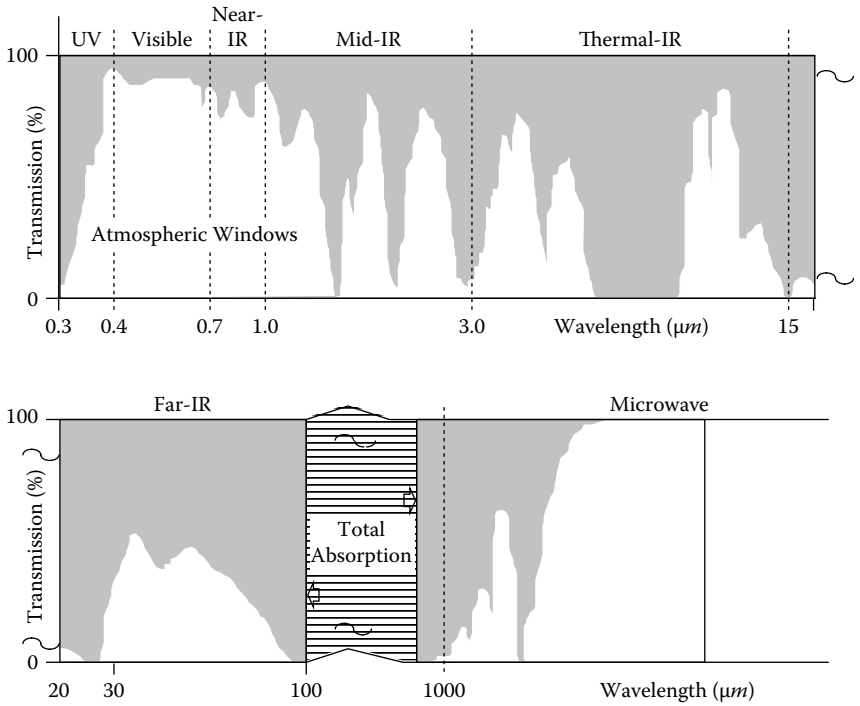

FIGURE 1.3 Atmospheric windows (unshaded). Vertical axis is atmospheric transmission (%). Horizontal axis is the logarithm of the wavelength in micrometers.

absorbed, and reflected. Surface material reflectance characteristics may be quantified by the spectral reflectance, which is a percentage measure obtained simply by dividing reflected energy in a given waveband by incident energy. The quantity of the reflected energy depends mainly on three factors: the magnitude of the incident energy, the roughness of the material, and the material type. Normally, the first two factors are regarded as constants. Therefore, only the third factor (i.e., the material type) is considered. However, it is worthwhile to first describe how roughness affects the reflected energy.

Surface roughness is a wavelength-dependent phenomenon. Given the same material, the longer the wavelength the smoother the material appears. For a perfectly smooth (specular) surface, reflected energy travels only in one direction such that the reflection angle is the same as incidence angle. In the case of a perfectly rough (Lambertian) surface, incident energy is reflected equally in all directions (Figure 1.4). However, in practical applications, most surface materials act neither as specular nor Lambertian reflectors; their roughness lies somewhere between these two extremes.

Figure 1.5 shows the average reflectance over the optical region of the spectrum for three ideal surface materials: dry bare soil, clear water, and green vegetation. This graph shows how these surface materials can be separated in terms of their reflectance spectra. It is apparent that vegetation reflectance varies considerably

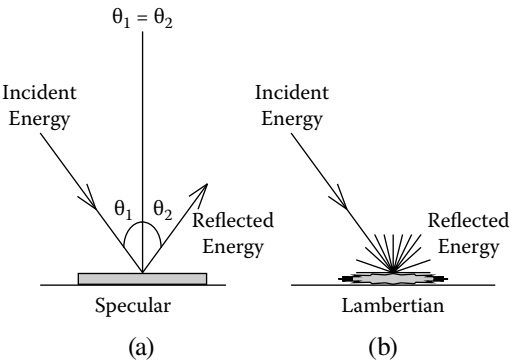

FIGURE 1.4 (a) Specular and (b) Lambertian reflectance.

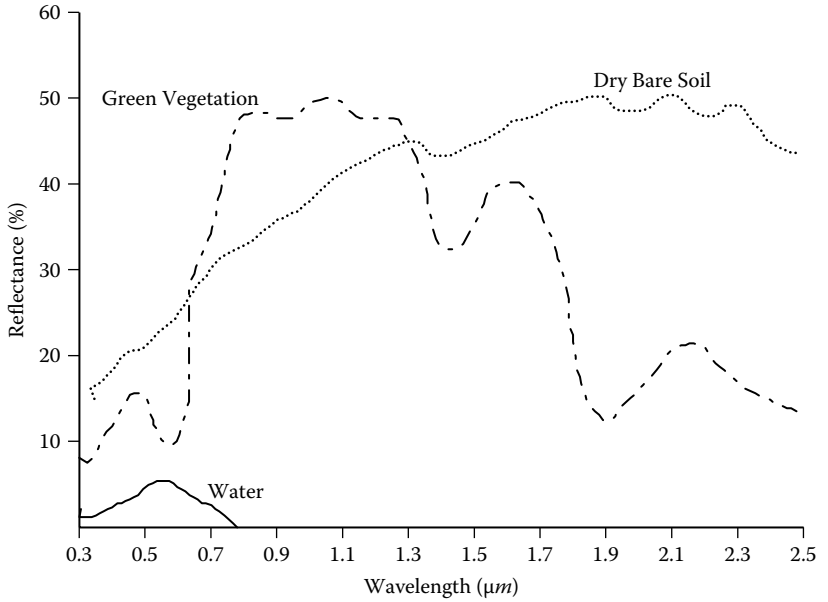

FIGURE 1.5 Typical spectral reflectance (%) of three materials: green vegetation, dry bare soil, and water.

across these wavebands. The lowest reflectance values occur at 0.4 μm (i.e., in the blue waveband), while the highest reflectance values occur around the near-infrared and part of the mid-infrared bands. The reflectance spectrum of bare soil, in contrast, shows reflectance increasing smoothly with wavelength. Its reflectance in the visible waveband is greater than that of vegetation, while in near-infrared and part of mid-infrared bands bare soil reflectance becomes less than that of vegetation, and eventually it dominates again beyond wavelengths of around 1.4 μm. The high near-infrared reflectance of vegetation, combined with its low reflectance in the

red waveband, is used in the construction of vegetation indices. One such index, the NDVI (Normalized Difference Vegetation Index), is described in the following text.

Recent interest in global environmental change has led to the development of global climate models, which require inputs describing land cover type. The AVHRR sensor carried by the National Oceanographic and Atmospheric Administration (NOAA) satellite series (from NOAA-6 to NOAA-18) provides data that are useful for large-scale studies of terrestrial vegetation (Eidenshink and Faundeen, 1994; Lim and Kafatos, 2002). A variety of mathematical combinations (e.g., subtraction, ratioing) of AVHRR band 1 (red) and band 2 (near infrared) have been developed to characterize the spatial distribution of vegetation and its condition. The best known of these vegetation indices is the Normalized Difference Vegetation Index (NDVI), defined as

$$\text{NDVI} = \frac{(\text{Near Infrared Band}) - (\text{Red Band})}{(\text{Near Infrared Band}) + (\text{Red Band})} \tag{1.1}$$

This index is based on the observation that vegetation has a high reflectance in the near infrared band, while reflectance is lower in the red band (Figure 1.5). NDVI is less sensitive to the changes of atmospheric conditions than are other indices (Jackson, 1983; Holben and Kimes, 1986) and therefore has been widely applied for vegetation monitoring. Data from other sensors that provide red and near-infrared (near-IR) images can also be used to generate NDVI images. For instance, in the case of Landsat Thematic Mapper ™ images, NDVI is based on bands 5 and 7, while for SPOT HRV, NDVI is derived from bands 3 and 2.

Reflectance from water surfaces is relatively low, and is more or less zero at wavelengths beyond the visible red. Knowledge of surface material reflectance characteristics provides us with a principle on the basis of which suitable wavebands to scan the Earth surface for a particular mission can be selected (e.g., for vegetation monitoring, sea surface observation, or lithological identification). Such knowledge also provides an important basis to make the objects more distinguishable in terms of multiband image manipulations such as overlay, subtraction, or ratioing.

1.1.3 Spatial and Radiometric Resolution

The resolution of a remote sensing instrument can be expressed in terms of its spatial and radiometric resolution. The higher the spatial resolution the smaller the ground objects that can be distinguished. The spatial resolution is related to the *instantaneous field of view* (IFOV) of the sensor, which denotes the size of the area from which the sensor receives the energy at the given instant in time. In Figure 1.6 the energy transmission path to the sensor takes a conelike shape, and ground resolution is roughly equivalent to the diameter of the circle formed by the intersection of this cone and the ground surface. As the sensor scanning area moves away from the nadir, the larger the IFOV will be (Figure 1.6), and thus results in the distortion of the resulting image as the spatial scale decreases from the left and right edges of

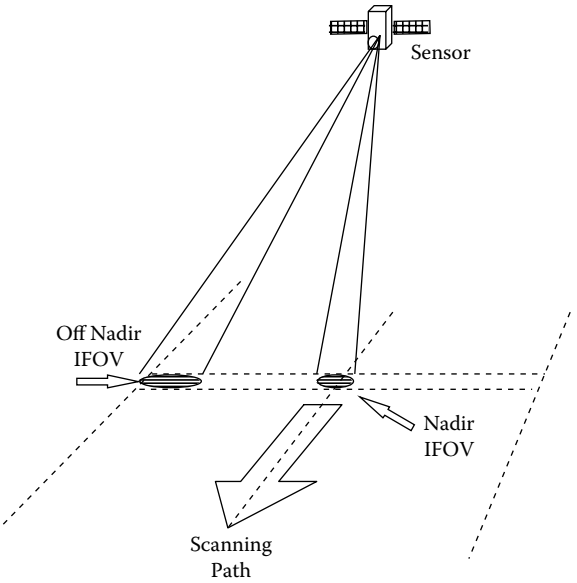

FIGURE 1.6 Showing the variation in the size of the instantaneous field of view (IFOV) of a sensor across a scan line.

the image toward the center. The correction for this scale distortion effect (and other effects due principally to the platform's orbit characteristics and to the eastward rotation of the Earth during scanning) is called *geometric correction*. This correction is usually performed by constructing a transform (using either an empirical procedure based on least squares methods or an analytical procedure using orbital information) in order to map ground coordinates to their corresponding image coordinates, and vice-versa. A review of local and global methods of geometric correction and image registration is provided by Brown (1992) and Zitová and Flusser (2003).

One's instinctive feeling might be that the finer the spatial resolution the better. However, in practice, this may not always be the case. The choice of spatial resolution should depend on what we want to see. For instance, in everyday life, we recognize a human face from the combination of features such as eyes, nose, lips, etc. Therefore, the appropriate spatial resolution should be set at a level to allow us to recognize each feature in the context of the whole face. It is arguable whether an increase in the spatial resolution of our eyes is likely to improve our identification of faces, once a certain limit has been reached. Thus, the choice of spatial resolution is case dependent.

Reducing the spatial resolution in terms of narrowing the instrument's IFOV also affects a related issue. The use of a smaller IFOV implies that the quantity of energy received by a detector is less (because area from which energy is collected is smaller, and the time available for the sensor to detect the upwelling energy is also shorter). It follows that the instrument's sensitivity to changes in the levels of energy will decrease, and thus the sensor may not be able to distinguish slight energy differences along a scan line. In other words, the radiometric resolution is degraded. A smaller

IFOV may thus result in a worse signal-to-noise ratio, which means that the signal is contaminated by more noise as IFOV decreases (assuming that the same radiometric resolution applies). Although such a decrease in signal-to-noise ratio can be compensated for by enlarging the scanning bandwidth (i.e., the region of the electromagnetic spectrum from which sensor receives energy), this will cause a reduction in the spectral resolution (i.e., sensor's ability to quantify spectral differences). Overall, it can be concluded that enhancement of both spatial and radiometric resolution cannot be achieved together, and some kind of compromise is needed.

1.2 OPTICAL REMOTE SENSING SYSTEMS

Over the past 20 to 25 years, the most widely used optical remote sensing systems have been the Landsat TM and Multispectral Scanning (MSS), the SPOT HRV, and the NOAA AVHRR instruments. Other remote sensing satellites carrying optical sensors have been launched by a number of national space agencies and private companies, and these have also gradually become the main sources for serving scientific study and environmental monitoring purposes. Examples are the Chinese-Brazilian remote sensing system, the Terra spacecraft, the Space Imaging Corporation's IKONOS satellite the European Envisat, the Indian IRS series, and several Japanese experimental projects. High-resolution sensing devices (4 m in multispectral mode, one meter or less in panchromatic mode) are now well established (e.g., the QuickBird satellite, and IKONOS). Radar systems are also becoming more numerous (Canada's Radarsat 1 and 2, the German TerraSAR-X, the European Advanced Synthetic Aperture Radar (ASAR) on Envisat, and the Italian COSMO-SkyMed X-band system). Considerable interest is also being shown in the application of hyperspectral imagery. Whereas multispectral sensors such as the Landsat ETM+ collect upwelling radiation in a small number of broad wavebands (seven in the case of the ETM+ instrument), a hyperspectral sensor collects data in a large number of very narrow wavebands. An example is the DAIS instrument, which collects data in 79 bands in the wavelength range 0.4 to 12.6 μm. The width of each spectral band varies from 15 to 20 nm in the visible to 2 μm in the middle infrared. The Compact Airborne Spectrographic Imager (CASI) instrument allows data to be collected for any 545-nm segment of the 0.4- to 1.0-μm region in 288 bands, with the bands spaced at intervals of approximately 1.9 nm. NASA's AVIRIS acquires data in 224 bands in the range 0.38 to 1.5 μm with a bandwidth of 10 nm. Up until the present time, hyperspectral data have been collected by aircraft-mounted sensors. NASA's Earth Observer I, launched in 2000, is the first orbiting spacecraft to carry a hyperspectral imager, Hyperion. The Hyperion instrument collects data over a narrow swath in 220 bands of 10 μm width. The large number of spectral bands produced by hyperspectral sensors (i.e., the high dimensionality of the data) poses significant problems in the pattern recognition process. These problems are discussed in Chapter 2.

Another class of satellites is the *small sat*, constructed using off-the-shelf components. The leader in this area is Surrey Satellite Technology Limited, which has developed the DMC or Disaster Monitoring Constellation of small satellites, which

have been purchased by several governments, including Algeria, Nigeria, China, and the United Kingdom. The imaging sensor carried by these satellites is comparable to Landsat's TM in the visible and near-IR bands.

An exhaustive list of sensors and satellites is not supplied here; such lists tend to become outdated very quickly. The advent of the World Wide Web (WWW) means that researchers, teachers, and students can readily obtain up-to-date information via the Internet. Professional and learned societies, such as the Remote Sensing and Photogrammetry Society, maintain WWW pages that provide links to international and national space agencies and projects. The Committee for Earth Observation Satellites (CEOS) also maintains an information site.

Details of the operation of the main types of sensor carried by remote sensing satellites can be found in textbooks (e.g., Lillesand and Keifer, 2000; Mather, 2004) and readers who may be unfamiliar with these details are referred to one of these sources.

1.3 ATMOSPHERIC CORRECTION

Electromagnetic energy detected by remote sensing instruments (especially those that operate in the optical region of the spectrum) consists of a mixture of energy reflected from or emitted by the ground surface and energy that has been scattered within or emitted by the atmosphere. The magnitude of the electromagnetic energy in the visible and near-infrared region of the spectrum that is detected by a sensor above the atmosphere is dependent on the magnitude of incoming solar energy (irradiance), which is attenuated by the process of atmospheric absorption, and by the reflectance characteristics of the ground surface. Hence, energy received by the sensor is a function of incident energy (irradiance), target reflectance, atmospherically scattered energy (path radiance), and atmospheric absorption. Interpretation and analysis of remotely sensed images in the optical region of the spectrum is based on the assumption that the values associated with the image pixels accurately represent the spatial distribution of ground surface reflectance, and that the magnitude of such reflectance is related to the physical, chemical, or biological properties of the ground surface. Clearly, this is not the case unless corrections are applied to take account of variations in solar irradiance and in the magnitude of atmospheric absorption and scattering, as well as in the sensitivity of the detectors used in the remote sensing instrument. The response of these detectors to a uniform input tends to change over time. Correction for these effects is vital if thematic images of a given area are to be compared over time; for example, over a crop-growing season.

The necessity for atmospheric correction depends on the objectives of the analysis. In general, land cover identification exercises that are based on single-date images do not require atmospheric correction, as pixels are being compared to other pixels within the image in terms of similarity, for example. The validity of this statement depends also on the quality of the image (for example, an image displaying severe haze effects, spatially varying haze phenomena, or cloud–cloud shadow effects may be unsuitable for classification). Atmospheric correction and sensor calibration are necessary when multisensor or multidate images are being classified, or where the aim of pattern recognition is to identify land cover change over time, in order to

ensure that pixel values are comparable from one image to the next in a temporal sequence. A more radical view is taken by Smith and Milton (1999, p. 2653), who emphasize that "to collect remotely sensed data of lasting quantitative value then data must be calibrated to physical units such as reflectance."

The value recorded for each pixel in a remotely sensed image is a function of the sensor-detected radiance. Owing to the atmospheric interaction, this *apparent* radiance is the combination of the contribution of the target object and the atmospheric effect. Their relationship can be approximated as

$$L_{app} = \rho TE/\pi + L_p. \tag{1.2}$$

Here, L_{app} denotes the apparent radiance received by the sensor, L_p is the path radiance, ρ is the target reflectance (%), T is the atmospheric transmittance (%), and E is the solar irradiance on the target. Radiance is expressed in units of $Wm^{-2}\ sr^{-1}\ \mu m^{-1}$, and irradiance is expressed in the units of $Wm^{-2}\ \mu m^{-1}$. As these two terms are not expressed in equivalent units, solar irradiance is converted into *equivalent solar radiance* by introducing the term π into the denominator. This conversion is based on the assumption that the target behaves as a Lambertian reflector (as described in Figure 1.4) (Mackay et al., 1994).

In Equation (1.2), only the first term ρ contains information about the target. The atmosphere contributes the second term, the path radiance *Lp*, which varies inversely in magnitude with wavelength. In the case of multispectral images, the magnitude of the L_p term in the visible bands will be higher than that in the near- or mid-IR bands.

1.3.1 Dark Object Subtraction

Two kinds of methods are used for atmospheric effect correction. The first kind consists of the dark object subtraction techniques (Chavez, 1988; Ouaidrari and Vermote, 2001), which involve subtraction of a constant value (offset) from all pixels in a given spectral band. These methods are based on the assumption that some pixels in the image should have a reflectance of zero, and that the values recorded for these zero pixels result from atmospheric scattering. Thus, these pixel values represent the effects of atmospheric scattering. For example, the reflectance of deep clear water in the near-IR waveband is near zero. Dark object subtraction methods assume that nonzero pixel values over deep, clear, water areas in the near-IR band are contributed by the path radiance L_p, and that the path radiance is spatially constant (meaning that a single value of path radiance is subtracted from all pixel values in the image). In case the of the visible bands, one may use shadow areas due to topography as dark objects. In effect, one is using the histogram offset as a measure of atmospheric path radiance, as shown in Figure 1.7.

The empirical line method is described and evaluated by Smith and Milton (1999). The method requires that ground measurements of surface reflectance of dark and bright areas in the image are taken simultaneous with the overflight, though if the areas are spectrally stable, the measurements need not be simultaneous (though they must be taken under similar atmospheric and illumination conditions). The image data are converted to radiance using the standard calibration, and surface

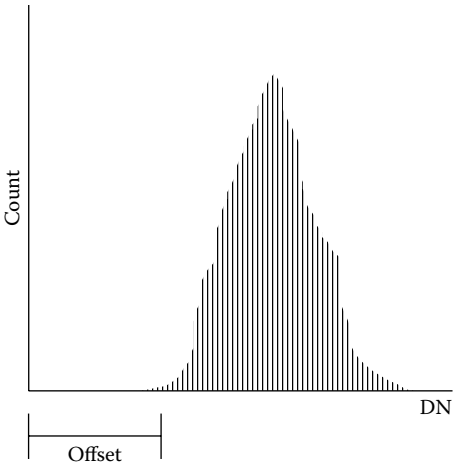

FIGURE 1.7 An estimate of path radiance is the image histogram offset from zero.

reflectance R is regressed against sensor radiance L to give a relationship of the form $R = (L - a) \times s$. The term a represents atmospheric radiance, which is subtracted from apparent radiance L before conversion to reflectance. Other descriptions of the empirical line methods are found in Moran et al. (2001) and Karpouzli and Malthus (2003).

1.3.2 Modeling Techniques

The methods described in Section 1.3.1 above involve the subtraction of the same pixel value from the whole image. They are easy to apply, but only provide an approximate correction. If the magnitude of the ground-leaving reflectance for each pixel is required, a more sophisticated method based on modeling techniques is necessary (e.g., Tanré et al., 1986, 1990; Vermote et al., 1997). These methods attempt to model atmospheric interactions, through which one can retrieve estimates of true target reflectance.

1.3.2.1 Modeling the Atmospheric Effect

The 5S model (*S*imulation of the *S*ensor *S*ignal in the *S*olar *S*pectrum) developed by Tanré et al. (1986, 1990) is the best-known atmospheric calibration model. An improved version is the 6S (*S*econd *S*imulation of the *S*ensor *S*ignal in the *S*olar *S*pectrum) model (Vermote et al., 1997), which is capable of simulating a non-Lambertian surface to model the signal measured by the sensor. The 6S model also includes data for calculating atmospheric absorption using an increased number of atmospheric gases. In what follows, the core of the model is described in order to provide an introduction to atmospheric modeling.

Assume unit solar irradiance incident on top of the atmosphere. A fraction of the incident solar irradiance is scattered from the path between the sun and the ground target into the atmospheric volume, with the remainder of the radiation being

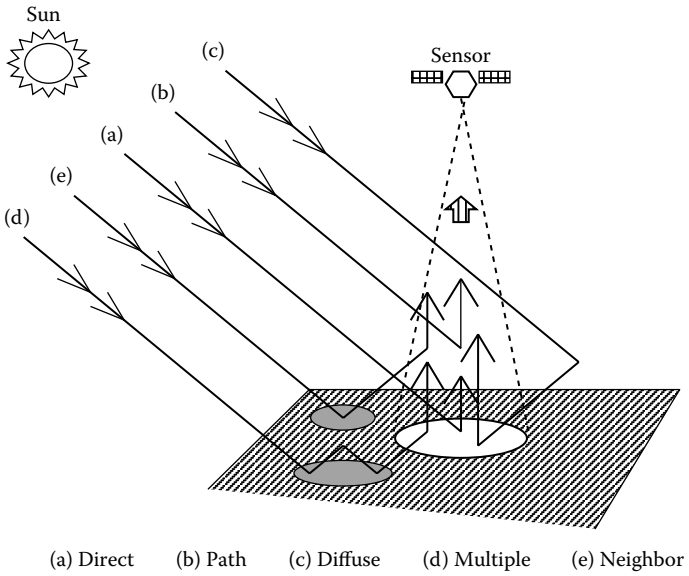

FIGURE 1.8 Five kinds of radiative interaction with the atmosphere.

incident on the ground target as direct solar radiation (Figure 1.8a). This transmitted fraction, denoted by $T(\theta_s)$, is defined as

$$T(\theta_s) = \exp\left(\frac{-\tau}{\cos(\theta_s)}\right). \tag{1.3}$$

The term τ is known as the optical depth, and θ_s is the solar zenith angle, which is illustrated in Figure 1.9.

A fraction of the solar radiation that is scattered into the atmosphere will also appear to contribute to the illumination of the ground target (Figure 1.8c, marked "diffuse") and will compensate for some of the attenuation of the direct beam. If we

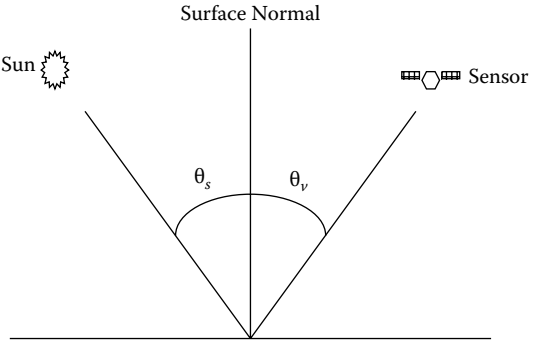

FIGURE 1.9 Solar and sensor view angles on a horizontal surface.

denote this diffuse skylight as $t_d(\theta_s)$, then the fraction of solar irradiance incident at the ground target becomes

$$T(\theta_s) = \exp\left(\frac{-\tau}{\cos(\theta_s)}\right) + t_d(\theta_s). \tag{1.4}$$

A second scattering flux that also should be taken into consideration is the trapping mechanism. The effect of this mechanism corresponds to the successive reflection and scattering of solar radiation between the ground target neighborhood and the atmosphere, so that the radiation then becomes incident upon the ground target, as shown in Figures 1.8d and 1.8e. The magnitude of this effect depends on the spherical albedo of the atmosphere, S, and the surface reflectance, ρ_s. The illumination at the ground target now becomes

$$\frac{1}{1-\rho_s S} \times T\left(\theta_s\right). \tag{1.5}$$

The proportion of the solar radiation reflected from the ground target is expressed as

$$\frac{\rho_s}{1-\rho_s S} \times T\left(\theta_s\right). \tag{1.6}$$

Consider a sensor that is receiving the reflectance from the ground target. The reflectance is generated by two main sources: one is the contribution of the total solar radiation reflected by the ground target and directly transmitted from the surface to the sensor, while the other is the contribution from the target neighborhood, which is scattered into the field of view of the sensor. The reflectance received by the sensor can thus expressed by

$$\frac{\rho_s}{1-\rho_s S} \times T\left(\theta_s\right) \times T\left(\theta_v\right). \tag{1.7}$$

In this equation, θ_v is the sensor view zenith angle, and Equation (1.4) can be again applied to express $T(\theta_v)$ as

$$T(\theta_v) = \exp\left(\frac{-\tau}{\cos(\theta_v)}\right) + t_d\left(\theta_v\right). \tag{1.8}$$

The sensor also receives a fraction of the solar radiation that has been scattered out of the downward solar beam into the sensor's field of view without interaction with the ground target, as shown in Figure 1.8b. This component is the atmospheric reflectance, denoted by the function $\rho_a(\theta_s,\theta_v, \phi)$, where ϕ is the relative azimuth

between the sun and the sensor. Therefore, the apparent reflectance ρ* at the sensor is

$$\rho^* = \frac{\rho_s}{1-\rho_s S} \times T\left(\theta_s\right) \times T\left(\theta_v\right) + \rho_a\left(\theta_s, \theta_v, \phi\right). \tag{1.9}$$

Equation (1.9) is a linear equation that specifies the relationship between the apparent reflectance ρ* and the surface reflectance ρ_s. The term $T(\theta_s) \times T(\theta_v)$ is the total atmospheric transmittance along the sun–target–sensor path.

A second atmospheric interaction should be considered, namely, the process of absorption. In the solar (optical) spectrum, atmospheric gaseous absorption is principally due to the presence of ozone (O_3), oxygen (O_2), water vapor (H_2O), and carbon dioxide (CO_2). Both O_2 and CO_2 are uniformly mixed in the atmosphere and are constant in terms of their concentrations, whereas H_2O and O_3 concentrations vary with time and geographical location. If $T_g(\theta_s, \theta_v)$ denotes atmospheric gas transmittance after absorption, then Equation (1.9) can be modified to give

$$\rho^* = T_g\left(\theta_s, \theta_v\right) \times \left[\frac{\rho_s}{1-\rho_s S} \times T\left(\theta_s\right) \times T\left(\theta_v\right) + \rho_a\left(\theta_s, \theta_v, \phi\right)\right]. \tag{1.10}$$

In order to retrieve the surface target reflectance, ρ_s, Equation (1.10) is further expanded as

$$\begin{aligned} &\frac{\rho^*}{T_g\left(\theta_s, \theta_v\right)} - \rho_a\left(\theta_s, \theta_v, \phi\right) = \frac{\rho_s}{1-\rho_s S} \times T\left(\theta_s\right) \times T\left(\theta_v\right) \\ &\Rightarrow \frac{\rho^*}{T_g\left(\theta_s, \theta_v\right) \times T\left(\theta_s\right) \times T\left(\theta_v\right)} - \frac{\rho_a\left(\theta_s, \theta_v, \phi\right)}{T\left(\theta_s\right) \times T\left(\theta_v\right)} = \frac{\rho_s}{1-\rho_s S} \\ &\Rightarrow \frac{\rho^*}{T_g\left(\theta_s, \theta_v\right) \times T\left(\theta_s\right) \times T\left(\theta_v\right)} - \frac{\rho_a\left(\theta_s, \theta_v, \phi\right)}{T\left(\theta_s\right) \times T\left(\theta_v\right)} = \frac{\rho_s}{1-\rho_s S}. \end{aligned} \tag{1.11}$$

If we define

$$A = \frac{1}{T_g\left(\theta_s, \theta_v\right) \times T\left(\theta_s\right) \times T\left(\theta_v\right)}, \text{ and } B = -\frac{\rho_a\left(\theta_s, \theta_v, \phi\right)}{T\left(\theta_s\right) \times T\left(\theta_v\right)}$$

then Equation (1.11) eventually gives

$$\rho_s = \frac{A \times \rho^* + B}{[1 + S \times (A \times \rho^* + B)]}. \tag{1.12}$$

Thus, knowing the apparent reflectance ρ*, the spherical albedo S, and the coefficients A and B, the surface target reflectance ρ_s can be obtained. Methods for obtaining these parameters are illustrated in Section 1.3.2.2.

1.3.2.2 Steps in Atmospheric Correction

The procedure to obtain estimates of the ground target reflectance involves three steps, as illustrated in Figure 1.10. The first step, converting the pixel value to radiance, is sensor-dependent. For instance, in the case of Landsat TM images, the relationship between the pixel values and apparent radiance L_{app} is expressed as

$$L_{app} = A_i \times DN + B_i \tag{1.13}$$

while in the case of SPOT HRV data the relationship is

$$L_{app} = DN/A_i \tag{1.14}$$

where A_i and B_i are the calibration *gain* and *offset* for band i, respectively. These calibration coefficients can be found either from the literature (e.g., Gellman et al., 1993; Thome et al., 1997; Teillet et al., 2001; Meygret, 2005) or from image header files. Note that header files may contain prelaunch calibrations that may differ significantly from the actual calibrations due to sensor degradation over time.

The second step, conversion from apparent radiance L_{app} to apparent reflectance ρ*, is based on the observation that in case of 100% reflectance, the radiance measured by the sensor is the result of multiplication of equivalent solar radiance (E/π), the cosine of solar zenith angle ($\cos(\theta_s)$), and the Earth-to-sun distance multiplicative factor d (Kowalik and Marsh, 1982). The factor d is measured in astronomical units (au) and is described further below. One au is equal to the average Earth-to-sun distance. About January 3, at perihelion, the Earth-to-sun distance is approximately 0.983 au, and on July 5, at aphelion, the Earth-to-sun distance is about 1.0167 au.

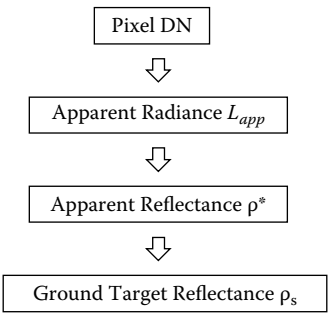

FIGURE 1.10 Procedure for retrieving ground radiance.

If the required coefficients are known, then the variation in sensor-detected apparent radiance L_{app} is caused by the difference in reflectance. One then obtains the following relation:

$$L_{app} = \frac{\rho^* \times \cos(\theta_s) \times E}{d\pi}$$

or, equivalently,

$$\rho^* = \frac{d \times L_{app}}{\cos(\theta_s) \times E/\pi}. \tag{1.15}$$

The value of the solar zenith angle can be retrieved from the image header file. The distance multiplicative factor d is used to compensate for the variation in solar irradiance E caused by the change in distance between the sun and the Earth. It is obtained from

$$d = au^2. \tag{1.16}$$

An alternative way to approximate Equation (1.16) is given by

$$d = \left(1 - 0.01673 \times \cos\left(0.9856 \times (JD - 4)\right)\right)^2 \tag{1.17}$$

where the term JD denotes the Julian day (e.g., in the case of 5th February, $JD = 36$).

The introduction of the factor d into Equation (1.15) is justified by the following observations. Since at perihelion, the magnitude of solar irradiance is greater than that at aphelion, if a sensor obtains the same radiance L_{app} at perihelion and aphelion, respectively, the apparent reflectance ρ^* at perihelion should be less than that at aphelion. Thus, if the sun-to-Earth distance is smaller than the average sun-to-Earth distance, one should use a lower (< 1) weighting factor d, and as the Earth is approaching aphelion, a higher value of d should be used.

The final step—that of converting apparent reflectance to ground target reflectance—uses Equation (1.12). We already know the apparent reflectance ρ^* from Equation (1.15), while other parameters such as the spherical albedo, S, and the coefficients A and B can be obtained by running either the 5S or the 6S model. An example is given in Table 1.1, which shows part of the output generated by the 5S model. The spherical albedo S and relevant parameters for deriving A and B are displayed in bold type. For a detailed description of 5S and 6S usage, readers are referred to Tanré et al. (1986, 1990) and Vermote et al. (1997). Once ground reflectance is retrieved, one may use Equation (1.15) to retrieve radiance followed by using either Equation (1.13) or Equation (1.14) to convert the radiance back to a corrected pixel value.

TABLE 1.1
Results from the 5S Model Used for Atmospheric Correction

	Downward	Upward	Total
Global gas transmission	0.961	0.965	**0.932** = $T_g(\theta s, \theta_v)$
Water transmission	0.988	0.989	0.980
Ozone transmission	0.975	0.978	0.954
CO_2 transmission	1.000	1.000	1.000
O_2 transmission	0.999	0.999	0.998
NO_2 transmission	1.000	1.000	1.000
CH_4 transmission	1.000	1.000	1.000
CO transmission	1.000	1.000	1.000
Rayleigh scattering transmission	0.967	0.971	0.939
Aerosol scattering transmission	0.953	0.962	0.917
Total scattering transmission	0.922	0.934	**0.861** = $T(\theta_s)\ T(\theta_v)$
	Rayleigh	**Aerosols**	**Total**
Spherical albedo	0.048	0.087	**0.123** = S
Optical depth total	0.054	0.362	0.416
Optical depth plane	0.054	0.362	0.416
Atmospheric reflectance	0.019	0.017	**0.037** = $\rho_a(\theta s, \theta v, \varphi)$
Phase function	0.993	0.099	0.215
Single scattering albedo	1.000	0.990	0.992

1.4 CORRECTION FOR TOPOGRAPHIC EFFECTS

Normally, the surface being measured by the remote sensor is assumed to be flat with a Lambertian reflectance behavior. Under this assumption, the magnitude of the radiance detected by the sensor is affected only by variations in the solar zenith angle, the wavelength, and the atmospheric interaction. The atmospheric correction model introduced in Section 1.3 is also based on such ideal assumptions, which may be invalid in the case of rugged terrain because the solar incidence angle will vary with topographic properties and will further contribute to differences in the level of radiance detected by the sensor. This is known as *topographic effect*. More specifically, the topographic effect can be defined as the variation in radiance exhibited by inclined surfaces compared to radiance from a horizontal surface as a function of orientation of the surface relative to the radiation source. Moreover, if we assume non-Lambertian reflectance for the surface being measured, the sensor position is another important variable that should be considered.

Calibration for topographic effects is intended to normalize the sensor-detected signal difference caused by the topographic variation. Various techniques (e.g., Smith et al., 1980; Colby, 1991; Dymond and Shepherd, 1999; Riano et al., 2003; Law and Nichol, 2004) have been published. Here, we present two approaches, using

band ratioing and the Minnaert model, due to their better performance (Smith et al., 1980; Colby, 1991; Law and Nichol, 2004).

Band ratioing (Colby, 1991, Mather, 2004) is the most commonly used method for reducing the topographic effect. Colby (1991) uses a Landsat TM band 5/4 ratio image to study the effectiveness of topographic effect calibration by comparing several sample sites having the same vegetation cover but with differences in topography. In other words, the same vegetation cover should have a similar spectral response, irrespective of location, thus the differences between sample sites are assumed to be caused by topographic effects. Results showed that the variance of spectral response between sample sites in ratio image was lower than that obtained from original TM band 4 and 5 images. Colby (1991) concludes that band ratioing does partially compensate for topographic effects.

Smith et al. (1980) present two empirical photometric functions for studying the effect of topography on the radiance field. The first such function is based on a Lambertian reflectance assumption, while the second function assumes that reflectance is non-Lambertian. Although this is a relatively old model, it generates quite robust calibration results (Colby, 1991; Law and Nichol, 2004).

Figure 1.11 shows the geometrical relationships among the sun, the sensor, and an arbitrary surface element. The Lambertian model assumes that the surface reflects the incident radiation uniformly in all directions. If we treat wavelength as a constant and ignore atmospheric interactions, the variation in radiance detected by the sensor is mainly caused by the local incidence angle θ_i (i.e., the angle formed between the

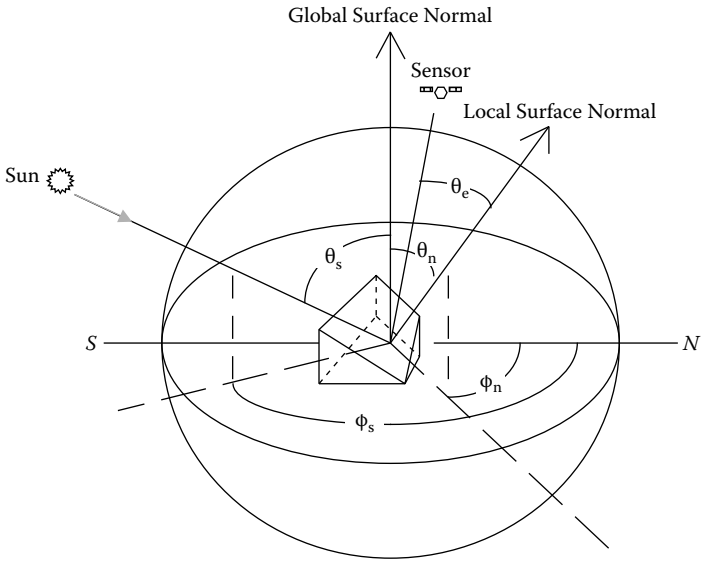

FIGURE 1.11 Geometrical relationships among the sun, the sensor, and the target position. Modified from Smith, J. A., T. L. Lin, and K. Ranson. "The Lambertian Assumption and Landsat Data," Figure 1. *Photogrammetric Engineering and Remote Sensing* 46 (1980): 1183–1189. (Reprinted with permission from the American Society for Photogrammetry and Remote Sensing).

solar radiation path and local surface normal). In this case, sensor-detected radiance L can be normalized in terms of

$$L_n = L/\cos(\theta_i). \tag{1.18}$$

where L_n denotes the normalized radiance. The $\cos(\theta_i)$ term can be derived from the spherical law as follows:

$$\cos(\theta_i) = \cos(\theta_s)\cos(\theta_n) + \sin(\theta_s)\sin(\theta_n)\cos(\phi_s - \phi_n) \tag{1.19}$$

where θ_s is solar zenith angle, θ_n is the angle of slope of terrain surface, ϕ_s is the solar azimuth angle, and ϕ_n is the surface aspect of the slope angle (see Figure 1.11). Slope is defined as a plane tangent to the surface containing two components: one is gradient, which specifies the rate of change in elevation, and the other is aspect, which measures the direction of the gradient. The values of several parameters are required to solve these equations, namely, solar zenith angle θ_s, solar azimuth angle ϕ_s, the surface slope θ_n, and aspect ϕ_n. Both θ_s and ϕ_s can be obtained from the image header file, while slope and aspect can be derived by co-registering the image with a digital elevation model (DEM). A variety of approaches can be employed to calculate the slope and aspect from a DEM (Skidmore, 1989; Jones, 1998).

In the case of the non-Lambertian reflectance assumption, Smith et al. (1980) suggest the following function to correct for the topographic effect:

$$L \times \cos(\theta_e) = L_n \times [\cos(\theta_i)\cos(\theta_e)]^k \tag{1.20}$$

where θ_e is effective view angle (Figure 1.11), $\cos(\theta_i)$ is defined in Equation (1.19), and k is known as the Minnaert constant (Minnaert, 1941) describing the bidirectional reflection distribution function of the surface, the type of scattering dependence, and surface roughness, respectively. A Lambertian surface is defined by a k value of 1.0, and Equation (1.20) then reduces to Equation (1.18).

In order to solve Equation (1.20), one needs to relate the effective view angle θ_e and k (the method for deriving $\cos(\theta_i)$ is described in Equation [1.19]). If Landsat TM or MSS imagery is used, θ_e can be regarded as the same as θ_n (i.e., the slope of terrain surface) since Landsat has a narrow view angle. In the case of SPOT HRV data, which can acquire imagery through an angle of ±27°, θ_e should be set to $\theta_e = \theta_n$, the satellite view angle. To estimate the Minnaert constant k, Equation (1.20) is converted into logarithmic form as

$$\log(L \times \cos(\theta_e)) = k \times \log(\cos(\theta_i)\cos(\theta_e)) + \log(L_n). \tag{1.21}$$

The term k is then equal to the slope of regression line of the plot made by the samples $log(cos(\theta_i)cos(\theta_e))$ plotted on the x-axis and $log(Lcos(\theta_e))$ plotted on the y-axis.

To calibrate for the topographic effect using a non-Lambertian assumption is more complicated than that based on a Lambertian reflectance assumption. As far as the computational cost and calibration accuracy is concerned, Smith et al. (1980)

suggest that when surface slopes are less than 25° and effective illumination angles are less than 45°, then the Lambertian assumption is more valid. Under such circumstances, one can use Equation (1.18) to carry out topographic effect correction, and the calibration accuracy should be preserved. If either of the above conditions is not satisfied, the use of Equation (1.20) is recommended.

It should also be appreciated that surface topographic variations will also cause distortions in the geometry of images. The map to which the image is referenced represents the relationship between features reduced to some datum such as sea level, while the image shows the actual terrain surface. If the terrain surface is significantly above sea level then the image pixel position will be displaced by an amount proportional to the pixel's elevation above sea level (or whatever datum is used).

1.5 REMOTE SENSING IN THE MICROWAVE REGION

The word *radar* is an acronym derived from the phrase "Radio Detection And Ranging." Imaging microwave sensors are known as *imaging radars*. These instruments transmit a signal in the wavelength range approximately 3 cm to 1 m, and receive reflection (backscatter) from the target. The level of backscatter for each pixel over the imaged area is recorded and the set of pixels forms the radar image. Remote sensing in the microwave region differs from optical remote sensing in a number of ways, the most important of which are

1. Radar backscatter is related to the roughness and electrical conductivity of the target. This information is complementary to that which is acquired by optical and thermal sensors.
2. Energy in the microwave region can penetrate clouds.
3. Microwave imaging radars are active, not passive instruments, and thus can operate independently of solar illumination.

An increasing number of space-borne radar systems is now in orbit, including the recently launched German TerraSAR-1 and the Italian COSMO-SkyMed, and it is probable that radar imagery will play an increasingly important role in supporting our understanding and monitoring of our environment. The main disadvantage of active microwave systems vis-à-vis optical systems is their power requirements, for the sensor transmits as well as receives energy. Optical sensors passively detect reflected solar radiation. Passive microwave sensors, which are not considered in this chapter, detect microwave radiation that is generated by the target.

This section introduces radar remote sensing. In Section 1.6, basic ideas underlying the use of radar images, including geometrical effects and the main factors affecting surface reflection or backscatter at radar wavelengths, are introduced. Section 1.7 considers the extraction of surface information from this backscattered signal. One of the main problems associated with the interpretation of radar imagery is the presence of noise, or *radar speckle*. The use of filters to reduce the noise effect is described in Section 1.8.

1.6 RADAR FUNDAMENTALS

An active radar system repetitively transmits short microwave energy pulses (normally of the order of microseconds, i.e., 10^{-6} second, denoted by μs) toward the area to be imaged. The energy pulse is likely to scatter in all directions when it reaches the surface. Part of the backscattered energy is reflected back to the radar antenna and recorded for later processing. Normally, each energy pulse has a duration of between 10 and 50 μs, and utilizes a small range of microwave wavelengths. A waveform can be characterized in terms of its wavelength and amplitude. Wavelength is defined as the distance between two adjacent crests or troughs of the waves (Figure 1.12). Amplitude measures the strength of an electromagnetic wave in terms of the maximum distance achieved by the waveform relative to the mean position (shown by the horizontal line in Figure 1.12). The amplitude may be a function of a complex signal including both magnitude and the phase; this point is discussed further below.

Frequency, rather than wavelength, can also be used to describe wavebands. *Frequency* is the number of oscillations per unit time or number of wavelengths that pass a point per unit time. One can obtain the frequency f (normally of the order of Gigahertz, GHz) corresponding to wavelength λ in terms of

$$f = \frac{c}{\lambda} \tag{1.22}$$

where c is the velocity of light ($3 \times 10^8\ ms^{-1}$).

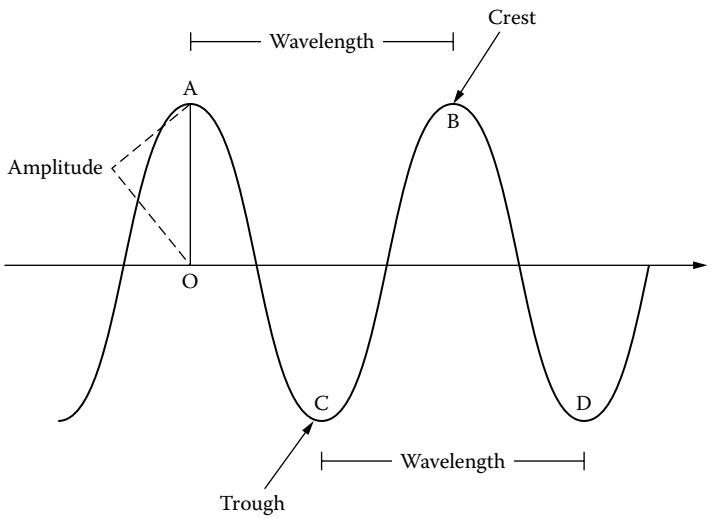

FIGURE 1.12 Wavelength is the distance between two adjacent crests (e.g., A and B) or troughs (e.g., C and D). The amplitude of a waveform (distance AO) measures the "power" or information carried by the wave.

The description of radar operation in the following pages is based on the most widely used radar system installed on aircraft platforms, the side-looking airborne radar (SLAR). Space-borne imaging radars operate on a similar basis, but use a synthetic rather than a real antenna. They are known as synthetic aperture radars (SAR).

1.6.1 SLAR Image Resolution

SLAR transmits and receives microwave energy using an antenna located to the side of the platform. The area imaged by the sensor is thus a strip of ground parallel to the flight track (known as the *azimuth direction*). SLAR image resolution is mainly dependent on pulse duration and antenna beam width, which is the ground area "illuminated" by the radar pulse at a given instant in time (Figure 1.13). Pulse duration affects the resolution in the range (cross-track) direction, while antenna beam width controls the azimuth (along-track) resolution. The ground range resolution and azimuth resolution are computed by

$$\text{Range Resolution} = \frac{c\tau}{2\cos\theta} \tag{1.23}$$

$$\text{Azimuth Resolution} = \beta \times d \tag{1.24}$$

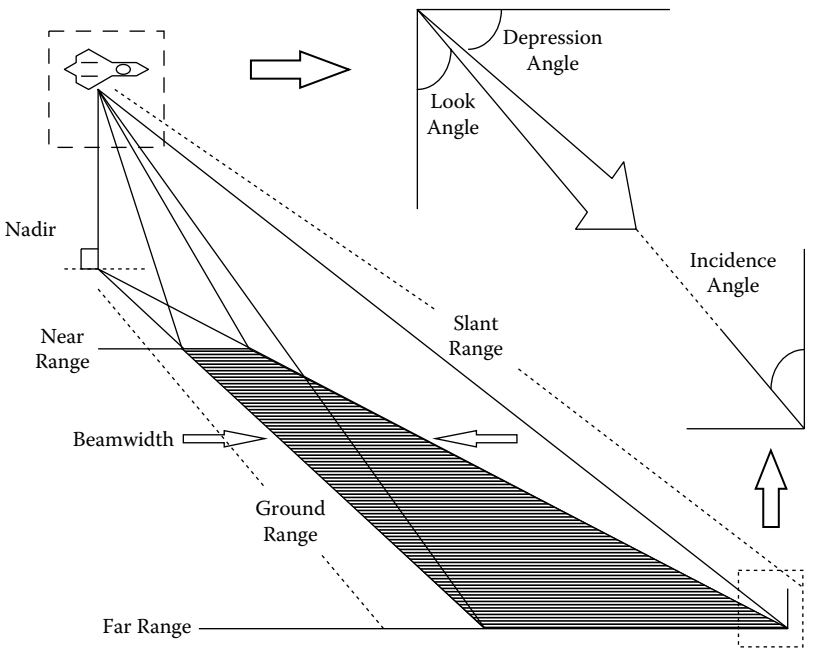

FIGURE 1.13 Some basic parameters of a SLAR system.

The term c is defined in Equation (1.22), while τ is the pulse duration, θ is the depression angle defined as the angle between the horizontal plane and the direction of emitted microwave energy (Figure 1.13), d is the ground range, and β is the antenna beam width. Range resolution can also be analyzed in terms of incidence angle or look angle (Figure 1.13). *Incidence angle* is defined as the angle between the radar beam and a line perpendicular to the illuminated surface. The *look angle* is complementary to the *depression angle*. If the illuminated surface is assumed to be flat, then one can also regard the incidence angle as the complement of the depression angle. The antenna beam width β, antenna length L, and wavelength λ are related as follows:

$$\beta = \frac{\lambda}{L}. \tag{1.25}$$

The combination of azimuth and range resolution determines the ground resolution of each pixel on a radar image.

It can be inferred from Equation (1.23) that the shorter the pulse duration τ, or the smaller the value of θ, the finer the range resolution. The depression angle θ varies across an image. The value of θ in the near range is relatively larger than that in the far range (Figure 1.13). Thus, the ground range resolution will also vary with respect to θ.

Equation (1.24) shows that the smaller the values of β and d, the finer the azimuth resolution will be. Thus, near ground range has a higher resolution than that in far ground range because both are smaller in near range than that in far range (Figure 1.13). According to Equation (1.25), one can use a long antenna length and short wavelength to obtain finer azimuth resolution. However, shorter wavelengths are more likely to be affected by the atmosphere and, furthermore, antenna length is constrained by physical limitations. For instance, to obtain an antenna beam width of 1×10^3 m at a wavelength of 20 cm, the required antenna length will be 200 m (Equation [1.25]). Clearly, if finer azimuth resolution is sought in terms of increasing antenna length, then serious practical difficulties will be encountered. An alternative strategy is to use a synthetic aperture radar (SAR), where the term *aperture* means the opening used to collect the reflected energy that is used to generate an image. In the case of radar, this opening is the antenna, while in the case of a camera, the opening is the shutter opening.

SAR increases the antenna length not in physical terms but by synthesizing a long antenna using the forward motion of a short antenna, a process that requires more complicated and expensive technology. SAR uses the Doppler principle in order to synthesize a longer antenna. The *Doppler effect* is the change in wave frequency as a function of the relative velocities of transmitter and reflector. A radar sensor can image a given target repeatedly from successive locations, as illustrated in Figure 1.14. Here, the frequency of the waveform reflected by the target will increase from location a to b because the distance between the sensor and the object is reducing. As the platform moves away from the target, from b to c, the frequency of the returned signal decreases. SAR uses the Doppler information to compute frequency shifts and thus determine the location and scattering properties of the target.

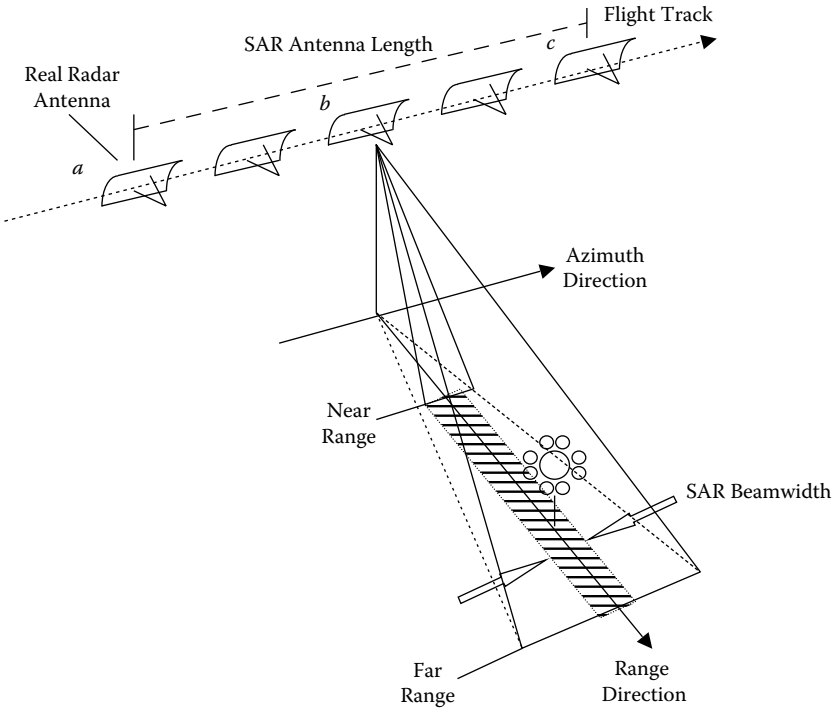

FIGURE 1.14 Concept of the synthetic aperture.

1.6.2 Geometric Effects on Radar Images

A radar image is generated from the timing data for transmitted energy to be returned to the radar antenna. This timing delay is dependent on the distance between the radar antenna and the target. This distance is the *slant range* (Figure 1.13), which is the path along which the microwave energy travels. Therefore, every target located on the terrain being observed by the radar will be mapped onto the slant range domain. Because of this slant range mapping, radar imagery is likely to be affected by geometric distortions. The most common distortions are those of layover, foreshortening, and shadow.

The *layover* effect results when the top of an illuminated target is seen by the radar as the bottom, and the bottom of the target is recorded by radar as the top. This phenomenon occurs when the time for the microwave energy to travel from the antenna to the top of an object is less than the time needed to travel to the bottom of the same object. Figure 1.15 shows two targets (a building and a mountain) that are illuminated by a radar sensor. The microwave energy transmitted by the radar will reach the tops of both objects (points *a* and *b* in Figure 1.15) before the bottoms (points *c* and *d*). The antenna will first receive the reflected energy from *a* and *b*, then some time later, the energy reflected from *c* and *d*. After projection onto the slant range domain, the result is called the *layover effect.*

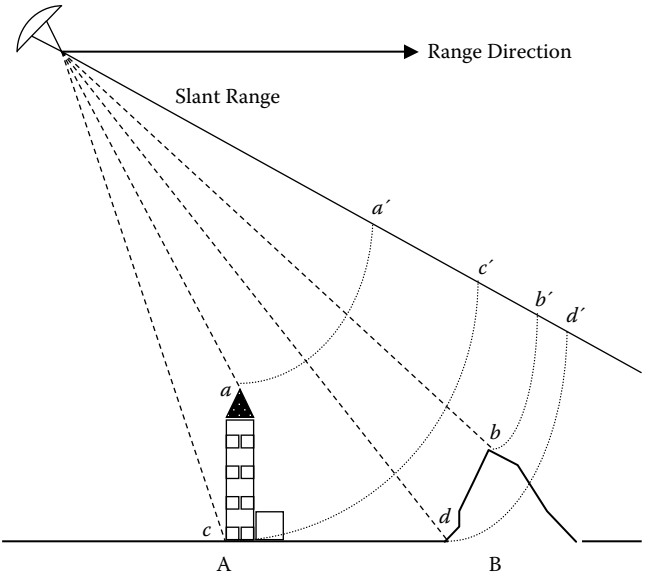

FIGURE 1.15 The layover effect in radar remote sensing.

It might be inferred from the preceding discussion that the higher the isolated target the greater the layover effect. However, layover is also controlled by another important factor: the angle, θ_f, between the front of the target and the energy path (Figure 1.16). Layover will occur only if θ_f exceeds 90° (see object *A* in Figure 1.16). If θ_f is smaller than 90°, as in the case of object *B* in Figure 1.16, then microwave

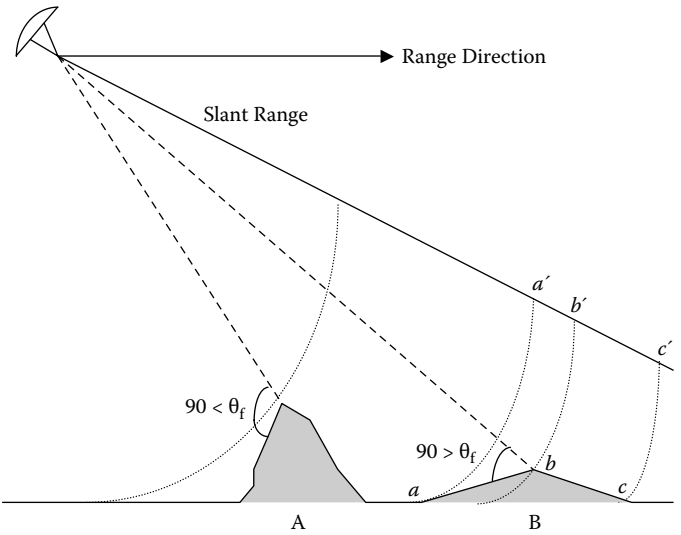

FIGURE 1.16 The angle θ_f controls layover effects (see text for discussion).

energy will first illuminate the bottom then the top of the object, and there will be no layover effect.

Foreshortening, like layover, results from the fact that radar is a side-looking sensor. The object labeled *B* in Figure 1.16 is symmetrical in cross-section, but the angle between its front slope *ab* and the microwave radiation emitted by the instrument is less than 90°. Hence, the front slope distance *ab* appears to be less than the back slope distance *bc* when projected onto slant range. Since the front slope also tends to reflect microwave energy more strongly than does the back slope, it will appear to be brighter, steeper, and shorter, while the back slope is shallower and darker. The darker back slope demonstrates another radar image geometry effect, that of shadow, as illustrated in the following text.

Radar shadow is due to the returned back energy from targets being affected by the nature of the terrain. A radar image is effectively a representation of returned energy levels plotted against the time taken for the energy to travel to and from the target. It follows that if, during a certain period, the antenna receives no reflection, then the image area corresponding to this time period will contain zero (dark) values.

The effect of radar shadow is controlled by the target height and angle θ_b (Figure 1.17), which is defined as the angle between the back slope of the target and the horizontal line parallel to the range direction. In Figure 1.17 the angle θ_b of object *A* is smaller than the corresponding depression angle θ_1. Thus, the back slope of object *A* is illuminated by the microwave energy. However, since the angle θ_b of object *B* is larger than the corresponding depression angle θ_2, the radar antenna will not receive any reflection from the back slope of object *B*, and this period of zero reflection is likely to continue until point *a* is reached. The resulting radar shadow after projection onto slant range is also illustrated in Figure 1.17.

The description of radar image distortions given above is a simplification. In real-world applications where terrains are often continuously sloping and rapidly varying,

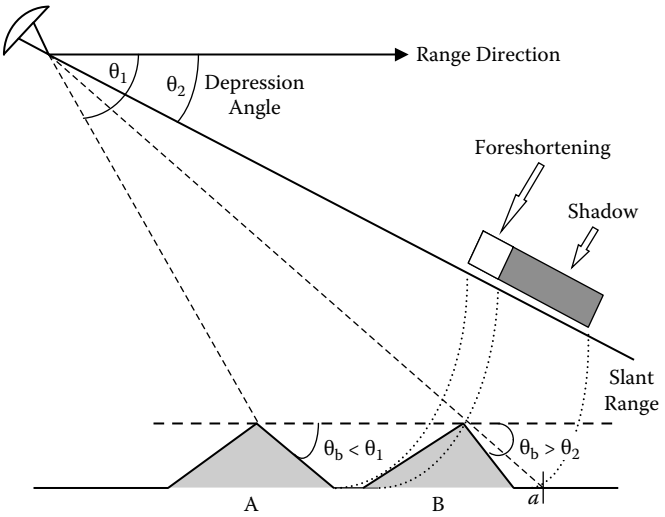

FIGURE 1.17 Showing the relationship between angle θ_j and radar shadow.

the resulting image will be a combination of different geometric effects. Hence, in order to compensate for these effects, one has to make careful case-by-case analyses (Kropatsch and Strobl, 1990; Goyal et al., 1999). That is, if one knows what effects are occurring at a given pixel, then one can use suitable algorithms to carry out calibration. As in the case of topographic calibration of optical imagery described above, geometric and radiometric correction of radar images requires a co-registration to a DEM. However, the calibration procedures are generally more complicated. Kwok et al. (1987), Riegler and Mauser (1998), and Hein (2003) provide descriptions.

1.6.3 Factors Affecting Radar Backscatter

It has already been noted that a radar image is a record of the strength of the backscatter from the targets making up the imaged area. The stronger the backscatter, the brighter the corresponding image element. The level of backscatter is determined by terrain conditions (such as roughness and electrical characteristics), and also by the parameters of the radar system. Understanding the factors affecting radar backscatter can help analyze landscape properties more knowledgeably.

1.6.3.1 Surface Roughness

Radar backscatter is stronger where the ground surface is rough relative to the radar wavelength. The roughness of a surface is dependent on both the wavelength of the incident energy and the angle of incidence. Rough surfaces act as Lambertian reflectors (Section 1.4) so that incident microwave energy is scattered in all directions and a portion is reflected back to the radar antenna. Smooth surfaces are specular, in that they act like a mirror and reflect the incident energy away from the sensor, resulting in extremely weak backscatter (Figure 1.18, point *a*). Normally, as the wavelength decreases, the surface appears rougher because smaller facets of the surface

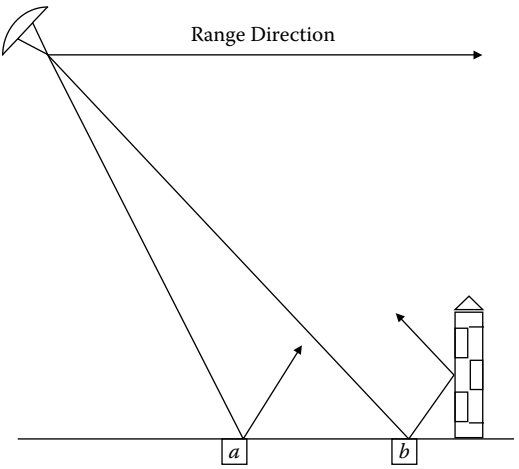

FIGURE 1.18 Microwave energy impinging on a smooth surface (point *a*) at which energy is reflected away from the sensor, and exhibiting a double bounce at point *b* when the reflected energy is reflected by a vertical wall.

contribute to the scattering process and thus stronger backscatter results. Likewise, as the wavelength increases, the surface tends to appear smoother. The strength of backscatter is also affected by the incidence angle. For a given wavelength, as the incidence angle increases, backscatter becomes weaker, and so the illuminated surface appears smoother. Some ground objects can behave like corner reflectors, which can reflect high energy back to the antenna and cause bright spots on the radar image. Such phenomena often occur in urban areas because energy can be returned by means of a *double bounce* from the corners of buildings (Figure 1.18, point *b*).

1.6.3.2 Surface Conductivity

Highly conductive ground surfaces tend to have higher reflectivity than surfaces with lower conductivities. Water and metal are good conductors. As a result, radar backscatter will be sensitive to metal objects and to the presence of moisture in the illuminated target area, even though the amount of moisture may be small. In a radar image, metal objects such as railway tracks and metal bridges generally result in bright spots. Moisture also affects the depth of microwave energy penetration of the soil surface. If soil contains a large amount of moisture, the signal does not penetrate the soil surface and is reflected back to the radar antenna. If the soil is dry, then the radar signal can penetrate more deeply into the soil surface layer. Wavelength is also another control on the depth of penetration. Lakes and other water bodies might be expected to exhibit high backscatter, but in fact the surfaces of rivers and lakes are generally smooth relative to radar wavelengths and act as specular reflectors. The ocean surface is generally rougher, and therefore the magnitude of backscatter depends on sea state as well as on wavelength and depression angle.

1.6.3.3 Parameters of the Radar Equation

The parameters of the radar equation (Van Zyl et al., 1993) are fundamental factors that influence the level of the returned signal. The radar equation is expressed as

$$P_r = \frac{P_t \lambda G_t(\gamma) G_r(\gamma)}{(4\pi)^3 R^4} \sigma^0 A. \tag{1.26}$$

P_t is the transmitted power from the antenna, λ is the transmitted wavelength, R is the distance to imaging area, γ is the radar look angle, A is the area on the ground responsible for scattering, G_t and G_r are the transmitted and received antenna gains (describing the system's ability to focus the transmitted microwave energy) at look angle γ, and σ^0 is the radar backscatter coefficient measured in decibels (dB). All of the parameters in Equation (1.26) affect the received power P_r. However, only σ^0 is related to the properties of the illuminated surface. Thus, the quantized pixel values (0 to 255) in a radar image are sometimes converted to σ^0 before being interpreted. The received power P_r in Equation (1.26) can also be characterized in terms of other parameters such as the scattering matrix (Equation [1.31]) and the coefficient of variation (Equation [1.35]), which also relate to the properties of surface objects, and can be used for classification purposes. A discussion of the scattering matrix is presented in the next section.

1.7 IMAGING RADAR POLARIMETRY

The polarimetry theory presented in this section is mainly derived from Evans et al. (1988), Zebker and Van Zyl (1991), Zebker et al. (1987, 1991), Van Zyl et al. (1987, 1993), Kim and Van Zyl (2000) and Hellmann (2002). Knowledge of radar polarimetry enables us to use a variety of features (such as complex format data, the elements of the scattering matrix, and the coefficient of variation of polarization signature) to perform image interpretation. Some basic concepts are described first.

An electromagnetic wave, besides being described in terms of wavelength and amplitude, can also be characterized using *complex number* format (a complex number consists of a two components, termed the *real* and *imaginary* parts). When the coordinate system is translated into both the real and imaginary axes (Figure 1.19), the wave is described by two parameters, namely, the *in-phase I* ($I = m \times \cos\varphi$) and *quadrature Q* ($Q = m \times \sin\varphi$) components. Both the I and Q parameters provide the wave's overall phase φ ($\varphi = \tan^{-1}(Q/I)$) and magnitude m ($m = (I^2 + Q^2)^{0.5}$) as illustrated in Figure 1.19. Radar phase represents the degree of coincidence in time between a repetitive radar signal and a reference signal having the same frequency. Over the complex domain, the amplitude a is expressed as $a = I + iQ$, where $I = (-1)^{0.5}$. The relationship between the magnitude m and a complex amplitude a, by definition, can be expressed as $m = |a|$, i.e., the absolute value of amplitude. The radar image can thus be formed by using any of the m, I, or Q components. As a result, this kind of radar image is said to be represented in *complex* format.

Complex format radar imagery can be used to generate interferometric information (Massonnet and Rabaute, 1993; Zebker et al., 1994; Gens and Van Genderen, 1996; Kim and Van Zyl, 2000), which is useful in producing digital elevation models (DEM) (Zebker et al., 1994; Lanari et al., 1996; Kim and Van Zyl, 2000), or in monitoring large-scale surface changes (Massonnet et al., 1993; Preiss et al., 2003). The potential of SAR interferometry (in the form of coherence maps) in land cover classification is the subject of current investigations (e.g., Ichoku et al., 1998).

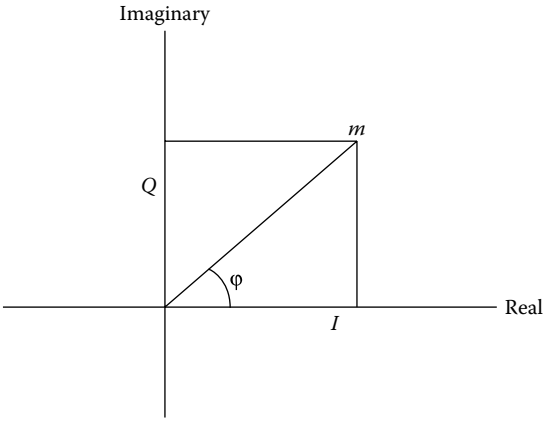

FIGURE 1.19 Wave described by complex (real and imaginary) coordinates.

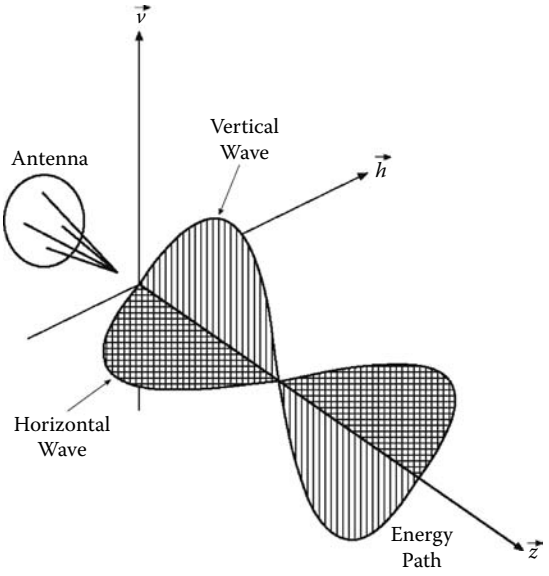

FIGURE 1.20 Polarized microwaves.

1.7.1 Radar Polarization State

Normally, microwave energy transmitted and received by a radar antenna can travel in all directions perpendicular to the direction of wave propagation. However, most radar systems polarize microwaves in such a way that the transmitted and received waves are restricted to a single plane perpendicular to the direction of wave propagation (Figure 1.20). The polarized wave is therefore transmitted and received in either the horizontal (H) or the vertical (V) plane. Consequently, there are four combinations of transmission and reception for the polarized waves. These combinations are HV, HH, VV, and VH, where HV denotes a wave transmitted in V direction and received in H direction. The other combinations can be inferred in a similar manner. Radar imagery generated in terms of HH or VV is called co- or like-polarized imagery, while imagery resulting from HV or VH polarization is called cross-polarized imagery. Cross-polarization detects multiple scattering from the target and thus generally results in weaker backscatter than that measured by a co-polarization configuration.

The coordinate system shown in Figure 1.20 determines the radar polarimetry, in which horizontally and vertically polarized waves lie in the unit vector $\vec{h}$ and $\vec{v}$ directions, respectively, while unit vector $\vec{z}$ denotes the direction of wave propagation. The relationship among unit vectors $\vec{h}$, $\vec{v}$, and $\vec{z}$ can be represented by

$$\vec{z} = \vec{h} \times \vec{v}\,. \tag{1.27}$$

The overall electric field can be represented by

$$\vec{E}(z,t) = \Re\left[(E_h\ \vec{h} + E_v\ \vec{v})e^{-i(\omega t - kz)}\right] \tag{1.28}$$

where E_h and E_v denote the electric field of vertical and horizontal plane, respectively, which are expressed by

$$\begin{aligned} E_h &= a_h e^{-i\delta_h} \\ E_v &= a_v e^{-i\delta_v}. \end{aligned} \tag{1.29}$$

The terms a_h and a_v denote the positive amplitudes in the $\vec{h}$ and $\vec{v}$ directions (Figure 1.21), respectively, and the corresponding phases are δ_h and δ_v relative to the phase factor $\omega t - kz$, where ω is frequency, t is time, k is wave number, and z is distance traveled in the $\vec{z}$ direction (i.e., the direction of wave propagation).

In the most general case, the electric field vector of a plane monochromatic wave rotates in a plane perpendicular to the direction of microwave energy propagation, and in doing so traces out an ellipse, as shown in Figure 1.21. The wave is said to be *elliptically polarized*. If one refers to the relative amplitude and phase relationships of the components of a given wave as the elliptic polarization state, Equation (1.28) can be rewritten as

$$\vec{E}(z,t) = a\vec{p}\cos\chi\sin(\omega t - kz + \delta) + a\vec{q}\sin\chi\cos(\omega t - kz + \delta) \tag{1.30}$$

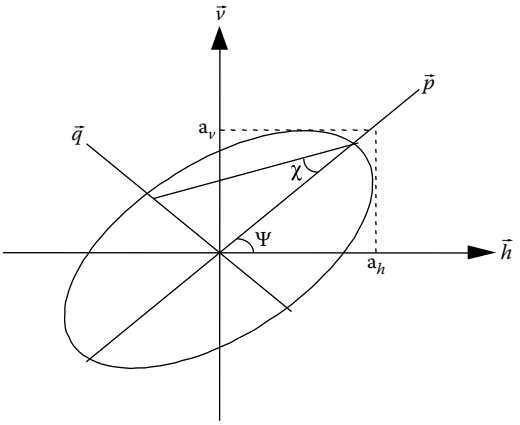

FIGURE 1.21 Elliptical polarization state for polarization synthesis. See text for explanation. Modified from Evans, D. L., T. G. Farr, J. J. Van Zyl, and H. A. Zebker. "Radar Polarimetry: Analysis Tools and Application." *IEEE Transactions on Geoscience and Remote Sensing* 26 (1988):774–789 © 1988 IEEE.

where $a^2 = a_h^2 + a_v^2$ is the intensity of the wave, $\delta = \delta_h - \delta_v$ is the phase angle, both $\vec{p}$ and $\vec{q}$ are unit vectors in a coordinate system rotated by angle ψ with respect to $\vec{h}$, and χ is the ellipticity angle. Note that the width of the ellipse is given by the parameter χ; so that $\chi = \pm 45°$ results in left- and right-handed circular polarizations, respectively. The orientation parameter ψ determines the orientation of the major axis of the ellipse; if $\chi = 0°$, then the values $\psi = 0°$ or $180°$ represent horizontal polarizations, while $\psi = 90°$ represents vertical polarization.

A polarimetric imaging radar measures the magnitude of the backscatter from a target as a vector quantity in such a way that the complex backscattered characteristics of any transmitting and receiving polarization configuration can be determined. Such backscattered characteristics are represented in terms of a scattering matrix [**S**] (Van de Hulst, 1981):

$$[\mathbf{S}] = \begin{pmatrix} \mathbf{S_{hh}} & \mathbf{S_{hv}} \\ \mathbf{S_{vh}} & \mathbf{S_{vv}} \end{pmatrix} \tag{1.31}$$

where element $\boldsymbol{S_{hv}}$ is determined by measuring both the amplitude and phase of the electric field where a vertically polarized wave is transmitted and the scattered wave is received in horizontal polarization. The remaining elements are obtained in a similar fashion. The relationship among the electric field E_s of the scattered wave, the electric field E_t of the transmitting wave, and [**S**] is expressed as

$$E_s = \frac{e^{ikr}}{kr}[\mathbf{S}]E_t \quad \Rightarrow \quad \begin{pmatrix} E_h \\ E_v \end{pmatrix}_s = \frac{e^{ikr}}{kr} \begin{pmatrix} \mathbf{S_{hh}} & \mathbf{S_{hv}} \\ \mathbf{S_{vh}} & \mathbf{S_{vv}} \end{pmatrix} \begin{pmatrix} E_h \\ E_v \end{pmatrix}_t \tag{1.32}$$

where r is the distance between the scatterer and the receiving antenna and k denotes the wave number of the illuminating wave. The scattering matrix thus describes how the ground scatterer transforms the illuminating electric field.

1.7.2 Polarization Synthesis

Knowledge of the scattering matrix [**S**] permits calculation of the received power P_r for any possible combination of transmit and receive antenna polarizations. This process is called *polarization synthesis*. The observed power P_r can be derived by evaluating the matrix equation:

$$P_r = K(\lambda, \theta, \phi)\left|E_s[S]E_t\right|^2 \tag{1.33}$$

where

$$K(\lambda, \theta, \phi) = \frac{1}{2}\frac{\lambda^2}{4\pi}\sqrt{\frac{\varepsilon_0}{\mu_0}}\frac{g(\theta, \phi)}{\left|E_s\right|^2} \tag{1.34}$$

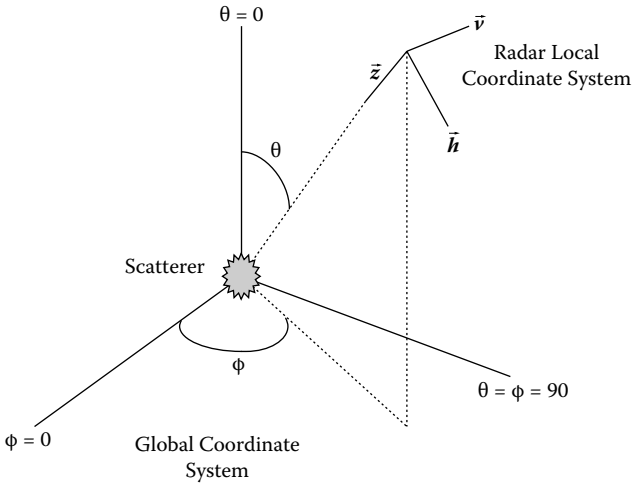

FIGURE 1.22 The local and global coordinate systems determine the angles θ and ϕ.

and $g(\theta, \phi)$ is the antenna gain function, θ and ϕ are the angles between the radar local coordinate system and the scatterer-centered global coordinate system shown in Figure 1.22, $[(\lambda^2/4\pi) \times g(\theta, \phi)]$ is the effective area of the antenna, and ε_0 and μ_0 are the permittivity and permeability of free space (i.e., transmission medium), respectively. Note that both permittivity ε_0 and permeability μ_0 determine the propagation velocity v (or phase velocity) of the wave; the relationship can be expressed as $v = 1/(\varepsilon_0 \times \mu_0)^{0.5}$.

Polarization synthesis can also be expressed in terms of either the Stokes matrix or the covariance matrix. Both of these representations consist of linear combinations of the cross-products of the four basic elements of the scattering matrix. The entries of these matrices can also provide a variety of features for classification purposes.

1.7.3 Polarization Signatures

A particular graphical representation of the variation of received power (or cross-section σ) as a function of polarization is called the *polarization signature* of an object. A polarization signature is a three-dimensional representation consisting of a plot of synthesized scattering power as a function of the ellipticity and orientation angles (i.e., χ and ψ in Figure 1.21) of the transmitted and received wave. Normally, analyses are based on only two types of polarization signatures, namely, co-polarization and cross-polarization.

Figure 1.23 illustrates the polarization signature based on a theoretical model of a large conducting sphere. Note that at the ellipticity angle $\chi = 0°$, the co-polarization signature reaches its highest value of cross-section, while the cross-polarization signature shows the lowest value at the same point. There is a measurement of surface roughness in accordance with polarization signature called the *coefficient of variation* (*CoV*), which is defined as

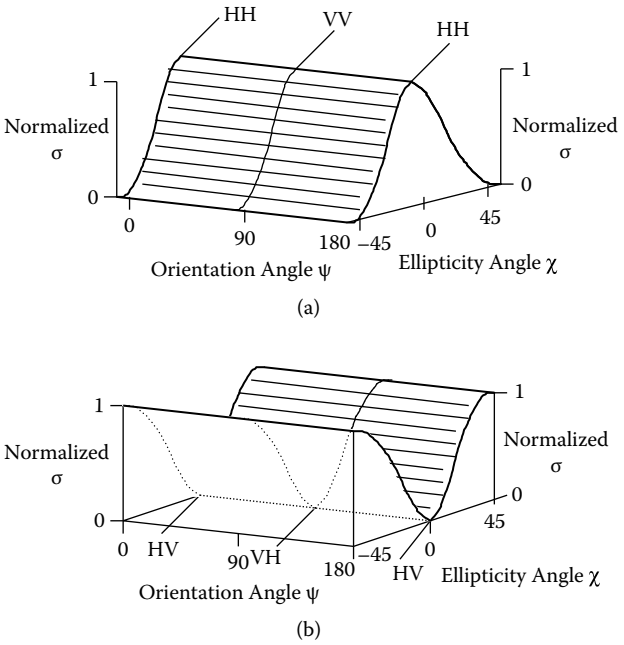

FIGURE 1.23 Polarization signature based on a theoretical model of a large conducting sphere. (a) At ellipticity angle 0 degrees the co-polarization signature reaches its highest cross-section value. (b) The cross-polarization value reaches its minimum point at the same ellipticity angle.

$$CoV = \frac{P_{r\min}}{P_{r\max}}. \tag{1.35}$$

$P_{r\min}$ and $P_{r\max}$ each denote minimal power and maximal power occurring within a polarization signature, respectively. Since *CoV* relates to the surface roughness, it can be used as a discriminating feature in classification. As the value of *CoV* increases, the measured surface tends to be rougher. The concept of *CoV* is based on the following observations. The polarization signature for each resolution element represents the sum of the polarization signatures of many individual measurements. If the surface being measured is smooth, the scattering mechanisms from a group of scatterers should be identical. Therefore, the maxima (minima) of a scattering mechanism should coincide with the maxima (minima) of the other scattering mechanisms. When the composite polarization signature is derived, it will produce a composite signature in which there is a large difference in magnitude between maximal and minimal backscatter, and thus the polarization signature will result in more peak- and valley-like shapes. As a result, the value of the *CoV* will be small (i.e., closer to 0). Conversely, if the measured ground surface is rough, several different scattering mechanisms may result, the backscatter maxima and minima may occur together from different individual scatterers, and a relatively flat polarization signature shape will be produced (equivalently, *CoV* will be large, i.e., close to 1).

1.8 RADAR SPECKLE SUPPRESSION

Due to random fluctuations in the signal observed from a spatially extensive target represented by a pixel (or image resolution element), *speckle noise* is generally present on a radar image. Speckle has the characteristics of a random multiplicative noise (defined below) in the sense that as the average grey level of a local area increases, the noise level increases. In a SAR imaging system, speckle effects are more serious (Lopez-Martinez and Fabregas, 2003). SAR can achieve high resolution in the azimuth direction independent of range, but the presence of speckle decreases the interpretability of the SAR imagery. If such imagery is to be used in classification, then some form of preprocessing to reduce or suppress speckle is necessary.

There are two approaches to the suppression of radar image speckle. The first method is known as the multilook process, while the second method uses filtering techniques to suppress the speckle noise.

1.8.1 Multilook Processing

Radar speckle can be suppressed by averaging several looks (images) to reduce the noise variance. This procedure is called *multilook processing*. As the radar sensor moves past the target pixel, it obtains multiple looks (i.e., returned samples). If these looks are spaced sufficiently far apart they can be considered to represent individual observations. The relationships among the radar aperture length L, the resolution R, and the number of independent samples N_s is expressed by (Ulaby et al., 1982, 1986a)

$$N_s \approx \frac{R}{0.5L}. \tag{1.36}$$

For instance, if radar aperture length is 10 m, and the desired spatial resolution is 25-m resolution, then the number of independent samples is 25/5 = 5. Figure 1.24 illustrates the relationship between the resolution and number of samples. Although the averaging of independent looks can reduce the noise variance, it also causes degradation in image resolution.

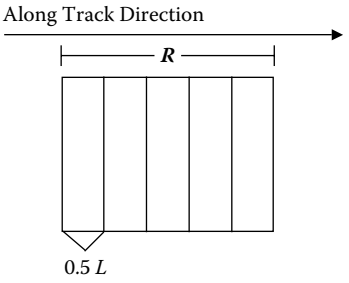

FIGURE 1.24 The relationship between resolution and number of looks in a SAR image. See text for explanation.

1.8.2 Filters for Speckle Suppression

The second method of speckle suppression uses filtering methods, which fall into two main categories, namely, adaptive and nonadaptive filters. *Adaptive filters* use weights that are dependent on the degree of speckle in the image, whereas *nonadaptive* filters use the same set of weights over the entire image. Adaptive filters are more likely to preserve details such as edges or high-texture areas (e.g., forest or urban areas) because the degree of smoothing is dependent on local image statistics.

The best-known nonadaptive filters are those based on the use of the mean or the median. The mean filter uses the same set of smoothing weights for the whole image without regard for differences in image texture, contrast, etc. The median filter does not use a weighting procedure, but is based on the ranking of image pixel values within a specified rectangular window (Mather, 2004). Both of these filters have a speckle-suppression capability, but they also smooth away other high-frequency information. The median is more effective than the mean in eliminating spike noise while retaining sharp edges. Both filters are easily implemented and require less computation than adaptive filters.

In comparison with nonadaptive speckle filters, adaptive speckle filters are more successful in preserving subtle image information. A number of adaptive speckle filters have been proposed, the best known being the Lee filter (Lee, 1980, 1981, 1986), the Kuan filter (Kuan et al., 1987), the Frost filter (Frost et al., 1982), and the Refined Gamma Maximum-A-Posteriori (RGMAP) filter (Touzi et al., 1988; Lopes et al., 1990; Baraldi and Parmiggiani, 1995). The effectiveness of these adaptive filters is dependent on the following three assumptions (Lee, 1980; Lopes et al., 1990; Baraldi and Parmiggiani, 1995a,b):

1. SAR speckle is modeled as a multiplicative noise (note that the visual effect of multiplicative noise is that the noise level is proportional to the image gray level).
2. The noise and signal are statistically independent.
3. The sample mean and variance of a pixel is equal to its local mean and local variance computed within a window centered on the pixel of interest.

All of the speckle filters described above rely strongly on a good estimate of local statistics (e.g., σ_z and μ_z) from a window. If the window center is located close to the boundary of an image segment (such as a boundary between agricultural fields), the resulting local statistics are likely to be biased and will thus degrade the filtering result. Nezry et al. (1991) notes this point, and proposes a refined GMAP filter called the RGMAP filter in which the local statistics extracted from a window do not cross image feature boundaries. Readers are referred to Sheng and Xia (1996) and Liu, Z. (2004) for comparisons of the above filters.

In recent years, the wavelet transform has been used for radar imagery denoising (Donoho, 1995; Fukuda and Hirosawa, 1998, 1999; Achim et al., 2003). The wavelet transform can decompose the multiplicative noise, and so simplify the speckle filtering process. Details of the wavelet transform are described in Chapter 7. Normally, using the wavelet transform for speckle suppression involves

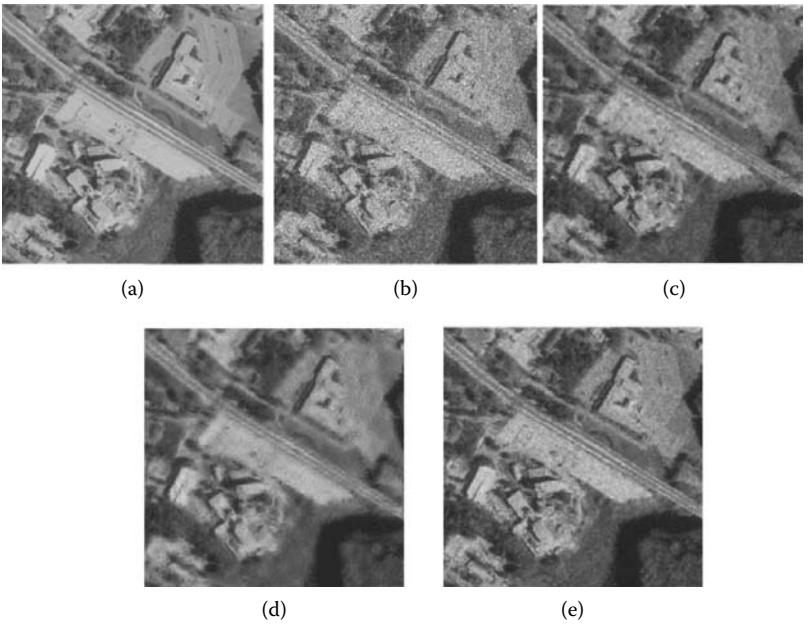

FIGURE 1.25 Calculation of median and mean filters for 3×3 window.

three steps as follows. First, the SAR image is translated into logarithmic domain and is then decomposed by means of the wavelet transform in a multiscale sense. Note that translating the raw SAR image into logarithmic domain is to convert the multiplicative noise to an additive noise. Second, the empirical wavelet coefficients are shrunk using a thresholding mechanism. Finally, the denoised signal is synthesized from the processed wavelet coefficients through the inverse wavelet transform. It is noted that the quality of wavelet transform for speckle suppression is closely related to the thresholding method used (Donoho, 1995). Some good estimators and modeling techniques proposed by Simoncelli (1999), Pizurica et al. (2001), and Achim et al. (2003) can be applied for solving such thresholding issues and so as to make the speckle suppression quality well controlled. Gagnon and Jouan (1997) and Achim et al. (2003) conducted comparative studies between wavelet-based filters and several statistical adaptive speckle filters described in the previous paragraph and show that, from the perspectives of both qualitative and quantitative measures, the wavelet-based approaches outperform other kinds of filters for speckle removal. Figure 1.25 illustrates the results of speckle suppression in terms of various filters. In Figure 1.25a, the original remotely sensed imagery is shown. The image contaminated by the noise is displayed in Figure 1.25b. The noisy image is then subjected to a GMAP filter (Figure 1.25c), and wavelet based filters developed by Donoho (1995) (Figure 1.25d) and Achim et al. (2003) (Figure 1.25e), respectively.

Further reading on the material covered in this chapter is provided in Elachi (1987), Liang (2004), Slater (1980), and contributors to Asrar (1989).

Bibliography

Abe, S., and M. S. Lan. 1995. A method for fuzzy rules extraction directly from numerical data and its application to pattern classification. *IEEE Transactions on Fuzzy Systems* 3:18–28.

Achim, A., P. Tsakalides, and A. Bezerianos. 2003. SAR image denoising via Bayesian wavelet shrinkage based on heavy-tailed modelling. *IEEE Transactions on Geoscience and Remote Sensing* 41:1773–1784.

Agterberg, F. P., and Q. Cheng. 1999. Introduction to special issue on "Fractals and Multifractals." *Computers and Geosciences* 25:947–948.

Aiazzi, B., L. Alparone, S. Baronti, and A. Garzelli. 2002. Context-driven fusion of high spatial and spectral resolution images based on oversampled multi-resolution analysis. *IEEE Transactions on Geoscience and Remote Sensing* 40:2300–2312.

Aires, F., C. Prigent, and W. B. Rossow. 2004. Neural network uncertainty assessment using Bayesian statistics: A remote sensing application. *Neural Computation* 16:2415–2458.

Aiyer, S. V. B., M. Niranjan, and F. Fallside. 1990. A theoretical investigation into the performance of the Hopfield model. *IEEE Transactions on Neural Networks* 1:204–215.

Aizerman, M. A., E. M. Braverman, and L.I. Rozoner. 1964. Theoretical foundations of the potential function method in pattern recognition learning. *Automation and Remote Control* 25:821–837.

Alilat, F., S. Loumi, and B. Sansal. 2006. Modified fuzzy ARTMAP and supervised fuzzy ART: Comparative study with multispectral classification. *International Journal of Computer Science* 1:232–238.

Allen, T. R., and J. A. Kupfer. 2000. Application of spherical statistics to change vector analysis of Landsat data: Southern Appalachian spruce-fir forests. *Remote Sensing of Environment* 74:482–493.

Alt, M. 1990. *Exploring Hyperspace—A Non-mathematical Explanation of Multivariate Analysis*. London: McGraw-Hill.

Ardö, J., P. Pilesjö, and A. Skidmore. 1997. Neural networks, multi temporal TM data and topographic data to classify forest damage in the Czech Republic. *Canadian Journal of Remote Sensing* 23:217–229.

Asner, G. P., and K. B. Heidebrecht. 2002.Spectral unmixing of vegetation, soil and dry carbon cover in arid regions: Comparing multispectral and hyperspectral observations. *International Journal of Remote Sensing* 23:3939–3958.

Asner, G. P., and D. B. Lobell. 2000. A biophysical approach for automated SWIR unmixing of soils and vegetation. *Remote Sensing of Environment* 74:99–112.

Atkinson, P. M. 1991. Optimal ground-based sampling for remote sensing investigations: Estimating the regional mean. *International Journal of Remote Sensing* 12:559–567.

Atkinson, P. M. 1996. Optimal sampling strategies for raster-based geographical information systems. *Global Ecology and Biogeographical Letters* 5:271–280.

Atkinson, P. M., and P. Lewis. 2000. Geostatistical classification for remote sensing: An introduction. *Computers and Geosciences* 26:361–371.

Atkinson, P. M., and A. R. L. Tatnall. 1997. Introduction: Neural networks in remote sensing. *International Journal of Remote Sensing* 18:699–709.

Ball,, G. H., and D. J. Hall. 1967. A clustering technique for summarising multivariate data. *Behavioral Science* 12:153–155.

Baraldi, A., and F. Parmiggiani. 1995a. A refined Gamma MAP SAR speckle filter with improved geometrical adaptivity. *IEEE Transactions on Geoscience and Remote Sensing* 33:1245–1257.

Baraldi, A., and F. Parmiggiani. 1995b. An alternative form of the Lee filter for speckle suppression in SAR images. *Computer Vision, Graphics and Image Processing—Graphical Models and Image Processing* 57:75–78.

Baronti, S., R. Carla, S. Sigismondi, and L. Alparone. 1994. Principal component analysis for change detection on polarimetric multitemporal SAR data. In *Proceedings of the International Geoscience and Remote Sensing Symposium (IGARSS'94)*, 8–12 August, Pasadena, CA, 2152–2154. Piscataway, NJ: Institute of Electrical and Electronics Engineers (IEEE).

Bardossy, A., and L. Samaniego. 2002. Fuzzy rule-based classification of remotely sensed imagery. *IEEE Transactions on Geoscience and Remote Sensing* 40:362–374.

Barnett, J. A. 1981. Computational methods for a mathematical theory of evidence. In *Proceedings of the 7th International Conference on Artificial Intelligence*, Vancouver, British Columbia, 868–875. Los Altos, CA: William Kaufmann.

Barnsley, M. F. 1993. *Fractals everywhere*. London: Academic Press Limited.

Barnsley, M. F., and L. P. Hurd. 1993. *Fractal image compression*. Wellesley, MA: AK Peters Ltd.

Bastin, L. 1997. Comparison of fuzzy c-means classification, linear mixture modelling and MLC probabilities as tools for unmixing coarse pixels. *International Journal of Remote Sensing* 18:3629–3648.

Bavarian, B., and Z. Lo. 1991. On the rate of convergence in topology preserving neural networks. *Biological Cybernetics* 65:55–63.

Belousov, A. I., S. A. Verzakov, and J. Von Frese. 2002. A flexible classification approach with optimal generalisation performance: Support vector machines. *Chemometrics and Intelligent Laboratory Systems* 64:15–25.

Benediktsson, J. A., P. H. Swain, and O. K. Esroy. 1990. Neural network approaches versus statistical methods in classification of multisource remote sensing data. *IEEE Transactions on Geoscience and Remote Sensing* 28:540–552.

Benson, B. J., and M. D. Mackenzie. 1995. Effects of sensor spatial resolution on landscape structure parameters. *Landscape Ecology* 10:113–120.

Berry, B. J. L., and A. M. Baker. 1968. Geographical sampling. In *Spatial analysis*, ed. B. J. L. Berry and D. F. Marble. Englewood Cliffs, NJ: Prentice-Hall.

Bersini, H., M. Saerens, and L. G. Sotelino. 1994. Hopfield net generation, encoding and classification of temporal trajectories. *IEEE Transactions on Neural Networks* 5:945–953.

Besag, J. 1974. Spatial interaction and the statistical analysis of lattice systems. *Journal of the Royal Statistical Society* 36:192–236.

Besag, J. 1986. On the statistical analysis of dirty pictures. *Journal of the Royal Statistical Society* 48:259–302.

Bezdek, J. C. 1981. *Pattern recognition with fuzzy objective function algorithms*. New York: Plenum Press.

Bezdek, J. C., R. Ehrlich, and W. Full. 1984. FCM: The fuzzy c-means clustering algorithm. *Computers and Geosciences* 10:191–203.

Bian, L. 2003. Retrieving urban objects using a wavelet transform approach. *Photogrammetric Engineering and Remote Sensing* 69:133–141.

Bishop, C. M. 1996. *Neural networks for pattern recognition*. Oxford: Clarendon Press.

Blake, A., and A. Zisserman. 1987. *Visual reconstruction*. Cambridge, MA: MIT Press.

Blamire, P. A. 1996. The influence of relative sample size in training artificial neural networks. *International Journal of Remote Sensing* 17:223–230.

Blanz, V., B. Schölkopf, H. Bülthoff, C. Burges, V. N. Vapnik, and T. Vetter. 1996. Comparison of view–based object recognition algorithms using realistic 3D models. In *Proceedings of International Conference on Artificial Neural Networks—ICANN'96*, Berlin, 1112, 251–256.

Borak, J. S., and A. H. Strahler. 1999. Feature selection and land cover classification of a MODIS-like data set for semi-arid environment. *International Journal of Remote Sensing* 20:919–938.

Borel, C. C., and S. A. W. Gerstl. 1994. Nonlinear spectral mixing models for vegetative and soil surfaces. *Remote Sensing of Environment* 47:403–416.

Bork, E. W., N. E. West, and K. P. Price. 1999. Calibration of broad- and narrow-band spectral variables for rangeland cover component quantification. *International Journal of Remote Sensing* 20:3641–3662.

Born, M., and E. Wolf. 1980. *Principles of optics*. New York: Pergamon.

Bosdogianni, P., M. Petrou, and J. Kittler. 1997. Mixture models with higher order moments. *IEEE Transactions on Geoscience and Remote Sensing* 33:341–353.

Boser, B. E., I. M. Guyon, and V. N. Vapnik. 1992. A training algorithm for optimal margin classifiers. In *Proceedings of the 5th Annual Workshop on Computational Learning Theory*, 144–152. Pittsburgh, PA: ACM Press.

Breim, G. J., J. A. Benediktsson, and J. R. Sveinsson. 2002. Multiple classifiers applied to multisource remote sensing data. *IEEE Transactions on Geoscience and Remote Sensing* 40:2291–2299.

Breiman, L. 1996. Bagging predictors. *Machine Learning* 26:123–140.

Breiman, L. 2001. Random forests. *Machine Learning* 45:5–32.

Breiman, L., J. H. Friedman, R. A. Olsen, and C. J. Stone. 1984. *Classification and Regression Trees*. Belmont, CA: Wadsworth.

Brigham, E. O. 1974. *The fast Fourier transform*. Englewood Cliffs, NJ: Prentice-Hall.

Brodatz, P. 1966. *Texture: A photographic album for artists and designers*. New York: Dover Books.

Brodley, C., and M. A. Friedl. 1996. Improving automated land cover mapping by identifying and eliminating mislabelled observations from training data. *Proceedings of the International Geoscience and Remote Sensing Symposium* (*IGARSS'96)*, Lincoln, NE, May 27–31, 1996, 1382–1384. Piscataway, NJ: Institute of Electrical and Electronics Engineers (IEEE).

Brodley, C., and M. A. Friedl. 1999. Identifying mislabelled training data. *Journal of Artificial Intelligence Research* 11:131–167.

Brogaard, S., and R. Ólafsdóttir. 1997. *Ground-truth or Ground-lies? Environmental sampling for remote sensing application exemplified by vegetation cover data.* Lund Electronic Reports in Physical Geography, No. 1 (October). Lund, Sweden: University of Lund, Department of Physical Geography. (http://www.lub.lu.se/luft/rapporter/lerpg/1/1Abstract.htm).

Brown, D. E., V. Corruble, and C. L. Pittard. 1993. A comparison of decision tree classifiers with backpropagation neural networks for multimodal classification problems. *Pattern Recognition* 26:953–961.

Brown, L. G. 1992. A survey of image registration techniques. *ACM Computing Surveys* 24:325–376.

Bruzzone, J., R. Gossu, and G. Vernazza. 2004. Detection of land-cover transitions by combining multidate classifiers. *Pattern Recognition Letters* 25:1491–1500.

Burges, C. J. C. 1998. A tutorial on support vector machines for pattern recognition. *Data Mining and Knowledge Discovery* 2:121–167.

Burges, C. J. C., and B. Schölkopf. 1997. Improving the accuracy and speed of support vector learning machines. In *Advances in neural information processing systems*, ed. by M. Mozer, M. Jordan, and T. Petsche, 9, 375–381, Cambridge, MA: MIT Press.

Burrus, C. S., R. A. Gopinath, and H, Guo. 1998. *Introduction to wavelets and wavelet transforms: A primer*. Upper Saddle River, NJ: Prentice Hall.

Camacho-De Coca, F., F. J. Carcía-Haro, M. A. Gilabert, and J. Meliá. 2004. Vegetation cover seasonal changes assessment from TM imagery in a semi-arid landscape. *International Journal of Remote Sensing* 25:3451–3476.

Campbell, J. B. 1987. *Introduction to remote sensing*. London: Guilford Press.

Cannon, R. L., J. V. Dave, J. C. Bezdek, and M. M. Trivedi. 1986. Segmentation of a Thematic Mapper image using the fuzzy c-means clustering algorithm. *IEEE Transactions on Geoscience and Remote Sensing* GE-24:400–408.

Cappellini, V., and A. Chiuderi. 1994. Neural networks in remote sensing multisensor data processing. *Proceedings of the 14th EARSeL Symposium*, Sweden, ed. by J. Askne, 457–462. Rotterdam: Balkema.

Carpenter, G. A., M. N. Gjaja, S. Gopal, and C. E. Woodcock. 1997. ART neural networks for remote sensing: Vegetation classification from Landsat TM and terrain data. *IEEE Transactions on Geoscience and Remote Sensing* 33:308–325.

Carpenter, G. A., and S. Grossberg. 1987a. A massively parallel architecture for a self-organising neural pattern recognition machine. *Computer Vision, Graphics and Image Processing* 37:54–115.

Carpenter, G. A., and S. Grossberg. 1987b. ART2: Stable self-organisation of pattern recognition codes for analogue input patterns. *Applied Optics* 26:4919–4930.

Carpenter, G. A., S. Grossberg, N. Markuzon, J. H. Reynolds, and D. B. Rosen. 1992. Fuzzy ARTMAP: A neural network architecture for incremental supervised learning of analogue multidimensional maps. *IEEE Transactions on Neural Networks* 3:698–713.

Carpenter, G. A., S. Grossberg, and J. H. Reynolds. 1991. ARTMAP: Supervisor real-time learning and classification of non-stationary data by a self-organising neural network. *Neural Networks* 4:565–588.

Carpenter, G. A., S. Grossberg, and D. B. Rosen. 1991. Fuzzy ART: Fast stable learning and categorisation of analogue patterns by an Adaptive Resonance system. *Neural Networks* 4:759–771.

Carper, W. J., T. M. Lillesand, and R. W. Kiefer. 1990. The use of IHS transformations for merging SPOT panchromatic and multispectral image data. *Photogrammetric Engineering and Remote Sensing* 56:459–467.

Carr, J. R. 1996. Spectral and textural classification of single and multiple band images. *Computers and Geosciences* 22:849–865.

Carr, J. R. 1999. Classification of digital image texture using variograms. In *Advances in remote sensing and GIS analysis*, ed. P. M. Atkinson and N. J. Tate, 135–146. Chichester, U.K.: John Wiley and Sons.

Carr, J. R., and F. P. Miranda. 1998. The semivariogram in comparison to the co-occurrence matrix for classification of image texture. *IEEE Transactions on Geoscience and Remote Sensing* 36:1945–1952.

Cestnik, B., and I. Bratko. 1991. On estimating probabilities in tree pruning. In *Proceedings of European Working Session on Learning*, ed. Y. Kodrato, 138–150. New York: Springer Verlag.

Chandler, D. 1987. *Introduction to modern statistical mechanics*. Oxford: Oxford University Press.

Chang, C. C., and C. J. Lin. 2007. LIBSVM: A library for support vector machines, 2001. Software available from http://www.csie.ntu.tw/~cjlin/libsvm (accessed May 16, 2008).

Chang, P. C., Y. W. Wang, and C. Y. Tsai. 2005. Evolving neural network for printed circuit board sales. *Expert Systems with Applications* 29:83–92.

Chapelle, O., V. Vapnik, O. Bousquet, and S. Mukherjee. 2002. Choosing multiple parameters for support vector machines. *Machine Learning* 46:131–159.

Chavez, P. S., Jr. 1988. An improved dark-object subtraction technique for atmospheric scattering correction of multispectral data. *Remote Sensing of Environment* 24:459–479.

Chen, C. F., and J. M. Lee. 2001. The validity measurement of fuzzy c-means classification for remotely sensed images. In *Proceedings of the 22nd Asian Conference on Remote Sensing*, November 5–9, Singapore, 208–210.

Chen, J., P. Gong, C. He, R. Pu, and P. Shi. 2003. Land-use/land-cover change detection using improved change-vector analysis. *Photogrammetric Engineering and Remote Sensing* 69:369–379.

Chen, Y., and T. Huang. 2001. Hierarchical MRF model for model-based multi-object tracking. In *Proceedings of the IEEE International Conference on Image Processing (ICIP'01)*, October 2001, Thessaloniki, Greece, 385–388.

Chen, Y. H., L. Den, J. Li, X. Li, and P. J. Shi. 2006. A new wavelet-based image fusion method for remotely sensed data. *International Journal of Remote Sensing* 27:1465–1476.

Cheung, Y. M. 2005. On rival penalization controlled competitive learning for clustering with automatic cluster number selection. *IEEE Transactions on Knowledge and Data Engineering* 17:1583–1588.

Chica-Olmo, M., and F. Abarca-Hérnandez. 2000. Computing geostatistical image texture for remotely sensed data classification. *Computers and Geosciences* 26:373–383.

Civco, D. 1989 Topographic normalisation of Landsat Thematic Mapper imagery. *Photogrammetric Engineering and Remote Sensing* 55:1303–1309.

Clarke, K. C. 1986. Computation of the fractal dimension of topographic surfaces using the triangular prism surface area method. *Computers and Geosciences* 12:713–722.

Clausi, M., and M. Jernigan. 1998. A fast method to determine co-occurrence texture features. *IEEE Transactions on Geoscience and Remote Sensing* 36:298–300.

Coburn, C. A., and A. C. B. Roberts. 2004. A multiscale texture analysis procedure for improved forest stand classification. *International Journal of Remote Sensing* 25:4287–4308.

Cochran, W. G. 1977. *Sampling techniques*. New York: John Wiley and Sons.

Cohen, A., and J. Kovavcevic. 1996. Wavelets: The mathematical background. *Proceedings of the IEEE* 84:514–522.

Cohen, J. 1960. A coefficient of agreement for nominal scales. *Educational and Psychological Measurement* 20(1):37–46.

Colby, J. D. 1991. Topographic normalisation in rugged terrain. *Photogrammetric Engineering and Remote Sensing* 57:531–537.

Colditz, R. C., T. Wehrmann, M. Bachmann, K. Steinnocher, M. Schmidt, G. Strunz, and S. Dech. 2006. Influence of image fusion approaches on classification accuracy: A case study. *International Journal of Remote Sensing* 27(15):3311–3335.

Collins, J. B., and C. E. Woodcock. 1994. Change detection using the Gramm-Schmidt transformation applied to mapping forest mortality. *Remote Sensing of Environment* 50:267–279.

Collins, J. B., and C. E. Woodcock. 1996. An assessment of several linear change detection techniques for mapping forest mortality using multitemporal Landsat TM data. *Remote Sensing of Environment* 56:66–77.

Congalton, R. G. 1988. A comparison of sampling schemes used in generating error matrices for assessing the accuracy of maps generated from remotely sensed data. *Photogrammetric Engineering and Remote Sensing* 54:593–600.

Congalton, R. G. 1991. A review of assessing the accuracy of classifications of remotely sensed data. *Remote Sensing of Environment* 37:35–46.

Congalton, R. G., and K. Green. 1999. *Assessing the accuracy of remotely sensed data: Principles and practice*. New York: Lewis Publishers.

Congalton, R. G., and L. C. Plourde. 2000. Sampling methodology, sampling placement and other important factors in assessing the accuracy of remotely sensed forest maps. In *Proceedings of the Accuracy 2000 Conference*, ed. G. B. M Heuvelink and M. J. P. M. Lemmens, 117–124. Amsterdam: Delft University Press.

Coppin, P. R., and M. E. Bauer. 1994. Processing of multitemporal Landsat TM imagery to optimise extraction of forest cover change features. *IEEE Transactions on Geoscience and Remote Sensing* 32:918–927.

Coppin, P. R., and M. E. Bauer. 1995. The potential contribution of pixel-based canopy change information to stand-based forest management in the northern US. *Journal of Environmental Management* 44:69–82.

Coppin, P. R., E. Lambin, I. Jonckheere, K. Nackaerts, and B. Muys. 2004. Digital change detection methods in ecosystem monitoring: A review. *International Journal of Remote Sensing* 25:1565–1596.

Cortes, C., and V. Vapnik. 1995. Support vector networks. *Machine Learning* 20:273–297.

Cortijo, F. J., and N. Pérez de la Blanca. 1999. The performance of regularised discriminant analysis versus non-parametric classifiers applied to high dimensional image classification. *International Journal of Remote Sensing* 20:3345–3365.

Cóté, S., and A. R. L. Tatnall. 1997. The Hopfield neural network as a tool for feature tracking and recognition from satellite sensor images. *International Journal of Remote Sensing* 18:871–885.

Courant, R., and D. Hilbert. 1953. *Methods of mathematical physics*, Volume 1. New York: Interscience Publishers.

Crammer, K., and Y. Singer. 2002. On the learnability and design of output codes for multiclass problems. *Machine Learning* 47:201–233.

Crapper, P. F. 1984. An estimate of the number of boundary cells in a mapped landscape coded to grid cells. *Photogrammetric Engineering and Remote Sensing* 50:1497–1503.

Craven, M. W. 1996. Extracting comprehensible models from trained neural networks. Ph.D. Thesis, University of Wisconsin, Madison, WI.

Crist, E. P., and R. C. Cicone. 1984a. A physically-based transformation of Thematic Mapper data—The TM Tasselled Cap. *IEEE Transactions on Geoscience and Remote Sensing* 22:256–263.

Crist, E. P., and R. C. Cicone. 1984b. Comparison of the dimensionality and features of simulated Landsat-4 MSS and TM data. *Remote Sensing of Environment* 14:235–246.

Cross, G. C., and A. K. Jain. 1983. Markov random field texture models. *IEEE Transactions on Pattern Analysis and Machine Intelligence* 5:25–39.

Csiszar, I., G. Guiman, P. Romanov, M. Leroy, and O. Hautecoeul. 2001. Using ADEOS/POLDER data to reduce angular variability of NOAA/AVHRR reflectances. *Remote Sensing of Environment* 76:399–409.

Curran, P. J. 1988. The semi-variogram in remote sensing: An introduction. *Remote Sensing of Environment* 24:493–507.

Curran, P. J., and P. M. Atkinson. 1998. Geostatistics and remote sensing. *Progress in Physical Geography* 22:61–78.

Cushnie, J. L. 1987. The interactive effect of spatial resolution and degree of internal variation within land cover types on classification accuracies. *International Journal of Remote Sensing* 8:15–29.

Daubechies, I. 1992. *Ten lectures on wavelets,* 2nd ed. Philadelphia, PA: Society for Industrial and Applied Mathematics (SIAM).

Davies, J. K. 1992. *Space Exploration*. New York: W & R Chambers.

De Bruin, S., and B. G. H. Gorte. 2000. Probabilistic image classification using geological map units applied to land-cover change detection. *International Journal of Remote Sensing* 21:2389–2402.

Decatur, S. E. 1989. Application of neural networks to terrain classification. In *Proceedings of International Joint Conference on Neural Networks*. Piscataway, NJ: Institute of Electrical and Electronics Engineers (IEEE), 1, 283–288.

De Colstoun, E. C. B., M. H. Story, C. Thompson, K. Commisso, T. G. Smith, and J. Irons. 2003. National park vegetation mapping using multitemporal Landsat 7 data and a decision tree classifier. *Remote Sensing of Environment* 85:316–327.

De Colstoun, E. C. B., and C. L. Walthall. 2006. Improving global scale land cover classifications with multi-directional POLDER data and a decision tree classifier. *Remote Sensing of Environment* 100:474–485.

De Jong, S. M., and P. A. Burrough. 1995. A fractal approach to the classification of Mediterranean vegetation types in remotely sensed images. *Photogrammetric Engineering and Remote Sensing* 61:1041–1053.

De Jong, S. M., and H. Van der Werff. 1998. The DAIS 7915 Peyne experiment: Using airborne imaging spectrometry for surveying minerals in vegetated and fragmented Mediterranean landscapes. In *Proceedings of the 1st EARSeL Workshop on Imaging Spectroscopy*, October 6–8, 1998, Remote Sensing Laboratories, University of Zurich, Switzerland, 341–347. Paris: EARSeL.

Dempster, A. P., N. M. Laird, and D. B. Bubin. 1977. Maximum likelihood from incomplete data via expectation-maximization (EM) algorithm. *Journal of the Royal Statistical Society*, Series B 39:1–38.

Dennison, P. E., and D. A. Roberts. 2003. Endmember selection for multiple spectral mixture analysis using endmember average RMSE. *Remote Sensing of Environment* 87:123–135.

Derin, H., and W. S. Cole. 1986. Segmentation of textured images using Gibbs random fields. *Computer Vision, Graphics and Image Processing* 35:72–98.

Derin, H., and H. Elliott. 1987. Modelling and segmentation of noisy and textured images using Gibbs random fields. *IEEE Transactions on Pattern Analysis and Machine Intelligence* 9:39–55.

Donoho, D. L. 1995. Denoising by soft-thresholding. *IEEE Transactions on. Information Theory* 41:613–627.

Dubes, R. C., and A. K. Jain. 1989. Random field models in image analysis. *Journal of Applied Statistics* 16:131–164.

Dubuc, B., J. F. Quiniou, C. Roques-Carmes, and S. W. Zucker. 1989. Evaluating the fractal dimension of profiles. *Physical Review* 39:1500–1512.

Duch, W., R. Adamczak, and K. Grabczewski. 2001. A new methodology of extraction, optimization and application of crisp and fuzzy logical rules. *IEEE Transactions on Neural Networks* 12:277–306.

Dymond, J. R., and J. D. Shepherd. 1999. Correction of the topographic effect in remote sensing. *IEEE Transactions on Geoscience and Remote Sensing* 37:2618–1619.

Eidenshink, J. C., and J. L. Faundeen. 1994. The 1 km AVHRR global land data set: First stages in implementation. *International Journal of Remote Sensing* 15:3443–3462.

Elachi, C. 1988. *Spaceborne Radar Remote Sensing: Applications and Techniques*. New York: IEEE Press.

Elmore, J. A., J. F. Mustard, S. J. Manning, and D. B. Lobell. 2000. Quantifying vegetation change in semiarid environments: Precision and accuracy of spectral mixture analysis and the normalized difference vegetation index. *Remote Sensing of Environment* 73:87–102.

El-Sheik, T. S., and A. G. Wacker. 1980. Effect of dimensionality and estimation on the performance of Gaussian classifiers. *Pattern Recognition* 12:115–126.

Erickson, W. K., and W. C. Lickens. 1984. An application of expert systems technology to remotely sensed image analysis. *IEEE Proceedings of Pecora IX Symposium*, October 2–4, 1984, Sioux Falls, SD, 258–276. Piscataway, NJ: Institute of Electrical and Electronics Engineers (IEEE), IEEE Catalogue Number CH2079 – 2/84/0000232.

Erwin, E., K. Obermayer, and K. Schulten. 1992a. Self-organizing maps: Stationary states, metastability and convergence rate. *Biological Cybernetics* 67:35–45.

Erwin, E., K. Obermayer, and K. Schulten. 1992b. Self-organizing maps: Ordering, convergence properties and energy functions. *Biological Cybernetics* 67:47–55.

Esposito, F., D. Malerba, and G. Semeraro. 1997. A comparative analysis of methods for pruning decision trees. *IEEE Transactions on Pattern Analysis and Machine Intelligence* 19:476–491.

Evans, D. L., T. G. Farr, J. J. Van Zyl, and H. A. Zebker. 1988. Radar polarimetry: Analysis tools and application. *IEEE Transactions on Geoscience and Remote Sensing* 26:774–789.

Evans, F. 1998. An investigation into the use of maximum likelihood classifiers, decision trees, neural networks and conditional probabilistic networks for mapping and predicting salinity. M.Sc. Thesis, Department of Computer Science, Curtin University of Technology, Australia.

Feder, J. 1988. *Fractals*. New York: Plenum Press.

Fioravanti, S. 1994. Multifractals: Theory and application to image texture recognition. In *Fractals in geoscience and remote sensing*. *Proceedings of a Joint JRC/EARSeL Expert Meeting, Ispra, Italy, 14th–15th April*, ed. G. G. Wilkinson, I. Kanellopoulos, and J. Megier, Image Understanding Research Series, 1, 152–175. Report EUR 16092, Office for Official Publications of the European Communities, Luxembourg.

Fitzpatrick-Lins, K. 1981. Comparison of sampling procedures and data analysis for a land-use and land-cover map. *Photogrammetric Engineering and Remote Sensing* 47(3):343–351.

Fletcher, R. 1987. *Practical methods of optimization*. 2nd ed. Chichester, U.K.: John Wiley and Sons.

Foley, J. D., and A. Van Dam. 1982. *Fundamentals of interactive computer graphics*. Reading, MA: Addison-Wesley.

Foody, G. M. 1992. On the compensation for chance agreement in image classification accuracy assessment. *Photogrammetric Engineering and Remote Sensing* 58:1459–1460.

Foody, G. M. 1996. Approaches for the production and evaluation of fuzzy land cover classifications from remotely-sensed data. *International Journal of Remote Sensing* 17:1317–1340.

Foody, G. M. 1998. Sharpening fuzzy classification output to refine the representation of sub-pixel land cover distribution. *International Journal of Remote Sensing* 19:2593–2599.

Foody, G. M. 1999a. The significance of border training patterns in classification by a feed-forward neural network using back-propagation learning. *International Journal of Remote Sensing* 20:3549–3562.

Foody, G. M. 1999b. Image classification with a neural network: From completely crisp to fully-fuzzy situations. In *Advances in remote sensing and GIS analysis*, ed. P. M. Atkinson and N. J. Tate, 17–37. Chichester, U.K.: John Wiley and Sons.

Foody, G. M. 2000a. Accuracy of thematic maps derived by remote sensing. In *Proceedings of the Accuracy 2000 Conference*, ed. G. B. M. Heuvelink and M. J. P. M. Lemmens, 217–224. Amsterdam: Delft University Press.

Foody, G. M. 2000b. Estimation of sub-pixel land cover composition in the presence of untrained classes. *Computers and Geosciences* 26:469–478.

Foody, G. M. 2002. Status of land cover classification accuracy assessment. *Remote Sensing of Environment* 80:185–201.

Foody, G. M., and P. J. Curran, eds.. 1994. *Environmental remote sensing from regional to global scales*. Chichester, U.K.: John Wiley and Sons.

Foody, G. M., R. M. Lucas, P. J. Curran, and M. Honzak. 1997. Non-linear mixture modelling without end-members using an artificial neural network. *International Journal of Remote Sensing* 18:937–953.

Foody, G. M., and A. Mathur. 2004. Toward intelligent training of supervised image classifications: Directing training data acquisition for SVM classification. *Remote Sensing of Environment* 93:107–117.

Foody, G. M., and A. Mathur. 2006. The use of small training sets containing mixed pixels for accurate hard image classification: Training on mixed spectral responses for classification by a SVM. *Remote Sensing of Environment* 103:179–189.

Foody, G. M., A. Mathur, C. Sanchez-Hernandez, and D. S. Boyd. 2006. Training set size requirements for the classification of a specific class. *Remote Sensing of Environment* 104:1–14.

Foody, G. M., M. B. McCullagh, and W. B. Yates. 1995. The effect of training set size and composition on artificial neural net classification. *International Journal of Remote Sensing* 16:1707–1723.

Franklin, S. E., and D. R. Peddle. 1990. Classification of SPOT HRV imagery and texture features. *International Journal of Remote Sensing* 11:551–556.

Franklin, S. E., D. R. Peddle, and J. A. Dechka. 2002. Evidential reasoning with Landsat TM, DEM and GIS data for landcover classification in support of grizzly bear habitat mapping. *International Journal of Remote Sensing* 23:4633–4652.

Frankot, R. T., and R. Chellappa. 1987. Lognormal random-field models and their applications to radar image synthesis. *IEEE Transactions on Geoscience and Remote Sensing* 25:195–207.

French, S. 1985. Group consensus probability distributions: A critical survey. In *Bayesian statistics 2*, ed. J. M. Bernardo, M. H. DeGroot, D. V. Lindley, and A. F. M. Smith, 183–202. New York: North Holland.

Freund, Y., and R. E. Schapire. 1999. A short introduction to boosting. *Journal of Japanese Society for Artificial Intelligence* 14:771–780.

Friedl, M. A., and C. E. Brodley. 1997. Decision tree classification of land cover from remotely sensed data. *Remote Sensing of Environment* 61:399–409.

Friedl, M. A., C. E. Brodley, and A. H. Strahler. 1999. Maximizing land cover classification accuracies produced by decision trees at continental to global scales. *IEEE Transactions on Geoscience and Remote Sensing* 37:969–977.

Friedman, J. H. 1994. An overview of predictive learning and function approximation. In *From statistics to neural networks*, ed. V. Cherkassky, J. Friedman, and H. Wechsler, 1–55. Proceedings of NATO/ISI Workshop. Berlin: Springer-Verlag.

Friedman, L. 1981. Extended plausible inference. In *Proceedings of the Seventh International Joint Conference on Artificial Intelligence*, Vancouver, BC, 487–495.

Frizzelle, B. G., and A. Moody. 2001. Mapping continuous distributions of land cover—a comparison of maximum likelihood estimation and artificial neural networks. *Photogrammetric Engineering and Remote Sensing*, 67693–67705.

Frost, V. S., J. A. Stiles, K. S. Shanmugan, and J. C. Holtzman. 1982. A model for radar images and its application to adaptive digital filtering of multiplicative Noise. *IEEE Transactions on Pattern Analysis and Machine Learning* 4:157–166.

Fukuda, S., and H. Hirosawa. 1998. Suppression of speckle in synthetic aperture radar images using wavelet. *International Journal of Remote Sensing* 19:507–519.

Fukuda, S., and H. Hirosawa. 1999. Smoothing effect of wavelet-based speckle filtering: The Haar basis case. *IEEE Transactions on Geoscience and Remote Sensing* 37:1168–1172.

Fukunaga, K. 1972. *Introduction to statistical pattern recognition*. New York: Academic Press.

Fung, T. 1990. An assessment of TM imagery for land cover change detection. *IEEE Transactions on Geoscience and Remote Sensing* 28:681–684.

Fung, T., and E. Le Drew. 1987. Application of principal components analysis to change detection. *Photogrammetric Engineering and Remote Sensing* 53:1649–1658.

Furrer, R., A. Barsch, C. Olbert, and M. Schaale. 1994. Multispectral imaging of land surface. *Geojournal* 32:7–16.

Gagnon, L., and A. Jouan. 1997. Speckle filtering of SAR images—a comparative study between complex-wavelet based and standard filters. *Proceedings of the SPIE* 3169:80–91.

Gahegan, M., and G. West. 1998. The classification of complex geographic datasets: An operational comparison of artificial neural networks and decision tree classifiers. In *Proceedings of the 3rd International Conference on GeoComputation* University of Bristol, United Kingdom, 17–19 September 1998, http://www.geocomputation.org/1998/61/gc_61.htm. Accessed 19 December 2008.

Garrigues, S., D. Allard, F. Baret, and M. Wesis. 2006. Quantifying spatial heterogeneity at the landscape scale using variogram models. *Remote Sensing of Environment* 103:81–96.

Garson, G. D. 1998. *Neural networks: An introductory guide for social scientists*. London: Sage Publications.

Garvey, T. D., J. D. Lowrance, and M. A. Fischler. 1979. An inference technique for integrating knowledge from disparate sources. In *Proceedings 7th International Conference on Artificial Intelligence*, Vancouver, British Columbia, 319–325.

Gellman, D. I., S. F. Biggar, M. C. Dinguirard, P. J. Henry, M. S. Moran, K. T. Thome, and P. N. Slater. 1993. Review of SPOT-1 and -2 calibration at White Sands from launch to present. *Proceedings of SPIE* 1938:118–125.

Geman, D., and B. Gidas. 1991. *Image analysis and computer vision*, chapter 2, 9–36. New York: Academic Press.

Geman S., and D. Geman. 1984. Stochastic relaxation Gibbs distributions and the Baysian restoration of the image. *IEEE Transactions on Pattern Analysis and Machine Intelligence* 6:721–741.

Gens, R., and J. L. Van Genderen. 1996. SAR interferometry—issues, techniques and applications. *International Journal of Remote Sensing* 17:1803–1835.

Gercek, D. 2004. Improvement of image classification with the integration of topographical data. In *Proceedings of 20th ISPRS Congress,* Istanbul, Turkey, 12–23 July 2004. 35-B8, 53–58.

Ghosh, J., K. Tumer, S. Beck, and L. Deser. 1995. Integration of neural classifiers for passive sonar signals. In *DSP theory and applications*, ed. C. T. Leondes, 301–338. New York: Academic Press.

Gillespie, A. R., A. B. Kahle, and R. E. Walker. 1986. Colour enhancement of highly correlated images. I. Decorrelation and HSI contrast stretches. *Remote Sensing of Environment* 20:209–235.

Ginevan, M. E. 1979. Testing land-use map accuracy: Another look. *Photogrammetric Engineering and Remote Sensing* 45:1371–1377.

Goldberg, D. E. 1989. *Genetic algorithms in search, optimization and machine learning*. Reading, MA: Addison-Wesley.

Goldon, J., and E. H. Shortliffe. 1985. Method for managing evidential reasoning in a hierarchical hypothesis space. *Artificial Intelligence* 26:323–357.

Goldstein, R. M., H. Engelhardt, B. Kamb, and R. M. Frolich. 1993. Satellite radar interferometry for monitoring ice sheet motion: Application to an Antarctic ice stream. *Science* 262:1525–1530.

Gong, P., and P. J. Howarth. 1990. An assessment of some factors influencing multispectral land cover classification. *Photogrammetric Engineering and Remote Sensing* 36:597–603.

González-Audícana, M., X. Otazu, O. Fors, and A. Seco. 2005. Comparison between Mallat's and the "a trous" discrete wavelet transform based algorithms for the fusion of multispectral and panchromatic images. *International Journal of Remote Sensing* 26(3):595–614.

Gonzato, G. 1998. A practical implementation of the box counting algorithm. *Computers and Geosciences* 24:95–100.

Gorte, B., and A. Stein. 1998. Bayesian classification and class area estimation of satellite images using stratification. *IEEE Transactions on Geoscience and Remote Sensing* 36:803–812.

Goth, I. and Geva, A.B. 1989. Unsupervised optimal fuzzy clustering. *IEEE Proceedings* on *Pattern Analysis and Machine Intelligence*, 11, 773–781.

Gouvernet, J., J. Ayme, S. Sanchez, E. Mattei, and F. Giraud. 1980. Diagnosis assistance in medical genetics based on belief functions and a tree structured thesaurus: A conversational mode realization. In *Proceedings of MEDINFO 80,* Tokyo, Japan, 798.

Goyal, S. K., M. S. Seyfried, and P. E. O'Neill. 1999. Correction of surface roughness and topographic effects on airborne SAR in mountainous rangeland areas. *Remote Sensing of Environment* 67:124–136.

Grasso, D. N. 1993. Applications of the IHS colour transformation for 1:24,000 scale geologic mapping: A low cost SPOT alternative. *Photogrammetric Engineering and Remote Sensing* 59:73–80.

Green, A. A., M. Berman, P. Switzer, and M. D. Craig. 1988. A transformation for ordering multispectral data in terms of image quality with implications for noise removal. *IEEE Transactions on Geoscience and Remote Sensing* 26:65–74.

Grossberg, S. 1976. Adaptive pattern classification and universal recoding, II: Feedback, expection, olfaction and illusions. *Biological Cybernetics* 23:187–202.

Gunn, S. R. 1997. Support vector machines for classification and regression. In *Technical Report ISIS-1-98,* Image Speech and Intelligent Systems Research Group (ISIS). Southampton, U.K.: University of Southampton.

Gurelli, M. I., and L. Onural. 1994. On a parameter estimation method for Gibbs-Markov random fields. *IEEE Transactions on Pattern Analysis and Machine Intelligence* 4:824–830.

Gurney, C. M. 1980. Threshold selection for line detection algorithms. *IEEE Transactions on Geoscience and Remote Sensing* 18:204–211.

Gurney, C. M. 1981. The use of contextual information to improve land cover classification of digital remotely sensed data. *International Journal of Remote Sensing* 2:379–388.

Guyon, I., J. Weston, S. Barnhill, and V. Vapnik. 2002. Gene selection for cancer classification using support vector machines. *Machine Learning* 46:389–422.

Haar, A. 1910. Zur Theorie der orthogonalen Funktionensysteme, *Mathematische Annalen* 69:331–371.

Halmos, P. R. 1967. *A Hilbert space problem book*. Princeton, NJ: D. Van Nostrand Company, Inc.

Hansen, L. K., and P. Salomon. 1990. Neural network ensembles. *IEEE Transactions on Pattern Recognition and Machine Intelligence* 12:993–1001.

Hansen, M. C., R. S. Defries, J. R. G. Townshend, M. Carroll, C. Dimicelli, and R. A. Sohlberg. 2003. Global percent tree cover at a spatial resolution of 500 metres: First results of the MODIS vegetation continuous fields algorithm. *Earth Interactions* 7:1–15.

Hansen, M. C., R. S. Defries, J. R. G. Townshend, and R. Sohlberg. 2000. Global land cover classification at 1km resolution using a classification tree approach. *International Journal of Remote Sensing* 21:1331–1364.

Hansen, M. C., R. Dubayah, and R. S. Defries. 1996. Classification trees: An alternative to traditional land cover classifiers. *International Journal of Remote Sensing* 17:1075–1081.

Haralick, R. M., and K. S. Fu. 1983. Pattern recognition and classification, In *Manual of Remote Sensing, Vol. I,* Second edition, ed. R. N. Colwell, D. S. Simonett and F. T. Ulaby, 881–884. Falls Church, VA: American Society of Photogrammetry.

Haralick, R. M., M. Shanmugam, and I. Dinstein. 1973. Texture feature for image classification. *IEEE Transactions on Systems, Man and Cybernetics* 3:610–621.

Harrell, F. E. 2001. *Regression modeling strategies: With applications to linear models, logistic regression, and survival analysis*. New York: Springer.

Harsanyi, J. C., and C. I. Chang. 1994. Hyperspectral image classification and dimensionality reduction: An orthogonal subspace projection approach. *IEEE Transactions on Geoscience and Remote Sensing* 32:779–785.

Haslett, J. 1985. Maximum likelihood discriminant analysis on the plane using a Markovian model of spatial context. *Pattern Recognition* 18:287–296.

Hassibi, B., and D. G. Stork. 1993. Second order derivatives for network pruning. In *Advances in neural information processing 5*, ed. S. J. Hansen, J. D. Cowan, and C. L. Giles, 164–171. San Mateo, CA: Morgan Kaufmann.

Hay, A. M. 1979. Sampling designs to test land-use map accuracy. *Photogrammetric Engineering and Remote Sensing* 45:529–533.

Hayes, D. J., and S. A. Sader. 2001. Comparison of change-detection techniques for monitoring tropical vegetation clearing and vegetation regrowth in a time series. *Photogrammetric Engineering and Remote Sensing* 67:1067–1075.

Haykin, S. 1999. *Neural networks: A comprehensive foundation*. Englewood Cliffs, NJ: Prentice-Hall.

Hebb, D. O. 1949. *The organisation of behaviour*. New York: John Wiley and Sons.

Hein, A. 2003. *Processing of SAR data: Fundamentals, signal processing, interferometry*. Berlin: Springer-Verlag.

Hellman, M. 2002. SAR polarimetry tutorial. http://epsilon.nought.de/. (Accessed 15 May 2008.)

Hentchel, H., and I. Procaccia. 1983. The infinite number of generalized dimensions of fractals and strange attractors. *Physica* 8D:435–444.

Hewitson, B. C., and R. G. Crane (eds.) 1994. *Neural nets: Applications in geography*. London: Kluwer Academic Publishers.

Hisdal, E. 1994. Interpretative versus prescriptive fuzzy set theory. *IEEE Transactions on Fuzzy Systems* 2:22–26.

Holben, B. N., and D. Kimes. 1986. Directional reflectance response in AVHRR red and near-infrared bands for three cover types and varying atmospheric conditions. *Remote Sensing of Environment* 19:213–226.

Holland, J. H. 1975. *Adaptation in natural and artificial systems*. Ann Arbor: University of Michigan Press.

Hong, D. H., and C. Hwang. 2003. Support vector fuzzy regression machines. *Fuzzy Sets and Systems* 138:271–281.

Hopfield, J. J. 1982. Neural networks and physical systems with emergent collective computational abilities. *Proceedings of the National Academy of Sciences of the USA* 79:2554–2558.

Hopfield, J. J. 1984. Neurones with graded response have collective computational properties like those of two-state neurones. *Proceedings of the National Academy of Sciences of the USA* 81:3088–3092.

Hopfield, J. J., and D. W. Tank. 1985. Neural computation of decisions in optimisation problems. *Biological Cybernetics* 52:141–152.

Hord, R. M., and W. Brooner. 1976. Land use map accuracy criteria. *Photogrammetric Engineering and Remote Sensing* 42:671–677.

Hostert, P., A. Röder, and J. Hill. 2003. Coupling spectral unmixing and trend analysis for monitoring of long-term vegetation dynamics. *Remote Sensing of Environment* 87:183–197.

Hseih, P. F., and D. Landgrebe. 1998. *Classification of high dimensional data*. Report TR-ECE 98-4, School of Electrical and Computer Engineering. W. Lafayette, IN: Purdue University.

Hsu, C. W., and C. J. Lin. 2002. A comparison of methods for multi-class support vector machines. *IEEE Transactions on Neural Networks* 13:415–425.

Hu, B., W. Lucht, A. H. Strahler, C. B. Schaaf, and M. Smith. 2000. Surface albedo and angle-corrected NDVI from AVHRR observations of South America. *Remote Sensing of Environment* 71:119–132.

Huang, C., L. S. Davis, and J. R. G. Townshend. 2002. An assessment of support vector machines for land cover classification. *International Journal of Remote Sensing* 23:725–749.

Huang, C., and J. R. G. Townshend. 2003. A stepwise regression for nonlinear approximation: Applications to estimating subpixel land cover. *International Journal of Remote Sensing* 24:75–90.

Huang, C., B. Wylie, L. Yang, C. Homer, and G. Zylstra. 2002. Derivation of a tasselled cap transformation based on Landsat 7 at-satellite reflectance. *International Journal of Remote Sensing* 23:1741–1748.

Huang, S. C., and Y. F. Huang. 1991. Bounds on the number of hidden neurons in multilayer perceptron. *IEEE Transactions on Neural Networks* 2:47–55.

Huber, P. 1981. *Robust statistics*. New York: John Wiley and Sons.

Hughes, G. F. 1968. On the mean accuracy of statistical pattern recognizers. *IEEE Transactions on Information Theory* 14:55–63.

Hur, A. B., D. Horn, H. T. Siegelmann, and V. Vapnik. 2001. Support vector clustering. *Journal of Machine Learning Research* 2:125–137.

Hutchinson, C. F. 1982. Techniques for combining Landsat and ancillary data for digital classification improvement. *Photogrammetric Engineering and Remote Sensing* 48:123–130.

Ichoku, C., A. Karnieli, Y. Arkin, J. Chorowicz, T. Fleury, and J. P. Rudant. 1998. Exploring the utility potential of SAR interferometric coherence images. *International Journal of Remote Sensing* 19:1147–1160.

Ince, F. 1987. Maximum likelihood classification, optimal or problematic: A comparison with nearest neighbour classification. *International Journal of Remote Sensing* 8:1829–1838.

Ishibuchi, H., and T. Nakashima. 2001. Effect of rule weights in fuzzy rule-based classification systems. *IEEE Transactions on Fuzzy Systems* 9:506–515.

Ishibuchi, H., T. Nakashima, and T. Morisawa. 1999. Voting in fuzzy rule-based systems for pattern classification problems. *Fuzzy Sets and Systems* 103:223–238.

Ishibuchi, H., K. Nozaki, and H. Tanaka. 1992. Distributed representation of fuzzy rules and its application to pattern classification. *Fuzzy Sets and Systems* 52:21–32.

Ishibuchi, H., and T. Yamamoto. 2002. Comparison of heuristic rule weight specification methods. *Proceedings of the 2002 IEEE International Conference on Fuzzy Systems*, Honolulu, USA, 12–17 May 2002, 908–913.

Ishibuchi, H., and T. Yamamoto. 2004. Fuzzy rule selection by multi-objective genetic local search algorithms and rule evaluation measures in data mining. *Fuzzy Sets and Systems* 141:59–88.

Ising, E. 1925. Beitrag zur Theorie des Ferromagnetismus. *Zeitschrift Physik* 31:253–258.

Jaakkola, T. S., and D. Haussler. 1999. Probabilistic kernel regression models. In *Proceedings of the 1999 Conference M on AI and Statistics*.

Jackson, Q., and D. Landgrebe. 2001. An adaptive classifier design for high dimensional data analysis with a limited training data set. *IEEE Transactions on Geoscience and Remote Sensing* 39:2664–2679.

Jackson, R. D. 1983. Spectral indices in *n*-space. *Remote Sensing of Environment* 13:409–421.

Jacobsen, A., K. B. Heidebreacht, and A. A. Neilsen. 1998. Monitoring grasslands using convex geometry and partial unmixing—a case study. *1st EARSeL Workshop on Imaging Spectroscopy*, 6–8 October 1998, Remote Sensing Laboratories, University of Zurich, Switzerland, 309–316. Paris: EARSeL.

Jansen, L. L. F., M. N. Jarsma, and E. T. M. Linden. 1990. Integrating topographic data with remote sensing for land-cover classification. *Photogrammetric Engineering and Remote Sensing* 56:1503–1506.

Jansen, L. L. F., and F. J. M. Van de Wel. 1994. Accuracy assessment of satellite derived land cover data: A review. *Photogrammetric Engineering and Remote Sensing* 48:595–604.

Jaynes, E. 1982. On the rationale of maximum-entropy methods. *Proceedings of IEEE* 70:939–952.

Jensen, J. R. 1983. Urban change detection mapping using Landsat digital data. *The American Cartographer* 81:127–147.

Jensen, J. R. 1986. *Introductory digital image processing: A remote sensing perspective*. Englewood Cliffs, NJ: Prentice-Hall.

Jhung, Y., and P. H. Swain. 1996. Bayesian contextual classification based on modified M-estimates and Markov random fields. *IEEE Transactions on Geoscience and Remote Sensing* 34:67–75.

Ji, C., R. R. Snapp, and D. Psaltis. 1990. Generalising smoothness constraints from discrete samples. *Neural Computation* 2:188–197.

Jin, Y. Q., and C. Liu. 1997. Biomass retrieval from high-dimensional active/passive remote sensing data by using an artificial neural network. *International Journal of Remote Sensing* 18:971–979.

Joachims, T. 1999. Transductive inference for text categorization using support vector machines. In *Proceedings of ICML-99*, *16th International Conference on Machine Learning*, San Francisco, CA, Morgan Kaufmann, 200–209.

Johnson, R. D., and E. S. Kasischke. 1998. Change vector analysis: A technique for the multi-spectral monitoring of land cover and condition. *International Journal of Remote Sensing* 19:411–426.

Jones, K. 1998. A comparison of algorithms used to compute hill slope as a property of the DEM. *Computers and Geosciences* 24:315–323.

Ju, J., E. D. Kolaczyk, and S. Gopal. 2003. Gaussian mixture discriminant analysis and sub-pixel land cover characterization in remote sensing. *Remote Sensing of Environment* 84:550–560.

Kalluri, S. N. V., C. Huang, S. Mathieu, J. Townshend, K. Yang, and R. Chellapa. 1997. A comparison of mixture modelling algorithms and their applicability to MODIS data. *Proceedings of the IEEE International Geoscience and Remote Sensing Symposium (IGARSS'97)*, Singapore, August 3–8, 1997. Piscataway, NJ: IEEE, 1, 171–173.

Kanellopoulos, I., A. Varfis, G. G. Wilkinson, and J. Mégier. 1992. Land-cover discrimination in SPOT HRV imagery using an artificial neural network: A 20-class experiment. *International Journal of Remote Sensing* 13:917–924.

Kanellopoulos, I., and G. G. Wilkinson. 1997. Strategies and best practice for neural network image classification. *International Journal of Remote Sensing* 18:711–725.

Kanellopoulos, I., G. G. Wilkinson, F. Roli, and J. Austin (eds.). 1997. *Neurocomputation in remote sensing data analysis*. Berlin: Springer-Verlag.

Kangas, J. A., T. K. Kohonen, and J. T. Laaksonen. 1990. Variants of self-organising maps. *IEEE Transactions on Neural Networks* 1:93–99.

Karen, C., K. C. Seto, and W. Liu. 2003. Comparing ARTMAP neural network with maximum likelihood for detecting urban change: The effect of class resolution. *Photogrammetric Engineering and Remote Sensing* 69:981–990.

Karnin, E. D. (1990) A simple procedure for pruning back-propagation trained neural networks. *IEEE Transactions on Neural Networks* 1:239–242.

Karpouzli, E., and T. Malthus. 2003. The empirical line method for the atmospheric correction of IKONOS imagery. *International Journal of Remote Sensing* 24:1143–1150.

Kashyap, R. L., and R. Chellappa. 1983. Estimation and choice of neighbors in spatial-interaction models of images. *IEEE Transactions on Information Theory* 29:60–72.

Kass, G. V. 1980. An exploratory technique for investigating large quantities of categorical data. *Applied Statistics* 29:119–127.

Kauth, R. J., and G. Thomas. 1976. The tasselled cap—a graphic description of the spectral-temporal development of agricultural crops as seen by Landsat. In *Proceedings of the Symposium on Machine Processing of Remotely-Sensed Data 1976*, 4 B-41–4 B-51. West Lafayette, IN: Purdue University.

Kavzoglu, T. 2001. An investigation of the design and use of feed-forward artificial neural networks in the classification of remotely sensed images. Ph.D. thesis, School of Geography, The University of Nottingham.

Kavzoglu, T., and P. M. Mather. 1999. Pruning artificial neural networks: An example using land cover classification of multi-sensor images. *International Journal of Remote Sensing* 20:2787–2803.

Kavzoglu, T., and P. M. Mather. 2002. The role of feature selection in artificial neural network applications. *International Journal of Remote Sensing* 23:2919–2937.

Keller, J. M., and S. Chen. 1989. Texture description and segmentation through fractal geometry. *Computer Vision, Graphics and Image Processing* 45:150–166.

Keuchel, J., S. Naumann, M. Heiler, and A. Siegmun. 2003. Automatic land cover analysis for Tenerife by supervised classification using remotely sensed data. *Remote Sensing of Environment* 86:530–541.

Kim, B., and D. A. Landgrebe. 1991. Hierarchical classifier design in high-dimensional, numerous class cases. *IEEE Transactions on Geoscience and Remote Sensing* 29:518–528.

Kim, D. W., K. H. Lee, and D. Lee. 2004. On cluster validity index for estimation of the optimal number of fuzzy clusters. *Pattern Recognition* 37:2009–2025.

Kim, H., and P. H. Swain. 1995. Evidential reasoning approach to multisource-data classification in remote sensing. *IEEE Transactions on Systems, Man and Cybernetics* 25:1257–1265.

Kim, Y., and J. Van Zyl. 2000. Overview of polarimetric interferometry. In *Proceedings of IEEE Aerospace Conference*, 3, 231 –236, Big Sky, MT, March 18–25.

Kindermann, R., and J. L. Snell. 1980. *Markov random fields and their applications*. Providence, RI: American Mathematical Society.

Knerr, S., L. Personnaz, and G. Dreyfus. 1990. Single-layer learning revisited: A stepwise procedure for building and training neural network. In *Neurocomputing: Algorithms, architectures and applications*, ed. J. Fogelman, NATO ASI, 41–50. Berlin: Springer-Verlag,.

Kneubuehler, M., M. Shaepman, D. Schlaepfer, and C. Itten. 1998. Endmember selection procedures for partial spectral unmixing of DAIS 7915 imaging spectrometer data in highly vegetated areas. In *1st EARSeL Workshop on Imaging Spectroscopy*, 6–8 October 1998, Remote Sensing Laboratories, University of Zurich, Switzerland, 255–261. Paris: EARSeL.

Koch, C. 1988. Computing motion in the presence of discontinuities: Algorithm and analog networks. In *Neural computers*, ed. R. Eckmiller and C. D. Malsburg, Volume F41, NATO ASI Series, 101–110. Berlin: Springer-Verlag.

Kohavi, R., and G. H. John. 1997. Wrappers for feature subset selection. *Artificial Intelligence Journal* 97:273–324.

Kohonen, T. 1982. Self-organized formation of topologically correct feature maps. *Biological Cybernetics* 43:59–69.

Kohonen, T. 1988a. An introduction to neural computing. *Neural Networks* 1:3–16.

Kohonen, T. 1988b. The "neural" phonetic typewriter. *Computer* 21:11–22.

Kohonen, T. 1989. *Self-organization and associative memory*. New York: John Wiley and Sons.

Kolmogorov, A. N., and S. V. Fomin. 1970. *Introductory real analysis*. Englewood Cliffs, NJ: Prentice-Hall, Inc.

Kosko, B. 1992. *Neural networks and fuzzy systems*. Englewood Cliffs, NJ: Prentice Hall.

Kowalik, W. S., and S. E. Marsh. 1982. A relation between Landsat Digital Numbers, surface reflectance and the cosine of the solar zenith angle. *International Journal of Remote Sensing* 12:39–55.

Kraaijveld, M. A., J. Mao, and A. K. Jain. 1995. A nonlinear projection method based on Kohonen's topology preserving maps. *IEEE Transactions on Neural Networks* 6:548–558.

Kriegel, H. P., R. Kroger, A. Pryakhin, and M. Schubert. 2004. Using support vector machines for classifying large sets of multi-represented objects. In *Proceedings of the International Conference on Data Mining (SDM'04)*, 102–114.

Krishnapuram, R., and J. M. Keller. 1993. A possibilitic approach to clustering. *IEEE Transactions on Fuzzy Systems* 1:98–110.

Krishnapuram, R., and J. M. Keller. 1996. The possibilitic *c*-means algorithm: Insights and recommendations. *IEEE Transactions on Fuzzy Systems* 4:385–393.

Kropatsch, W. G., and D. Strobl. 1990. The generation of SAR layover and shadow maps from digital elevation models. *IEEE Transactions on Geoscience and Remote Sensing* 28:98–107.

Kuan, D. T., A. A. Sawchuk, T. C. Strand, and P. Chavel. 1987. Adaptive restoration of images with speckle. *IEEE Transactions on Acoustics, Speech and Signal Processing* 35:373–383.

Kuemmerle, T., A. Röder, and J. Hill. 2006. Separating grassland and shrub vegetation by multidate pixel-adaptive spectral mixture analysis. *International Journal of Remote Sensing* 27:3251–3271.

Kulkarni, A. V., and N. K. Laveen. 1976. An optimisation approach to hierarchical classifier design. In *Proceedings of the Third International Joint Conference on Pattern Recognition*, IEEE Catalogue No. 76CH1140-3C, 459–466. Piscataway, NJ: IEEE.

Kurzynski, M. W. 1983. The optimal strategy of a tree classifier. *Pattern Recognition* 16:81–87.

Kwarteng, A. Y., and P. S. Chavez. 1998. Change detection study of Kuwait City and environs using multitemporal Landsat Thematic Mapper data. *International Journal of Remote Sensing* 19:1651–1662.

Kwok, R. J., J. C. Curlander, and S. Pang. 1987. Rectification of terrain induced distortions in radar imagery. *Photogrammetric Engineering and Remote Sensing* 53:507–513.

Lam, H. K., and F. H. F. Leung. 2007. Fuzzy controller with stability and performance rules for nonlinear systems. *Fuzzy Sets and Systems* 158:147–163.

Lambin, E. F., and A. H. Strahler. 1994. Change vector analysis in multitemporal space: A tool to categorise land-cover change processes using high-temporal-resolution satellite data. *Remote Sensing of Environment* 48:231–244.

Lanari, R., G. Fornaro, D. Riccio, M. Migliaccio, K. P. Papathanassiou, J. R. Moreira, M. Schwäbisch, L. Dutra, G. Puglisi, G. Franceschetti, and M. Coltelli. 1996. Generation of digital elevation models by using SIR-C/X-SAR multifrequency two-pass interferometry: The Etna case study. *IEEE Transactions on Geoscience and Remote Sensing* 34(5):1097–1114.

Landgrebe, D. 1998. Information extraction principles and methods for multispectral and hyperspectral image data. In *Information processing for remote sensing*, ed. C. H. Chen. River Edge, NJ: World Scientific Publishing.

Law, K. H., and J. Nichol. 2004. Topographic correction for differential illumination effects on IKONOS satellite imagery. In *Proceedings of 20th ISPRS Congress,* Istanbul, Turkey, 12–23 July 2004. 35-B3, 641–646.

Le Cun, Y., J. S. Decker, and S. A. Solla. 1999. Optimal brain damage. In *Advances in neural information processing 5*, ed. D. S. Touresky, 598–605. San Mateo, CA: Morgan Kaufmann.

Le Hegarat-Mascle, S., R. Seltz, L. Hubert-Moy, S. Corgne, and N. Stach. 2006. Performance of change detection using remotely sensed data and evidential fusion: Comparison of three cases of application. *International Journal of Remote Sensing* 27(16):3515–3532.

Lee, B. W., and B. J. Sheu. 1991. Modified Hopfield neural networks for retrieving the optimal solution. *IEEE Transactions on Neural Networks* 2:137–142.

Lee, J., R. C. Weger, S. K. Sengupta, and R. M. Welch. 1990. A neural network approach to cloud classification. *IEEE Transactions on Geoscience and Remote Sensing* 28:846–855.

Lee, J. B., A. S. Woodyatt, and M. Berman. 1990. Enhancement of high spectral resolution remote sensing data by noise-adjusted principal components transform. *IEEE Transactions on Geoscience and Remote Sensing* 28:295–304.

Lee, J. S. 1980. Digital image enhancement and noise filtering by use of local statistics. *IEEE Transactions on Pattern Analysis and Machine Intelligence* 2:165–168.

Lee, J. S. 1981. Speckle suppression and analysis for synthetic aperture radar images. *Optical Engineering* 15:380–389.

Lee, J. S. 1986. Speckle suppression and analysis for synthetic aperture radar. *Optical Engineering* 25:636–643.

Lee, S., and R. G. Lathrop. 2005. Sub-pixel estimation of urban land cover components with linear mixture model analysis and Landsat Thematic Mapper imagery. *International Journal of Remote Sensing* 26:4885–4905.

Lee, S., and R. G. Lathrop. 2006. Subpixel analysis of Landsat ETM+ using self-organizing map (SOM) neural network for urban land cover characterisation. *IEEE Transactions on Geoscience and Remote Sensing* 44(6):1642–1654.

Lee, T., and J. A. Richards. 1985. A low-cost classifier for multitemporal applications. *International Journal of Remote Sensing* 6:1405–1417.

Lee, T., J. A. Richards, and P. H. Swain. 1987. Probabilistic and evidential approaches for multisource data analysis. *IEEE Transactions on Geoscience and Remote Sensing* 25:283–293.

Lewis, H. G., S. Côté, and A. R. L. Tatnall. 1997. Determination of spatial and temporal characteristics as an aid to neural network cloud classification. *International Journal of Remote Sensing* 18:899–915.

Li, L., S. L. Ustin, and M. Lay. 2005. Application of multiple endmember spectral mixture analysis (MESMA) to AVIRIS imagery for coastal salt marsh mapping: A case study in China Camp, CA, USA. *International Journal of Remote Sensing* 26:5193–5207.

Li, S. Z. 1990. Invariant surface segmentation through energy minimization with discontinuities. *International Journal of Computer Vision* 5:161–194.

Li, S. Z. 1995a. Markov random field modelling in computer vision. In *Computer science workbench*, ed. T. L. Kunii. Berlin: Springer-Verlag.

Li, S. Z. 1995b. On discontinuity-adaptive smoothness priors in computer vision. *IEEE Transactions on Pattern Analysis and Machine Intelligence* 17:576–586.

Lillesand, T. M., and R. W. Keifer. 2000. *Remote sensing and image interpretation*. New York: John Wiley and Sons.

Lim, C., and M. Kafatos. 2002. Frequency analysis of natural vegetation distribution using NDVI/AVHRR data from 1981 to 2000 for North America: Correlations with SOI. *International Journal of Remote Sensing* 23:3347–3383.

Liu, D., M. Kelly, and P. Gong. 2006. A spatial-temporal approach to monitoring forest disease spread using multi-temporal high spatial resolution imagery. *Remote Sensing of Environment* 101:167–180.

Liu, W., K. C. Seto, E. Y. Wu, S. Gopal, and C. E. Woodcock. 2004. ART-MAP: A neural network approach to subpixel classification. *IEEE Transactions on Geoscience and Remote Sensing* 42:1976–1983.

Liu, W., and E. Y. Wu. 2005. Comparison of non-linear mixture models: Sub-pixel classification. *Remote Sensing of Environment* 94(2):145–154.

Liu, Y., S. Nishiyama, and Y. Tomohisa. 2004. Analysis of four change detection algorithms in bi-temporal space with a case study. *International of Remote Sensing* 25:2121–2139.

Liu, Z., A. Liu, C. Wang, and S. Qi. 2004. Statistical ratio rank-ordered differences filter for radar speckle removal. *Proceedings of the SPIE* 5238:524–531.

Lloyd, C. D., S. Berberoglu, P. J. Curran, and P. M. Atkinson. 2004. A comparison of texture measures for the per-field classification of Mediterranean land cover. *International Journal of Remote Sensing* 25:3943–3965.

Loh, W. Y., and Y. S. Shih. 1997. Split selection methods for classification trees. *Statistica Sinica* 7:815–840.

Lopes, A., E. Nezry, and R. Touzi. 1990. Maximum a posteriori speckle filtering and first order texture models in SAR images. In *Proceedings of the International Geoscience and Remote Sensing Symposium (IGARSS'90),* University of Maryland, College Park, MD, 20–24 May 1990, 3, 2409–2412. Piscataway, NJ: IEEE.

Lopez-Martinez, C., and X. Fabregas. 2003. Polarimetric SAR speckle model. *IEEE Transactions on Geosciences and Remote Sensing* 41:2232–2242.

Lu, C. S., P. C. Chung, and C. F. Chen. 1997. Unsupervised texture segmentation via wavelet transform. *Pattern Recognition* 30:729–742.

Lu, D., P. Mausel, M. Batistella, and E. Moran. 2005. Land-cover binary change detection methods for use in the moist tropical region of the Amazon: A comparative study. *International Journal of Remote Sensing* 26(1):101–114.

Lu, D., P. Mausel, E. Brondizio, and E. Moran. 2004. Change detection techniques. *International Journal of Remote Sensing* 25:2365–2407.

Luntz, A., and V. Brailovsky. 1969. On estimation of characters obtained in statistical procedure of recognition. *Technicheskaya Kibernetica*, 3 (in Russian).

Lyon, J., D. Yuan, R. Lunetta, and C. Elvidge. 1998. A change detection experiment using vegetation indices. *Photogrammetric Engineering and Remote Sensing* 64:143–150.

Mackay, G., M. D. Steven, and J. A. Clarke. 1994. A pseudo-5S code for atmospheric correction of ATSR-2 visible and near-IR land-surface data. In *Proceeding of the 6th International Symposium—Physical Measurements and Signatures in Remote Sensing*, Val d'lsère, France, 17–21st January, 103–110.

Macleod, R. B., and R. G. Congalton. 1998. A quantitative comparison of change-detection algorithms for monitoring eelgrass from remotely sensed data. *Photogrammetric Engineering and Remote Sensing* 64:207–216.

Magnussen, S., P. Boudewyn, and M. Wulder. 2004. Contextual classification of Landsat TM images to forest inventory cover types. *International Journal of Remote Sensing* 25:2421–2440.

Mali, K., and S. Mitra. 2005. Symbolic classification, clustering and fuzzy radial basis function network. *Fuzzy Sets and Systems* 152:553–564.

Malila, W. 1980. Change vector analysis an approach for detection forest changes with Landsat. In *Proceedings of the 6th Annual Symposium on Machine Processing of Remotely Sensed Data,* 3–6 June 1980, 326–335. West Lafayette, IN: Purdue University Press.

Mallat, S. G. 1989. A theory for multi-resolution signal decomposition: The wavelet representation. *IEEE Transactions on Pattern Analysis and Machine Intelligence* 11, 674–693.

Mallat, S., and S. Zhong. 1992. Characterization of signals from multiscale edges. *IEEE Transactions on Pattern Analysis and Machine Intelligence* 8:679–698.

Mandelbrot, B. B. 1977. *Fractals: Form, chance and dimension*. San Francisco. CA: Freeman.

Mandelbrot, B. B. 1982. *The fractal geometry of nature*. San Francisco, CA: Freeman.

Mannan, B., J. Rot, and A. K. Ray. 1998. Fuzzy ARTMAP supervised classification of multispectral remotely-sensed images. *International Journal of Remote Sensing* 19:767–774.

Marceau, D. J., and G. J. Hay. 1999. Remote sensing contributions to the scale issue. *Canadian Journal of Remote Sensing* 25:357–366.

Marceau, D. J., P. J. Howarth, and D.J. Gratton. 1994. Remote sensing and the measurement of geographical entities in a forested environment. Part I: The scale and spatial aggregation problem. *Remote Sensing of Environment* 49:93–104.

Marroquin, J. L., J. S. Mitter, and T. Poggio. 1987. Probabilistic solution of ill-posed problems in computational vision. *Journal of the American Statistical Association* 82:76–89.

Marsh, S. E., P. Switzer, W. S. Kowalik, and R. J. Lyon. 1980. Resolving the percentage of component terrains within single resolution elements. *Photogrammetric Engineering and Remote Sensing* 46:1079–1086.

Martin, R. S., and J. H. Wilkinson. 1971. Reduction of the symmetric eigenproblem $Ax = \lambda Bx$ and related problems to standard form. In *Handbook for automatic computation, volume II: Linear algebra*, ed. J. H. Wilkinson and C. Reinch, 303–314. Berlin: Springer-Verlag,.

Maselli, F., C. Conese, T. De Filippis, and S. Norcini. 1995. Estimation of forest parameters through fuzzy classification of TM data. *IEEE Transactions on Geoscience and Remote Sensing* 33:77–84.

Mason, D. C., D. G. Corr, A. Cross, D. C. Hogg, D. H. Lawrence, M. Petrou, and A. M. Taylor. 1988. The use of digital map data in the segmentation and classification of remotely-sensed images. *International Journal of Geographical Information Systems* 2:195–215.

Massonnet, D., and T. Rabaute. 1993. Radar interferometry: Limits and potential. *IEEE Transactions on Geoscience and Remote Sensing* 31:45–464.

Massonnet, D., M. Rossi, C. Carmona, F. Adragna, G. Peltzer, K. Feigi, and T. Rabaute. 1993. The displacement field of the Landers earthquake mapped by radar interferometry. *Nature* 364:138–142.

Mather, P. M. 1976. *Computational Methods of Multivariate Analysis in Physical Geography*. Chichester: John Wiley and Sons.

Mather, P. M. 1985. A computationally-efficient maximum-likelihood classifier employing prior probabilities for remotely-sensed data. *International Journal of Remote Sensing* 6:369–376.

Mather, P. M. 1987. Pre-processing of training data for multispectral image classification. In *13th Annual Conference of the Remote Sensing Society*, Nottingham, England, 111–120.

Mather, P. M. 1992. Remote sensing and the detection of change. In *Land use change: The cause and consequences. ITE Symposium Proceedings No. 27,* ed. M. C. Whitby, 60–68.

Mather, P. M. 1999. Land cover classification revisited. In *Advances in remote sensing and GIS analysis*, ed. P. M. Atkinson and N. J. Tate, 7–16. Chichester: John Wiley and Sons.

Mather, P. M. 2004. *Computer processing of remotely-sensed images: An introduction*, 3rd edition. Chichester: John Wiley and Sons.

Mather, P. M., B. Tso, and M. Koch. 1998. An evaluation of combining spectral and textural information for lithological classification. *International Journal of Remote Sensing* 19:587–604.

Mathieu-Marni, S., P. Leymarie, and M. Berthod. 1996. Removing ambiguities in a multispectral image classification. *International Journal of Remote Sensing* 17:1493–1504.

Mausel, P. W., W. J. Kramber, and J. K. Lee. 1990. Optimum band selection for supervised classification of multispectral data. *Photogrammetric Engineering and Remote Sensing* 56:55–60.

McConway, K. J. 1980. The combination of experts' opinions in probability assessment: Some theoretical considerations, Ph.D. thesis, University College London.

McCulloch, W. S., and W. Pitts. 1943. A logical calculus of the ideas imminent in nervous activity. *Bulletin of Mathematical Biophysics* 5:115–133.

Mégier, J., W. Mehl, and R. Ruppelt. 1984. Per-field classification and application to SPOT simulated SAR and combined SAR-MSS data. In *18th International Symposium on Remote Sensing of Environment*. Ann Arbor, MI: Environmental Research Institute of Michigan, 1011–1017.

Mehrotra, K. G., C. K. Mohan, and S. Ranka. 1991. Bounds on the number of samples needed for neural learning. *IEEE Transactions on Neural Networks* 2:548–558.

Metropolis, N., A. W. Rosenbluth, M. N. Rosenbluth, A. H. Teller, and E. Teller. 1953. Equations of state calculations by fast computational machine. *Journal of Chemical Physics* 21:1087–1091.

Metternicht, G. I., and A. Fermont. 1998. Estimating erosion surface features by linear mixture modelling. *Remote Sensing of Environment* 12:1887–1903.

Meygret, A. 2005. Absolute calibration: From SPOT1 to SPOT5. *Proceedings of SPIE* 5882:335–346.

Michalek, J. L., T. Wagner, J. J. Luczkovich, and R. W. Stoffle. 1993. Multispectral change vector analysis for monitoring coastal marine environments. *Photogrammetric Engineering and Remote Sensing* 59:381–384.

Michie, D., D. J. Spiegelhalter, and C. C. Taylor. 1994. *Machine learning, neural and statistical classification*. Chichester, U.K.: Ellis Horwood.

Miller, A. J. 1990. *Subset selection in regression*. New York: Chapman & Hall.

Miller, J. W. V., J. B. Farison, and Y. Shin. 1992. Spatially invariant image sequences. *IEEE Transactions on Image Processing* 1:148–161.

Milne, A. K. 1988. Change detection analysis using Landsat imagery: A review of methodology. *Proceedings of the IGARSS'88 Symposium*, Edinburgh, Scotland, ESA SP-284, 541–544.

Minnaert, M. 1941. The reciprocity principle in Lunar photometry. *Astrophysics Journal* 93:403–410.

Moran, M. S., R. Bryanta, K. Thomeb, W. Nia, and Y. Nouvellona. 2001. A refined empirical line approach for reflectance factor retrieval from Landsat-5 TM and Landsat-7 ETM+. *Remote Sensing of Environment* 78:71–82.

Moussouris, J. 1974. Gibbs and Markov systems with constraints. *Journal of Statistical Physics* 10:11–33.

Muchoney, D., J. Borak, H. Chi, M. Friedl, S. Gopal, J. Hodges, N. Morrow, and A. H. Strahler. 2000. Application of MODIS global supervised classification model to vegetation and land cover mapping in Central America. *International Journal of Remote Sensing* 21:1115–1138.

Muchoney, D. M., and B. N. Haack. 1994. Change detection for monitoring forest defoliation. *Photogrammetric Engineering and Remote Sensing* 60:1243–1251.

Murphy, S. K., F. Kasif, and S. Salzberg. 1994. A system for induction of oblique decision trees. *Journal of Artificial Intelligence Research* 2:1–32.

Mustard, J. F. 1993. Relationships of soil, grass and bedrock over the Kameah Serpentine Melange through spectral mixture analysis of AVIRIS data. *Remote Sensing of Environment* 44:293–308.

Nackaerts, K., K. Caesen, B. Muys, and P. Coppin. 2005. Comparative performance of a modified change vector analysis in forest change detection. *International Journal of Remote Sensing* 26:839–852.

Nelson, R. F. 1983. Detecting forest canopy change due to insect activity using Landsat MSS. *Photogrammetric Engineering and Remote Sensing* 49:1303–1314.

Nemmour, H., and Y. Chibani. 2006. Fuzzy neural network architecture for change detection in remotely sensed imagery. I*nternational Journal of Remote Sensing* 27:705–717.

Nezry, E., A. Lopes, and R. Touzi. 1991. Detection of structure and textural features for SAR images filtering. *Proceedings of the International Geoscience and Remote Sensing Symposium (IGARSS'91)*, Espoo, Finland, June 03–6, 1991, 3, 2169–2172. Piscataway, NJ: IEEE.

Nielsen, A. A. 1994. Analysis of regularly and irregularly sampled spatial, multivariate and multi-temporal data. Ph.D. thesis, Institute of Mathematical Modelling, Technical University of Denmark, Lyngsby, Denmark.

Nielsen, A. A. 1998. Linear mixture modelling and partial unmixing in multi- and hyperspectral data. In *EARSeL Workshop on Imaging Spectroscopy, University of Zurich, 6–8 October 1988*, 165–172. Paris: EARSeL.

Neilsen, A. A., K. Conradsen, and J. J. Simpson. 1998. Multivariate Alteration Detection (MAD) and MAF post-processing in multispectral, bi-temporal image data: New approaches to change detection studies. *Remote Sensing of Environment* 64:1–19.

Nikhil, R.P., and J. C. Bezdek. 1995. On cluster validity for the fuzzy c-means model. *IEEE Transactions on Fuzzy Systems* 3(3):370–379.

Nishii, R., and S. Eguchi. 2005. Supervised image classification by contextual AdaBoost based on posteriors in neighbourhoods. *IEEE Transactions on Geoscience and Remote Sensing* 43:2547–2554.

Núñez, J., X. Otazu, O. Fors, A. Prades, V. Palá, and R. Arbiol. 1999. Multiresolution-based image fusion with additive wavelet decomposition. *IEEE Transactions on Geoscience and Remote Sensing* 37:1204–1211.

Olsen, S. I. 1993. Estimation of noise in images: An evaluation. *Graphical Models and Image Processing* 55:319–323.

Opper, M., and O. Winter. 2000. Gaussian processes and SVM: Mean field and leave-one-out. In *Advances in Large Margin Classifiers,* ed.A. J. Smola, P. L. Bartlett, B. Schölkopf, and D. Schuurmans, 311–326. Cambridge, MA: MIT Press.

Ouaidrari, H., and E. F. Vermote. 2001. Operational atmospheric correction of Landsat TM data. *Remote Sensing of Environment* 70:4–15.

Ouma, Y. O., T. G. Ngigi, and R. Tateishi. 2006. On the optimization and selection of wavelet texture for feature extraction from high-resolution satellite imagery with application towards urban-tree delineation. *International Journal of Remote Sensing* 27:73–104.

Pal, M. 2005. Random forest classifiers for remote sensing classification. *International Journal of Remote Sensing* 26:217–222.

Pal, M. 2006. Support vector machine-based feature selection for land cover classification: A case study with DAIS hyperspectral data. *International Journal of Remote Sensing* 27:2877–2894.

Pal, M., and P. M. Mather. 2003. An assessment of the effectiveness of decision tree methods for land cover classification. *Remote Sensing of Environment* 86:554–565.

Pal, M., and P. M. Mather. 2005. Support vector machines for classification in remote sensing. *International Journal of Remote Sensing* 26:1007–1011.

Pal, M., and P. M. Mather. 2006. Some issues in the classification of DAIS hyperspectral data. *International Journal of Remote Sensing* 27:2895–2916.

Pal, N. R., and J. C. Bezdek. 1995. On cluster validity for fuzzy c-means model. *IEEE Transactions on Fuzzy Systems* 3:370–379.

Pal, N. R., and J. C. Bezdek. 1997. Correction to "On cluster validity for fuzzy c-means model." *IEEE Transactions on Fuzzy Systems* 5:152–153.

Pal, N. R., J. C. Bezdek, and C. K. Tsao. 1993. Generalised clustering networks and Kohonen's self-organising scheme. *IEEE Transactions on Neural Networks* 4:549–557.

Pal, N. R., A. Laha, and J. Das. 2005. Designing fuzzy rule based classifier using self-organizing feature map for analysis of multispectral satellite images. *International Journal of Remote Sensing* 26:2219–2240.

Pal, S. K., and S. Mitra. 1992. Multilayer perceptron, fuzzy sets and classification. *IEEE Transactions on Neural Networks* 3:683–697.

Paola, J. D., and R. A. Schowengerdt. 1995. A review and analysis of backpropagation neural networks for classification of remotely-sensed multi-spectral imagery. *International Journal of Remote Sensing* 16:3033–3058.

Papoulis, A. 1991. *Probability random variables and stochastic processes*. New York: John Wiley and Sons.

Parisi, G. 1988. *Statistical field theory*. Reading MA: Addison-Wesley.

Parisi, G., and U. Frish. 1985. A multifractal model of intermittency. In *Turbulence and predictability in geophysical fluid dynamics and climate dynamics*, ed. M. Ghil, 84–89. New York: North Holland.

Park, C. H., H. Park, and P. Pardalos. 2004. A comparative study of linear and nonlinear feature extraction methods. In *Proceedings of the Fourth IEEE International Conference on Data Mining (ICDM'04)*, 1–4 November, Brighton, U.K., 495–498.

Pecknold, S., S. Lovejoy, D. Scherter, and C. Hooge. 1997. Multifractals and resolution dependence of remotely sensed data: GSI to GIS. In *Scale in remote sensing and GIS*, ed. D. A. Quattrochi and M. F. Goodchild, 361–394. New York: Lewis Publishers.

Peddle, D. R., and A. M. Smith. 2005. Spectral mixture analysis of agricultural crops: Endmember validation biophysical estimation in potato plots. *International Journal of Remote Sensing* 26(22):4959–4979.

Pedrycz, W. 1989. *Fuzzy control and fuzzy systems*. New York: John Wiley and Sons.

Peleg, S., J. Naor, R. Hartley, and D. Avnir. 1984. Multiple resolution texture analysis and classification. *IEEE Transactions on Pattern Analysis and Machine Intelligence* 6:1984, 518–523.

Pena, J. M., J. A. Lozano, and P. Larranaga. 1999. An empirical comparison of four initialization methods for the k-means algorithm. *Pattern Recognition Letters* 20:1027–1040.

Pentland, A. P. 1984. Fractal based description of natural scenes. *IEEE Transactions on Pattern Analysis and Machine Intelligence* 6:661–674.

Pickard, D. K. 1980. Unilateral Markov fields. *Advance in Applied Probability*, 12:655–671.

Pierce, L. E., F. T. Ulaby, K. Sarabandi, and M. C. Dobson. 1994. Knowledge-based classification of polarimetric SAR images. *IEEE Transactions on Geoscience and Remote Sensing* 33(5):1081–1086.

Pizurica, A., W. Philips, I. Lemahieu, and M. Acheroy. 2001. Despeckling SAR images using wavelets and a new class of adaptive shrinkage estimators. In *Proceedings of IEEE International Conference on Image Processing*, Thessaloniki, Greece, 7–10 October 2001, 233–236.

Platt, J. C., N. Cristianini, and Shawe-Taylor. 2000. Large margin DAGs for multiclass classification. In *Advances in Neural Information Processing Systems*, 547–553. Cambridge, MA: MIT Press.

Prasad, N., S. Saran, S. P. S. Kushwaha, and P. S. Roy. 2001. Evaluation of various image fusion techniques and imaging scales for forest features interpretation. *Research Communication* 81:1218–1224.

Preiss, M., D. Gray, and N. Stacy. 2003. A change detection statistic for repeat pass interferometric SAR. In *Proceedings of IEEE International Conference on Acoustics, Speech and Signal Processing (ICASSP 2003)*, April 6 – 10 2003, Hong Kong. 5, 241–244.

Puissant, A. J. Hirsch, and C. Weber. 2005. The utility of texture analysis to improve per-pixel classification for high to very high spatial resolution imagery. *International Journal of Remote Sensing* 26:733–745.

Puyou-Lacassies, P. H., G. Flouzat, M. Gay, and C. Vignolles. 1994. Validation of the use of multiple linear regression as a tool for unmixing coarse spectral resolution images. *Remote Sensing of Environment* 49:155–166.

Qing-Yun, N, S., and K. S. Fu. 1983. A method for design of binary tree classifiers. *Pattern Recognition* 16:593–603.

Quattrochi, D. A., and M. A. Goodchild, eds. 1997. *Scale in remote sensing and GIS*. New York: Lewis Publishers.

Quinlan, J. R. 1979. Discovering rules by induction from large collections of examples. In *Expert systems in the micro-electronic age*, ed. D. Michie, 168–201. Edinburgh, Scotland: Edinburgh University Press.

Quinlan, J. R. 1986. Induction of decision trees. *Machine Learning* 1:81–106.

Quinlan, J. R. 1993. *C4.5: Algorithm for machine learning*. San Mateo: Morgan Kaufmann.

Quinlan, J. R. 1996. Bagging, boosting and C4.5. In *Thirteenth National Conference on Artificial Intelligence*, 725–730. Portland, OR: American Association for Artificial Intelligence.

Quintano, C., A. Fernández-Mando, O. Fernández-Manso, and Y. E. Shimabukuro. 2006. Mapping burned areas in Mediterranean countries using spectral mixture analysis from a uni-temporal perspective. *International Journal of Remote Sensing* 27:645–662.

Radeloff, V., D. Mladenoff, and M. Boyce. 1999. Detecting jack pine budworm defoliation using spectral mixture analysis: Separating effects from determinants. *Remote Sensing of Environment* 69:156–169.

Ramstein, G., and M. Raffy. 1989. Analysis of the structure of radiometric remotely-sensed images. *International Journal of Remote Sensing* 10:1049–1073.

Rashed, T., J. R. Weeks, D. Stow, and D. Fugate. 2005. Measuring temporal compositions of urban morphology through spectral mixture analysis: Toward a soft approach to change analysis in crowded cities. *International Journal of Remote Sensing* 26(4):699–718.

Raudys, S., and V. Pikelis. 1980. On dimensionality, sample size, classification error and complexity of classification algorithms in pattern recognition. *IEEE Transactions on Pattern Analysis and Machine Intelligence* 2:242–252.

Ray, T. W., and B. C. Murray. 1996. Non-linear mixing in desert vegetation. *Remote Sensing of Environment* 55:59–64.

Reed, R. 1993. Pruning algorithms—a survey. *IEEE Transactions on Neural Networks* 4:740–747.

Reeves, S. J. 1992. A cross-validation framework for solving image restoration problems. *Journal of Visual Communication and Image Representation* 3:433–445.

Reillt, D. L., L. N. Cooper, and C. Elbaum. 1982. A neural model for category learning. *Biological Cybernetics* 45:35–41.

Riano, D., E. Chuvieco, J. Salas, and I. Aguado. 2003. Assessment of different topographic corrections in Landsat-TM data for mapping vegetation types. *IEEE Transactions on Geoscience and Remote Sensing* 41:1056–1061.

Ricchetti, E. 2000. Multispectral satellite image and ancillary data integration for geological classification. *Photogrammetric Engineering and Remote Sensing* 66:429–436.

Richards, J. A. 1986. *Remote sensing digital image analysis: An introduction*. Berlin: Springer-Verlag.

Riegler, G., and W. Mauser. 1998. Geometric and radiometric terrain correction of ERS SAR data for applications in hydrologic modelling. In *Proceedings of the International Geoscience and Remote Sensing Symposium* (*IGARSS'98)*, Seattle, WA, July 6–10, 1998, 2603–2605. Piscataway, NJ: IEEE.

Ripley, B. D. 1996. *Pattern recognition and neural networks*. Cambridge: Cambridge University Press.

Ritter, H., and K. Schulten. 1988. Convergence properties of Kohonen's topology conserving maps: Fluctuations, stability and dimension selection. *Biological Cybernetics* 60:59–71.

Roberts, D. A., M. Gardner, R. Church, S. L. Ustin, G. Scheer, and R. O. Green. 1998. Mapping Chaparral in the Santa Monica Mountains using multiple endmember spectral mixture models. *Remote Sensing of Environment* 65:267–279.

Robinson, G. D., H. N. Gross, and J. R. Schott. 2000. Evaluation of two applications of spectral unmixing models to image fusion. *Remote Sensing of Environment* 71:272–281.

Roli, F., G. Giacinto, and G. Vernazza. 1997. Comparison and combination of statistical and neural net algorithms for remote sensing image classification. In *Neurocomputation in remote sensing data analysis,* ed. I. Kanellopoulos, G. G. Wilkinson, G. G. Roli, and J. Austin, 117–124. Berlin: Springer-Verlag.

Rosenblatt, R. 1959. *Principles of neurodynamics*. New York, Spartan Books.

Rosenfield, G. 1981. Analysis of variance of thematic mapping experiment data. *Photogrammetric Engineering and Remote Sensing* 47:1685–1692.

Rosenfield, G. H., K. Fitzpatrick-Lins, and H. S. Ling. 1982. Sampling for thematic map accuracy testing. *Photogrammetric Engineering and Remote Sensing* 48:131–137.

Rosin, P. L., and J. Hervás. 2005. Remote sensing image thresholding methods for determining landslide activity. *International Journal of Remote Sensing* 26(6):1075–1092.

Rumelhart, D. E., G. E. Hinton, and R. J. Williams. 1986a. Learning internal representation by error propagation. In *Parallel distributed processing: Explorations in the microstructures of cognition*, 318–362. Cambridge, MA: MIT Press.

Rumelhart, D. E., G. E. Hinton, and R. J. Williams. 1986b. Learning representations by back-propagating errors. *Nature* 323:533–536.

Sá, A. C. L., J. M. C. Pereira, M. J. P. Vasconcelos, J. M. N. Silva, N. Ribeiro, and A. Awasse. 2003. Assessing the feasibility of sub-pixel burned area mapping in Miombo woodlands of northern Mozambique using MODIS imagery. *International Journal of Remote Sensing* 24(8):1783–1796.

Sabol, D. E., A. R. Gillespie, J. B. Adams, M. O. Smith, and C. J. Tucker. 2002. Structural stage in Pacific Northwest forests estimated using simple mixing models of multispectral images. *Remote Sensing of Environment* 80:1–16.

Safavian, S. R., and D. Landgrebe. 1991. A survey of decision tree classifier methodology. *IEEE Transactions on Systems, Man and Cybernetics* 21*:*660–674.

Saguib, S. S., C. A. Bouman, and K. Sauer. 1998. ML parameter estimation for Markov random fields with applications to Bayesian tomography. *IEEE Transactions on Image Processing* 7:1029–1044.

Salford Systems. 2008. CART overview. http://www.Salford-systems.com/cart.php. (Accessed 20 December 2008.)

Sali, E., and H. Wolfson. 1992. Texture classification in aerial photographs and satellite data. *International Journal of Remote Sensing* 13:3395–3408.

Sarkar, N., and B. B. Chaudhuri. 1994. An efficient differential box-counting approach to compute the fractal dimension of images. *IEEE Transactions on Systems, Man and Cybernetics* 24:115–120.

Sarle, W. S. 2000. *Neural network frequently asked questions,* ftp://ftp.sas.com/pub/neural/FAQ.html (accessed 15 May 2008).

Schaale, M., and R. Furrer. 1995. Land surface classification by neural networks. *International Journal of Remote Sensing* 16:3003–3031.

Schaffer, C. 1993. Selecting a classification method by cross validation. *Machine Learning* 13:135–143.

Schapire, R. E., and Y. Singer. 1998. BoosTexter: A system for multiclass multi-label text categorization. *Machine Learning* 39:135–168

Schepers, J. 2004. Integrating remote sensing and ancillary information into management systems. In *Remote sensing for agriculture and the environment*, ed. S. Stamadiadis, J. M. Lynch, and J. S. Schepers, 254–259. Larissa Greece: Peripheral Editions.

Schistad, A. H., A. K. Jain, and T. Taxt. 1994. Multisource classification of remotely sensed data: Fusion of Landsat TM and SAR images. *IEEE Transactions on Geoscience and Remote Sensing* 32:768–778.

Schistad, A. H., T. Taxt, and A. K. Jain. 1996. A Markov random field model for classification of multisource satellite imagery. *IEEE Transactions on Geoscience and Remote Sensing* 34:100–113.

Schouten, T. E., and M. S. Klein Gebbinck. 1997. A neural net approach to spectral mixture analysis. In *Neurocomputation in remote sensing data analysis*, ed. I. Kanellopoulos, G. G. Wilkinson, F. Roli, and J. Austin, 79–85. Berlin: Springer-Verlag.

Schowengerdt, R. A. 1983. *Techniques for image processing and classification in remote sensing*. New York: Academic Press.

Schowengerdt, R. A. 1996. Soft classification and spectral-spatial mixing. In *Soft computing in remote sensing data analysis*, ed. E. Binaghi, P. A. Brivio, and A. Rampini, 1–6. Singapore: World Scientific.

Schowengerdt, R. A. 1998. *Remote sensing: Models and methods for image processing.* New York: Academic Press.

Schröder, M., M. Walessa, H. Rehrauer, K. Seidel, and M. Datcu. 2000. Gibbs random field models: A toolbox for spatial information extraction. *Computers and Geosciences* 26:423–432.

Serneels, S., M. Said, and E. F. Lambin. 2001. Land-cover changes around a major East African wildlife reserve: The Mara ecosystem. *International Journal of Remote Sensing* 22:3397–3420.

Settle, J. 1996. On the relationship between spectral unmixing and subspace projection. *IEEE Transaction on Geoscience and Remote Sensing* 34:1045–1046.

Settle, J. J., and N. A. Drake. 1993. Linear mixing and the estimation of ground cover proportions. *International Journal of Remote Sensing* 14:1159–1177.

Shafer, G. 1979. *A mathematical theory of evidence.* Princeton, NJ: Princeton University Press.

Shafer, G. 1987. Belief functions and possibility measures. In *Analysis of fuzzy information. Vol. 1: Mathematics and logic*, ed. J. C. Bezdek, 51–84. Boca Raton, FL: CRC Press.

Shafer, G., and R. Logan. 1987. Implementing Dempster's rule for hierarchical evidence. *Artificial Intelligence* 33:271–298.

Shannon, C. E. 1948. A mathematical theory of communication. *Bell System Technical Journal* 27:379–423, 623–656.

Shannon, C. E., and W. Weaver. 1963. *The mathematical theory of communication*. Chicago: University of Illinois Press.

Sheng, Y. 1996. *Wavelet transform. The transforms and applications handbook*, ed. A. D. Poularikas, 747–827. Boca Raton, FL: CRC Press.

Sheng, Y., and Z. G. Xia. 1996. A comprehensive evaluation of filters for radar speckle suppression. *Proceedings of the International Geoscience and Remote Sensing Symposium (IGARSS'96)*, Lincoln, Nebraska, May 27–31, 1996, 1559–1561. Piscataway, NJ: IEEE.

Shölkopf, B., K. K. Sung, C. Burges, F. Girosi, P. Niyogi, T. Poggio, and V. Vapnik. 1997. Comparing support vector machines with Gaussian kernels to radial basis function classifiers. *IEEE Transactions on Signal Processing* 45:2758–2765.

Shoshany, M., and T. Svoray. 2002. Multidate adaptive unmixing and its application to analysis of ecosystem transition along a climatic gradient. *Remote Sensing of Environment* 82:5–20.

Siegel, A. F. 1982. Robust regression using repeated medians. *Biometrika* 69:242–244.

Simard, M., G. De Grandi, S. Saatchi, and P. Mayaux. 2002. Mapping tropical coastal vegetation using JERS-1 and ERS-1 radar data with a decision tree classifier. *International Journal of Remote Sensing* 23:1461–1474.

Simoncelli, E. P. 1999. Bayesian denoising of visual images in the wavelet domain. In *Bayesian inference in wavelet based models*, ed. P. Muller and B. Vidakovic, 291–308. New York: Springer-Verlag.

Singh, A. 1984. Some clarifications about the pairwise divergence method in remote sensing. *International Journal of Remote Sensing* 5:623–627.

Singh, A. 1986. Change detection in the tropical forest environment of North-eastern India using Landsat. In *Remote sensing and tropical land management*, 237–254. New York: John Wiley and Sons.

Singh, A. 1989. Digital change detection techniques using remotely-sensed data. *International Journal of Remote Sensing* 10:989–1003.

Skidmore, A. K. 1989. A comparison of techniques for calculating gradient and aspect from a gridded digital elevation model. *International Journal of Geographical Information Systems* 3:323–334.

Skidmore, A. K., B. J. Turner, W. Brinkhof, and E. Knowles. 1997. Performance of a neural network: Mapping forests using GIS and remote sensing data. *Photogrammetric Engineering & Remote Sensing* 63(5):501–514.

Small, C. 2001. Estimation of urban vegetation abundance by spectral mixture analysis. *International Journal of Remote Sensing* 22:1305–1334.

Smith, G. M., and E. J. Milton. 1999. The use of the empirical line method to calibrate remotely sensed data to reflectance. *International Journal of Remote Sensing* 20:2653–2662.

Smith, J. A., T. L. Lin, and K. Ranson. 1980. The Lambertian assumption and Landsat data. *Photogrammetric Engineering and Remote Sensing* 46:1183–1189.

Smits, P. C. 2002. Multiple classifier systems for supervised remote sensing image classification based on dynamic classifier selection. *IEEE Transactions on Geoscience and Remote Sensing* 40:801–813.

Solaiman, B., M. C. Mouchot, and A. Hillion. 1996. Contextual dynamic neural networks learning in multispectral images classification. In *Proceedings of the International Geoscience and Remote Sensing Symposium* (*IGARSS'96)*, Lincoln, Nebraska, May 27–31, 1996, 523–525. Piscataway, NJ: IEEE.

Songh, C. W., C. E. Woodstock, K. C. Seto, M. P. Lenney, and S. A. Macomber. 2001. Classification and change detection using Landsat TM data: When and how to correct atmospheric effects. *Remote Sensing of Environment* 75:230–244.

SPSS. 2006. http://www.spss.com (accessed 20 December 2007).

Srinivasan, A., and J. A. Richards. 1990. Knowledge-based techniques for multi-source classification. *International Journal of Remote Sensing* 11:505–525.

Starck, J.-L., F. Murtagh, and A. Bijaoui. 1998. *Image processing and data analysis*. Cambridge: Cambridge University Press.

Steele, B. M. 2000. Combining multiple classifiers-an application using spatial and remotely sensed information for land cover type mapping. *Remote Sensing of Environment* 74:545–556.

Stehman, S. V. 1992. Comparison of systematic and random sampling for estimating the accuracy of maps generated from remotely sensed data. *Photogrammetric Engineering and Remote Sensing* 58:1343–1350.

Stehman, S. V., and R. L. Czaplewinski. 1998. Design and analysis for thematic map accuracy assessment—fundamental principles. *Remote Sensing of Environment* 64:331–344.

Strahler, A. H. 1980. The use of prior probabilities in maximum likelihood classification of remotely sensed data. *Remote Sensing of Environment* 10:135–163.

Strahler, A. H. 1981. Stratification of natural vegetation for forest and rangeland inventory using Landsat digital imagery and collateral data. *International Journal of Remote Sensing* 2:15–41.

Strahler, A. H., and N. A. Bryant. 1978. Improving forest cover classification accuracy from Landsat by incorporating topographic information. In *Proceeding 12th International Symposium on Remote Sensing of the Environment*, Ann Arbor, MI, 927–942.

Strand, E., A. M. S. Smith, S. C. Bunting, L. A. Verling, D. B. Hann, and P. E. Gessler. 2006. Wavelet estimation of plant spatial patterns in multi-temporal aerial photography. *International Journal of Remote Sensing* 27:2049–2054

Strat, T. M. 1984. Continuous belief functions for evidential reasoning. In *Proceedings of the Fourth National Conference on Artificial Intelligence*, 6–10, August, Austin, TX, 308–313.

Sun, W., G. Xu, P. Gong, and S. Liang. 2006. Fractal analysis of remotely sensed images: A review of methods and applications. *International Journal of Remote Sensing* 27:4963–4990.

Swain, P. H., and S. M. Davis. 1978. *Remote sensing: The quantitative approach*. New York: McGraw-Hill.

Swain, P. H., and H. Hauska. 1977. The decision tree classifier: Design and potential. *IEEE Transactions on Geoscience and Remote Sensing* 15:142–147.

Switzer, P., and A. A. Green. 1984. *Min/Max autocorrelation factors for multivariate spatial imagery*. Technical Report No. 6, Department of Statistics, Stanford University, Stanford, CA.

Szeliski, R. 1989. *Bayesian modeling of uncertainty in low-level vision*. Rotterdam: Kluwer.

Taha, I. A., and J. Ghosh. 1999. Symbolic interpretation of artificial neural networks. *IEEE Transactions on Knowledge and Data Engineering* 11:448–463.

Takagi, H., and L. Hayashi. 1991. NN-driven fuzzy reasoning. *International Journal of Approximate Reasoning*, 5:191–212.

Takagi, H., and M. Sugeno. 1985. Fuzzy identification of systems and its application to modelling and control. *IEEE Transactions on Systems, Man and Cybernetics* 15:116–132.

Tanré, D., C. Deroo, P. Duhaut, M. Herman, J. J. Morcette, J. Perbos, and P. Y. Deschamps. 1986. Simulation of the satellite signal in the solar spectrum (5S), *Technical Report*, Laboratoire d'Optique Atmospherique, Universite des Sciences et Techniques de Lille, 59655 Villeneuve d'ascq Cedex, France.

Tanré, D., C. Deroo, P. Duhaut, M. Herman, J. J. Morcette, J. Perbos, and P. Y. Deschamps. 1990. Description of a computer code to simulate the satellite signal in the solar spectrum: The 5S code. *International Journal of Remote Sensing* 11:659–668.

Tatem, A. J., H. G. Lewis, P. M. Atkinson, M. S. Nixon. 2002. Multiple-class land-cover mapping at the sub-pixel scale using a Hopfield neural network. *International Journal of Applied Earth Observation and Geoinformation* 3:184–190.

Teggi, S., R. Cecchi, and F. Serafina. 2003. TM and IRS-1C-PAN data fusion multiresolution decomposition methods based on the "a trous" algorithm. *International Journal of Remote Sensing* 24(6):1287–1301.

Teillet, P. M., J. L. Barker, B. L. Markham, R. R. Irish, G. Fedosejevs, and J. C. Storey. 2001. Radiometric cross-calibration of the Landsat-7 ETM+ and Landsat-5 TM sensors based on tandem data sets. *Remote Sensing of Environment* 78:39–54.

Terzopoulos, D. 1984. Multiresolution computation of visible-surface representation. Ph.D. Thesis, Department of Electrical Engineering and Computer Science, MIT, Cambridge, MA.

Therrien, C. W. 1989. *Decision, estimations and classification: An introduction to pattern recognition and related topics*. New York: John Wiley and Sons.

Theseira, M. A., G. Thomas, J. C. Taylor, F. Gemmell, and J. Varjo. 2003. Sensitivity of mixture modelling to end member selection. *International Journal of Remote Sensing* 24:1559–1575.

Thome, K, P. Slater, S. Biggar, B. Markham, and J. Barker. 1997. Radiometric calibration of Landsat. *Photogrammetric Engineering and Remote Sensing* 63:853–858

Thornton, M. W., P. M. Atkinson, and D. A. Holland. 2006. Sub-pixel mapping of rural land cover objects form fine spatial resolution satellite sensor imagery using super-resolution pixel-swapping. *International Journal of Remote Sensing* 27:473–491.

Tian, Y., P. Guo, and M. R. Lyu. 2005. Comparative studies on feature extraction methods for multispectral remote sensing image classification. *Proceedings of IEEE International Conference on Systems, Man and Cybernetics*, 10–12 October 2005, Waikoloa, Hawaii, 2, 1275–1279.

Tikhonov, A. N., and V. A. Arsenin. 1977. *Solutions of ill-posed problems*. Washington: Winston and Sons.

Touzi, R., A. Lopes, and P. Bousquet. 1988. A statistical and geometrical edge detector for SAR images. *IEEE Transactions on Geoscience and Remote Sensing* 26:764–773.

Towell, G., and J. Shavlik. 1994. Knowledge-based artificial neural networks. *Artificial Intelligence* 70:119–165.

Townshend, J. R. G., ed. 1981. *Terrain analysis and remote sensing*. London: George Allen & Unwin.

Townshend, J. R. G., C. Huang, S. N. V. Kalluri, R. S. Defries, S. Liang, and K. Yang. 2000. Beware of per-pixel characteristics of land cover. *International Journal of Remote Sensing* 21:839–843.

Townshend, J. R. G., C. O. Justice, C. Gurney, and J. McManus. 1992. The impact of misregistration on change detection. *IEEE Transactions on Geoscience and Remote Sensing* 30:1054–1060.

Tso, B. 1997. Investigation of alternative strategies for incorporating spectral, textural and contextual information in remote sensing image classification. Ph.D. Thesis, School of Geography, The University of Nottingham, Nottingham, England, U.K.

Tso, B., and P. M. Mather. 1999. Classification of multisource remote sensing imagery using a Genetic Algorithm and Markov Random Fields. *IEEE Transactions on Geoscience and Remote Sensing* 37:1255–1260.

Tso, B., and R. C. Olsen. 2005a. Combining spectral and spatial information into hidden Markov models for unsupervised image classification. *International Journal of Remote Sensing* 26:2113–2133.

Tso, B., and R. C. Olsen. 2005b. A contextual classification scheme based on MRF model with improved parameter estimation and multiscale fuzzy line process. *Remote Sensing of Environment* 97:127–136.

Tukey, J. W. 1977. *Exploratory data analysis*. Reading, MA: Addison-Wesley.

Tumer, K., and J. Ghosh. 1995. *Theoretical foundations of linear and order statistics combiners for neural pattern classifiers*, Technical Report TR-95-02-98, The Computer and Vision Research Center, The University of Texas at Austin.

Tupin, F., H. Maitre, J. F. Mangin, J. M. Nicolas, and E. Pechersky. 1998. Detection of linear features in SAR images: Application to road network extraction. *IEEE Transactions on Geoscience and Remote Sensing* 36:434–454.

Turket, P. D. 1995. Cost-sensitive classification: Empirical evaluation of a hybrid genetic decision tree induction algorithm. *Journal of Artificial Intelligence Research* 2:369–409.

Ulaby, F. T., A. K. Fung, and R. K. Moore. 1982. *Microwave remote sensing* (two volumes). Reading, MA: Addison-Wesley.

Ulaby, F. T., A. K. Fung, and R. K. Moore. 1986a. *Microwave remote sensing*, Vol. 3. Dedham, MA: Artech House.

Ulaby, F. T., F. Kouyate, B. Brisco, and L. Williams. 1986b. Texture information in SAR images. *IEEE Transactions on Geoscience and Remote Sensing* 24:235–245.

Ulfarsson, M. O., J. A. Benediktsson, and J. R. Sveinsson. 2003. Data fusion and feature extraction in the wavelet domain. *International Journal of Remote Sensing* 24:3933–3945.

Ustin, S. L., D. Dipietro, K. Olmstead, E. Underwood, and G. J. Scheer. 2002. Hyperspectral remote sensing for invasive species detection and mapping. In *Proceedings of the International Geoscience and Remote Sensing Symposium* (*IGARSS'02)*, 24–28 June, Toronto, Canada, 1658–1660. Piscataway, NJ: IEEE.

Van de Hulst, H. C. 1981. *Light scattering by small particles*. New York: Dover,

Van der Meer, F. 1995. Spectral unmixing of Landsat Thematic Mapper data. *International Journal of Remote Sensing* 16:3189–3194.

Van der Meer, F. 1999a. Iterative spectral unmixing. *International Journal of Remote Sensing* 20:3431–3436.

Van der Meer, F. 1999b. Geostatistical approaches for image classification and assessment of uncertainty in geologic processing. In *Advances in remote sensing and GIS analysis*, ed. P. M. Atkinson and N. J. Tate, 147–166. Chichester: John Wiley and Sons.

Van der Meer, F., and S. M. De Jong. 2000. Improving the results of spectral unmixing of Landsat TM imagery by enhancing the orthogonality of end-members. *International Journal of Remote Sensing* 21:2781–2797.

Van der Meer, F., K. Scholte, S. De Jong, and M. Dorrestijn. 1998. Scaling to MERIS resolution: Mapping accuracy and spatial variability. In *EARSeL Workshop on Imaging Spectroscopy,* University of Zurich, 6–8 October 1988, 147–153. Paris: EARSeL.

Van Genderen, J. L., and B. F. Lock. 1977. Testing land use map accuracy. *Photogrammetric Engineering and Remote Sensing* 43:1135–1137.

Van Zyl, J.J., B. D. Chapman, P. Dubois, and J. C. Shi. 1993. The effect of topography on SAR calibration. *IEEE Transactions on Geoscience and Remote Sensing*. 31:1036–1043.

Van Zyl, J. J., H. A. Zebker, and C. Elachi. 1987. Image radar polarization signatures: Theory and observation, *Radio Science* 22:529–543.

Vapnik, V. 1979. *Estimation of dependences based on empirical data* [in Russian]. Nauka, Moscow. (English translation: Springer-Verlag, New York).

Vapnik, V. 1995. *The nature of statistical learning theory*. New York: Springer-Verlag.

Vapnik, V. 1998. *Statistical learning theory*. New York: John Wiley.

Vapnik, V., and O. Chapelle. 2000. Bounds on error expectation for support vector machines. *Neural computation* 12:2013–2036.

Verbyla, D. L., and S. H. Boles. 2000. Bias in land cover change estimates due to misregistration. *International Journal of Remote Sensing* 21:3553–3560.

Vermote, E. F., D. Tanré, J. L. Deuze, M. Herman, and J. J. Morcette. 1997. Second simulation of the satellite signal in the solar spectrum, 6S: An overview. *IEEE Transactions on Geoscience and Remote Sensing* 35:675–686.

Vieira, C. A. O. 2000. Accuracy of remote sensing classification of agricultural crops: A comparative study. Ph.D. thesis, School of Geography, The University of Nottingham, Nottingham, UK.

Vieira, C. A. O., and P. M. Mather. 1999. Assessing the accuracy of classifications using remotely sensed data. In *Proceedings of the 4th International Airborne Remote Sensing Conference/21st Canadian Symposium on Remote Sensing*, Ottawa, Canada, 21–24 June 1999, 2, 823–830.

Voss, R. 1986. Random fractals: Characterization and measurement. In *Scaling phenomena in disordered systems*, ed. R. Pynn and A. Skjeltorp, 37–48. New York: Plenum Press.

Wahbe, G. 1990. *Spline models for observation data*. Philadelphia, PA: Society for Industrial and Applied Mathematics.

Wald, L. 1999. Some terms of reference in data fusion. *IEEE Transactions on Geosciences and Remote Sensing* 37(3):1190–1193

Wald, L. 2000. Quality of high resolution synthesized images: Is there a simple criterion. International Conference on Fusion of Earth Data, *France*, Nice, France, 99–105.

Wald, L. 2002. *Data fusion*. Paris: Ecole des Mines de Paris.

Wald, L., T. Ranchin, and M. Mangolini. 1997. Fusion of satellite images of different spatial resolutions: Assessing the quality of resulting images. *Photogrammetric Engineering and Remote Sensing* 63:691–699.

Walpole, R. E. 1982. *Introduction to statistics*. New York: Macmillan.

Wang, F. 1990a. Fuzzy supervised classification of remote sensing images. *IEEE Transactions on Geoscience and Remote Sensing* 28:194–201.

Wang, F. 1990b. Improving remote sensing image analysis through fuzzy information representation. *Photogrammetric Engineering and Remote Sensing* 56:1163–1169.

Wang, G., G. Gertner, and A. B. Anderson. 2005. Sampling design and uncertainty based on spatial variability of spectral variables for mapping vegetation cover. *International Journal of Remote Sensing* 26:3255–3274.

Wang, G. J., Y. D. Cheng, and K. Chang. 2005. A new neural fuzzy control system with heuristic learning. *International Journal of Fuzzy Systems* 7:158–168.

Wang, L., and D. C. He. 1990. A new statistical approach for texture analysis. *Photogrammetric Engineering and Remote Sensing* 56:61–66.

Wang, X., and H. Wang. 2004. Markov random field modeled range image segmentation. *Pattern Recognition Letters* 25(3):367–375.

Wang, Y., and D. Dong. 1997. Retrieving forest stand parameters from SAR backscatter data using a neural network trained by a canopy backscatter model. *International Journal of Remote Sensing* 18:981–989.

Wang, Z., and A. C. Bovik. 2002. A universal image quality index. *IEEE Signal Processing Letters* 9:81–84

Warner, T. 2005. Hyperspherical direction cosine change vector analysis. *International Journal of Remote Sensing*,\ 26:1201–1215.

Wei, J., and I. Gertner. 2003. MRF-MAP-MFT visual object segmentation based on motion boundary field. *Pattern Recognition Letters* 24(16):3125–3139.

Welch, R. M., S. K. Sengupta, A. K. Goroch, P. Rabindra, N. Rangaraj, and M. S. Navar. 1992. Polar cloud and surface classification using AVHRR imagery: An intercomparison of methods. *Journal of Applied Meteorology* 31:405–420.

Wessman, C. A., C. A. Bateman, and T. A. Benning. 1997. Detecting fire and grazing patterns in tallgrass prairie using spectral mixture analysis. *Ecological Applications* 7:493–511.

Whitsitt, S. J., and D. A. Landgrebe. 1977. *Error estimation and separability measures in feature selection for multiclass pattern recognition*, LARS Publication 082377, Laboratory for Application of Remote Sensing. W. Lafayette, IN: Purdue University.

Widrow, B., and M. E. Hoff. 1960. Adaptive switching circuits. In *IRE WESCON Convention Record, August,* Part 4*,* 96–104.

Wilkinson, G. G., F. Fierens, and I. Kanellopoulis. 1995. Integration of neural and statistical approaches in spatial data classification. *Geographical Systems* 2:1–20.

Wilkinson, G. G., and J. Mégier. 1990. Evidential reasoning in a pixel classification hierarchy—a potential method for integrating image classifiers and expert system rules based on geographic context. *International Journal of Remote Sensing* 11:1963–1968.

Winkler, R. L. 1968. The consensus of subjective probability distributions. *Management Science* 15:B61–B75.

Witten, I. H., and E. Frank. 2005. *Data Mining: Practical Machine Learning Tools and Techniques*. San Francisco, CA: Morgan Kaufmann.

Won, C. S., and H. Derin. 1992. Unsupervised segmentation of noisy and textured images using Markov random fields. *Computer Vision, Graphics and Image Processing (CVGIP): Graphics Models and Image Processing* 54:308–328.

Woodcock, C. E., and A. H. Strahler. 1983. Characterising spatial patterns in remotely sensed data. In *Proceedings of the 17th International Symposium on Remote Sensing of Environment*, 839–852. Ann Arbor, MI: University of Michigan.

Woodcock, C. E., and A. H. Strahler. 1987. The factor of scale in remote sensing. *Remote Sensing of Environment* 21:311–332.

Woodcock, C. E., and A. H. Strahler, and D. B. Jupp. 1988a. The use of variogram in remote sensing: I. Scene models and simulated images. *Remote Sensing of Environment* 25:323–348.

Woodcock, C. E., and A. H. Strahler, and D. B. Jupp. 1988b. The use of variogram in remote sensing: II. Real digital images *Remote Sensing of Environment* 25:349–379.

Wu, Y., and H. Maitre. 1992. Smoothing speckled synthetic aperture radar image by using maximum homogeneous region filters. *Optical Engineering* 31:1785–1792.

Xu, M., P. Watanachaturaporn, P. K. Varshney, and M. K. Arora. 2005. Decision tree regression for soft classification of remote sensing data. *Remote Sensing of Environment* 97:322–336.

Yang, X., and C. P. Lo. 2000. Relative radiometric normalization performance for change detection from multi-data satellite images. *Photogrammetric Engineering and Remote Sensing* 66:967–980.

Yokoya, N., K. Yamamoto, and N. Funakubo. 1989. Fractal-based analysis and interpolation of 3D natural surface shapes and their application to terrain modelling. *Computer Vision, Graphics and Image Processing* 46:284–302.

Zadeh, L. A. 1965. Fuzzy sets. *Information Control* 8:338–353.

Zebker, H.A., and J. J. Van Zyl. 1991. Imaging radar polarimetry: A review. *Proceedings of the IEEE* 79:1583–1606.

Zebker, H.A., J. J. Van Zyl, S. L. Durden, and L. Norikane. 1991. Calibrated imaging radar polarimetry: Technique, examples and applications. *IEEE Transactions on Geoscience and Remote Sensing* 29:942–961.

Zebker, H. A., J. J. Van Zyl, and D. N. Held. 1987. Imaging radar polarimetry from wave synthesis. *Journal of Geophysical Research* 92(B1):683–701.

Zebker, H.A., C. L. Werner, P. A. Rosen, and S. Hensley. 1994. Accuracy of topographic maps derived from ERS-1 interferometric radar. *IEEE Transactions on Geoscience and Remote Sensing* 32:823–836.

Zhang, C., S. E. Franklin, and M. A. Wulder. 2004. Geostatistical and texture analysis of airborne-acquired images used in forest classification. *International Journal of Remote Sensing* 25:859–865.

Zheng, J. S., and Y. W. Leung. 2004. Improved possibilistic c-means clustering algorithms. *IEEE Transactions on Fuzzy Systems* 12:209–217.

Zhong, J., and R. Wang. 2006. Multi-temporal remote sensing change detection based on independent component analysis. *International Journal of Remote Sensing* 27(10): 2055–2061.

Zhu, C., and X. Yang. 1998. Study of remote sensing image texture analysis and classification using wavelets. *International Journal of Remote Sensing* 13:3167–3187.

Zhu, H. 2005. Linear spectral unmixing assisted by probability guided and minimum residual exhaustive search for subpixel classification. *International Journal of Remote Sensing* 26(24):5585–5601.

Zhu, L., and R. Tateishi. 2006. Fusion of multisensor multitemporal satellite data for land cover mapping. *International Journal of Remote Sensing* 27(5):903–918.

Zitová, B., and J. Flusser. 2003. Image registration methods: A survey. *Image and Vision Computing* 21:977–1000.